STRUCTURAL VIBRATION CONTROL IN WIND TURBINES

A THESIS SUBMITTED TO
THE GRADUATE SCHOOL OF NATURAL AND APPLIED SCIENCES
OF
MIDDLE EAST TECHNICAL UNIVERSITY

BY

ÇAĞRI KOÇAN

IN PARTIAL FULFILLMENT OF THE REQUIREMENTS
FOR
THE DEGREE OF MASTER OF SCIENCE
IN
MECHANICAL ENGINEERING

SEPTEMBER 2019

Approval of the thesis:

STRUCTURAL VIBRATION CONTROL IN WIND TURBINES

submitted by **ÇAĞRI KOÇAN** in partial fulfillment of the requirements for the degree of **Master of Science in Mechanical Engineering Department, Middle East Technical University** by,

Prof. Dr. Halil Kalıpçılar _____
Dean, Graduate School of **Natural and Applied Sciences**

Prof. Dr. M. A. Sahir Arıkan _____
Head of Department, **Mechanical Engineering**

Assist. Prof. Dr. Gökhan O. Özgen _____
Supervisor, **Mechanical Engineering Department, METU**

Examining Committee Members:

Prof. Dr. Fevzi Suat Kadıoğlu
Mechanical Engineering, METU _____

Assist. Prof. Dr. Gökhan Osman Özgen
Mechanical Engineering, METU _____

Prof. Dr. Serkan Dağ
Mechanical Engineering, METU _____

Prof. Dr. Altan Kayran
Aerospace Engineering, METU _____

Assist. Prof. Dr. Selçuk Himmetoğlu
Mechanical Engineering, Hacettepe University _____

Date: _____

I hereby declare that all information in this document has been obtained and presented in accordance with academic rules and ethical conduct. I also declare that, as required by these rules and conduct, I have fully cited and referenced all material and results that are not original to this work.

Name, Last Name: Çağrı Koçan

Signature :

ABSTRACT

STRUCTURAL VIBRATION CONTROL IN WIND TURBINES

Koçan, Çağrı
M.S., Department of Mechanical Engineering
Supervisor : Assist. Prof. Dr. Gökhan O. Özgen

September 2019, 154 pages

Wind turbines are exposed to many different sources of loads which cause significant vibrations during their lifetime. Vibrations in the wind turbine system reduce efficiency and decrease the fatigue life. Although vibrations cannot be completely eliminated, they can be mitigated or converted to the other forms of energy by using various vibration control approaches which then increase the lifetime of the wind turbine system. Lowering the vibration response of the wind turbine provides stability under normal and extreme conditions, lesser amount of noise, maintain the high performance and manufacturability. Vibration control approaches usually aim to increase the damping characteristics of the system by using viscoelastic materials as well as additional external active or passive systems that include damping in themselves. In this thesis, dynamic response and fatigue load analyses are presented for a 5MW reference wind turbine, which has developed by United States National Renewable Energy Laboratory (NREL) as a reference model, by using aeroservoelastic simulation tool FAST. For both onshore and offshore cases, the effect of structural damping on the wind turbine in terms of vibration response and fatigue life is observed. Each structural tower and blade modes that induce significant vibrations are

taken into account under different environmental conditions such as normal and extreme turbulence model and transient events such as gusts. The parked and operating conditions are investigated under different mean wind speeds. The effect of blade pitch angle to the fatigue damage is observed. By examining the analyses, it is aimed to guide for damping treatment approaches to mitigate vibrations and increase fatigue life of the structure. In this aspect, in order to identify how much structural damping increase can be achieved, finite element model of the NREL 5MW wind turbine is created. Viscoelastic link treatment is applied to the finite element model by a parametric approach and investigated that remarkable vibration mitigation can be obtained by using viscoelastic links.

Keywords: Renewable energy, Wind turbine, Structural dynamics, Structural vibration control, Vibration mitigation, Fatigue life, Damping treatment, Viscoelastic link

ÖZ

RÜZGAR TÜRBİNLERİNDE YAPISAL TİTREŞİM KONTROLÜ

Koçan, Çağrı
Yüksek Lisans, Makina Mühendisliği Bölümü
Tez Yöneticisi : Dr. Öğr. Üyesi Gökhan O. Özgen

Eylül 2019 , 154 sayfa

Rüzgar türbinleri yaşam ömürleri boyunca ciddi titreşimlere sebep olacak birçok farklı yük kaynağına maruz kalmaktadır. Rüzgar türbini sistemindeki titreşimler yapının verimliliğini ve yorulma ömrünü ciddi oranda düşürür. Bu titreşimler tamamen ortadan kaldırılamasa bile farklı titreşim kontrol yaklaşımlarıyla azaltılabilmekte, veya başka enerjiye dönüştürebilmekte ve bu şekilde rüzgar türbini sisteminin yaşam ömrü arttırılabilmektedir. Rüzgar türbininin titreşim cevabını azaltmak normal ve uç koşullarda stabilite, daha az gürültü, yüksek performans ve üretilebilirliğe katkı sağlayabilmektedir. Titreşim kontrol yaklaşımları genellikle viscoelastik malzemeler ya da dışarıdan eklenen ve kendi içerisinde sönümlemeye sahip aktif veya pasif sistemler kullanılarak sistemin sönümleme karakteristiğini arttırmayı amaçlamaktadır. Bu tez Birleşik Devletler Ulusal Yenilenebilir Enerji Laboratuvarının referans olarak hazırladığı 5MW'lık bir rüzgar türbini modeli üzerinde, aeroservoelastic simülasyon aracı FAST kullanarak dinamik cevap ve yorulma ömrü analizlerini sunmaktadır. Kara ve denizdeki rüzgar türbini modelleri için, eklenen yapısal sönümleme oranının rüzgar türbinine titreşim ve yorulma ömrü açısından etkisi araştırılmaktadır. Normal ve uç türbülans modelleri gibi çeşitli durumlarda ciddi titreşimlere sebep olacak her bir

kule ve kanatçık modu hesaba katılmaktadır. Farklı rüzgar hızlarıyla park ve çalışan koşuldaki rüzgar türbini ayrı ayrı incelenmektedir. Analiz sonuçlarına bakarak, titreşim azaltacak ve yorulma ömrü arttıracak sönümleme yaklaşımları için bir rehber oluşturulması hedeflenmektedir. Ne kadar yapısal sönümleme oranının elde edilebileceğini saptamak için 5MW rüzgar türbininin sonlu elemanlar modeli tanımlanmakta ve sönümleme yaklaşımları uygulanmaktadır. Parametrik bir yaklaşımla viskoelastik bağlantılar kullanılarak kayda değer oranda titreşim sönümlemesi elde edilebilmektedir.

Anahtar Kelimeler: Yenilenebilir enerji, Rüzgar türbini, Yapı dinamiği, Yapısal titreşim kontrolü, Titreşim sönümleme, Yorulma ömrü, Sönümleme işlemi, Viskoelastik bağlantı

To my family...

ACKNOWLEDGMENTS

First of all, I would like to express my gratitude to supervisor Assist. Prof. Dr. Gökhan ÖZGEN for his technical support.

I would like to express my deep love and heartfelt gratitude to my family, to whom I dedicate my life and make me what I am today, my mother Belgin KOÇAN, my father Erol KOÇAN and my brother Çağlar KOÇAN for their supports in all aspects of my life. Without their moral supports, I could not handle the thesis.

I would like to thank my housemates Mert TUNALI and Ahmet Mert POLATER, who also write their thesis, for their support and companionship during my Master of Science life. I owe my special thanks to my oldest friends Yiğit SERİN and Kıvanç ÇETİN and Eran Ege AKAR for welcoming me all the time and for having a memorable time outside the home. I am also thankful to all my friends for the unforgettable special moments I spent with them.

Finally, my special thanks to my colleagues from Turkish Aerospace Industries, for their friendship and encouragement during my study.

TABLE OF CONTENTS

APPENDICES

LIST OF TABLES

TABLES

LIST OF FIGURES

FIGURES

LIST OF ABBREVIATIONS

ABBREVIATIONS

TwrBsFxt	Tower base fore-aft shear force
TwrBsFyt	Tower base side-side shear force
TwrBsFzt	Tower base axial force
TwrBsMxt	Tower base side-side moment
TwrBsMyt	Tower base fore-aft moment
TwrBsMzt	Tower base torsional moment
RootFxb1	Blade 1 root flapwise shear force
RootFyb1	Blade 1 root edgewise shear force
RootFzb1	Blade 1 root axial force
RootMxb1	Blade 1 root edgewise moment
RootMyb1	Blade 1 root flapwise moment
RootMzb1	Blade 1 root pitching (torsional) moment
DEL	Damage Equivalent Load
PSD	Power Spectral Density
NREL	National Renewable Energy Laboratory
HAWT	Horizontal Axis Wind Turbine
VAVT	Vertical Axis Wind Turbine
TMD	Tuned Mass Damper
TLD	Tuned Liquid Damper
FEM	Finite Element Model
FRF	Frequency Response Functions
SSI	Structure Soil Interaction
IEC	International Electrotechnical Commission

CHAPTER 1

INTRODUCTION

1.1 Motivation

As technology advances, there is an increase in energy demand. Although it has been mostly met by burning fossil fuels during industrialization, it is known that they threaten our world by causing global climate change. Therefore, there is an intensive amount of labor for researching alternative energy sources. Especially after 2015 when the Paris Agreement was signed, countries from all over the world make collaboration to take actions against climate change by investing in new energy sources.

The use of wind energy has been growing very fast and has the greatest potential for the future since they are nonpolluting and inexhaustible compared to the other sources of energy such as fossil fuels and nuclear power [21]. Wind energy has the greatest potential to meet the electricity requirement of the whole world. By 2030, it is expected that 20% of US energy is provided by wind energy [22].

Wind power is generated by the wind turbines which are classified as onshore and offshore in terms of their working area. The sizes of the wind turbines have been increasing exponentially to capture more energy from the wind. As size increases, the cost of the wind turbines also increases thus the recent improvements are related with obtaining an efficient size and cost balance. In addition, as size increases and structure becomes more slender, the fourth parameter takes part; which is the vibration related problems. Vibrations in the wind turbines produce noise, decrease user and operating comfort, production efficiency and fatigue life. As a result, wind turbine technology includes an optimization procedure between four parameters which are energy, cost, size and vibration problems.

Structural control is used in order to mitigate vibrations and increase fatigue life of a mechanical system. It can be achieved by increasing damping ratio of a system by either designing external passive or active systems that include damping in themselves or materials that convert vibration energy into strain energy. The effect of structural damping to the wind turbine dynamic response under different loading is usually overlooked by researchers. In addition, viscoelastic link treatment is not studied in the literature for the wind turbines. With an effective damping treatment, the lifetime of a wind turbine can be prolonged which leads cost reductions and reliability increase. In addition, in the near future, an effective structural control of a wind turbine can give rise to higher wind turbine sizes, more than even 10 MW, to generate more electricity.

1.1.1 Objectives of the Thesis

The main objectives of this Master's thesis are:

- To observe the effect of modal characteristics of a wind turbine to its dynamic response.
- To study the effect of structural damping on wind turbine response and fatigue life for different environmental and physical conditions by using aeroservoelastic wind turbine model.
- To investigate the effectiveness of viscoelastic link treatment approach in order to mitigate vibrations and fatigue loads in the wind turbine.

1.2 Organization of the Thesis

In Chapter 2, general information about wind turbine and relevant theory are presented. The chapter covers the characteristics and classifications of wind turbines, modeling techniques of wind turbines, characteristics of loads, as well as fatigue load estimation approaches used in this thesis. In Chapter 3, the aeroservoelastic simulation code FAST is described. This chapter involves the description of the different submodules of the simulation code and the coupling between them. In Chapter 4,

NREL 5 MW reference wind turbine model, which is used throughout the thesis is described in detail. In Chapter 5, the simulations are explained. It includes spectral analyses, sectional loads analyses, fatigue load estimations and lifetime fatigue load results for different structural damping ratios and different environmental conditions. In Chapter 6, viscoelastic link modeling is described. It includes finite element modeling, parametric approach developed for viscoelastic link implementation and simulation results for different viscoelastic link layouts. Chapter 7 includes the conclusion of the study.

CHAPTER 2

LITERATURE SURVEY

2.1 History

The first attempt to generate electricity by wind turbine was of Charles Brush who converted an electrical generator into a windmill in 1888. A photograph of his wind turbine is shown in Figure 2.1.

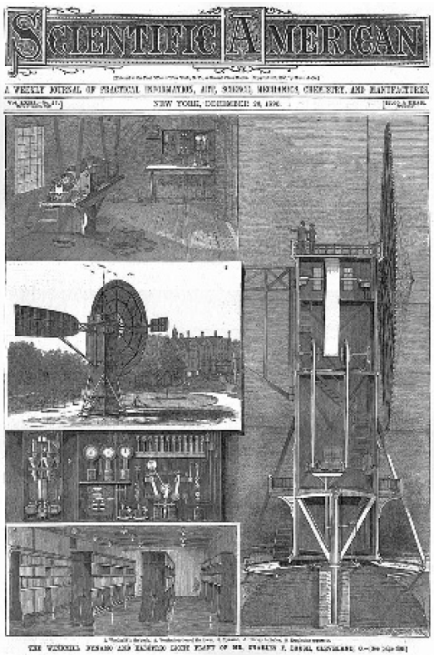

Figure 2.1: Scientific American page showing different views of brush turbine [1]

After his attempt, a small turbine which was three bladed and had an airfoil cross section was designed by Marcellus Jacobs as shown in Figure 2.2. Smith-Putnam machine was one of the most significant early large turbine, built in the late 1930s in the United States [23]. It had 1.25 MW power and with a rotor diameter of 53.3 m.

It was the largest wind turbine in 1930s. After that, in wind turbine technology, not much happened until when the world faced the first oil crisis.

Figure 2.2: Jacobs Turbine[5]

The first oil crisis attracted the attention to renewable energy sources and wind energy technology has developed significantly in the last decades. In 1970s, NASA developed one of the most remarkable large scale wind turbine in the renewable energy history. In 1980, the first wind farm was built in New Hampshire, United States with 20 wind turbines [24]. As the wind at sea is stronger and more stable than the land, the first offshore wind farm was built in Denmark in 1991 with a 5 MW total capacity [25]. Nowadays, the size of the largest commercial wind turbines has been increased up to 10 MW. As of 2017, the world's largest wind turbine named MHI Vestas V164 with 164 m rotor diameter and a rated power of 9.5 MW has been built [1]. A list of the largest wind turbines in 2017 is given in Table 2.1.

Table 2.1: The largest wind turbines[1]

Model	Rotor Diameter (m)	Rated Power (MW)
MHI Vestas V164	164	9.5
Adwen AD-80	180	7.5
Siemens SWT-8.0-154	120-154	6-8
Enercon E-126	127	7.5
Ming Yang SCD 6	140	6
Senvion 6.2M152	126	6.15
GE Haliade	151	6

Although increasing the rotor diameter provides higher power, this approach has eco-

nomic limits. Figure 2.3 shows the correlation between the rotor diameter and the cost of purchasing and maintaining a wind turbine.

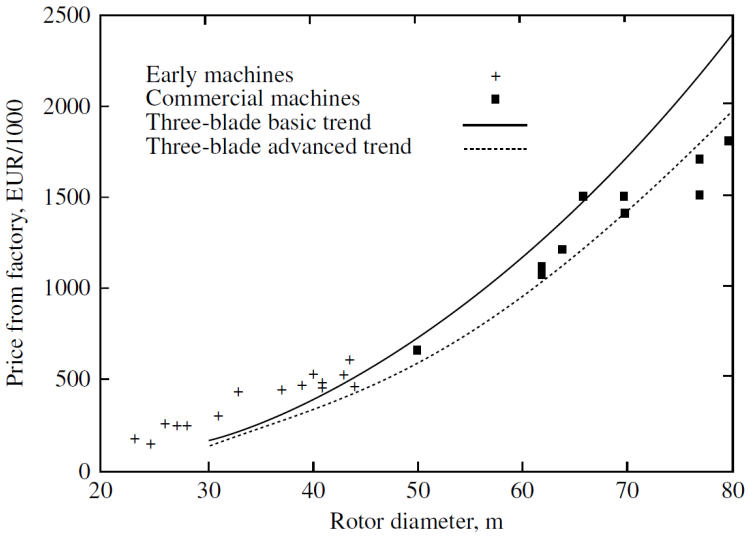

Figure 2.3: Relation between rotor diameter and cost[1]

In the future, wind energy ensures its viable role for maintaining world's energy. The next generation wind turbines must improve efficiency and reliability and lower the acquisition cost to compete with fossil fuel electric power plants.

2.2 Market Overview

Nowadays, more than 90 countries use wind energy source. Currently, 539 GW of installed power generation capacity are in operation with more than 340.000 wind turbines as shown in Table 2.2. China leads with a total wind energy capacity of 188.392 MW. US, Germany, India and Spain follow with 89.077 MW, 56.132 MW, 32.848 MW and 23.170 MW, respectively [2]. The total cumulative installed capacity by year is represented in Figure 2.4. The offshore wind turbines had a record with 4.334 MW of installations, corresponding to an 87% increase in 2016, and representing only about 8% of the global annual market. However, it is only 3.5% of total installed capacity, but it is growing quickly. Countries such as Spain, Germany and Denmark are close to meet 30% of their electricity from wind energy. In addition, project prices for onshore and offshore wind turbine continue to decrease. Better planning, more so-

phisticated power electronics and management contribute to increased reliability and reductions in prices. It is expected that there will be 1X wind turbine machines nearly soon. On March 2018, GE announced its next generation design, which is named as the 12 MW Haliade-X and will have 220 m rotor diameter, is planned to come into commercial operation as early as 2021 [26].

Table 2.2: Use of wind energy worldwide[2]

Country	MW	% Share
PR China	188,392	35
USA	89,077	17
Germany	56,132	10
India	32,848	6
Spain	23,170	4
United Kingdom	18,872	4
France	13,759	3
Brazil	12,763	2
Canada	12,239	2
Italy	9,479	2
Rest of the world	82,391	15
Total TO P10	**456,732**	**85**
World Total	**539,123**	**100**

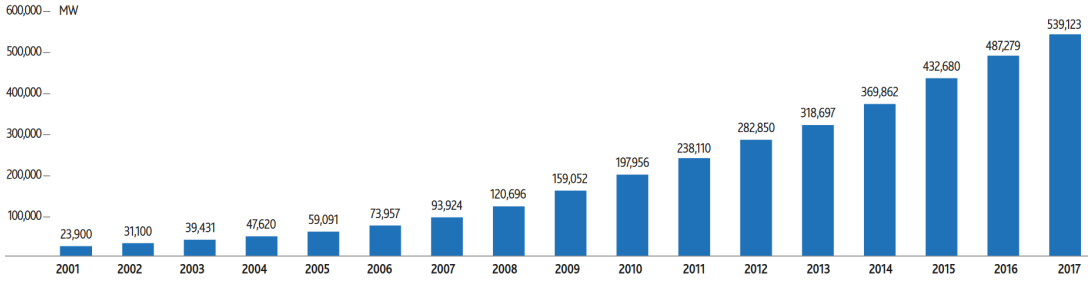

Figure 2.4: Total installed capacity worldwide by year[6]

2.3 Characteristics of the Wind Turbine

Wind turbines are classified into two groups as onshore and offshore in terms of their working area. In the early years of wind energy development, wind turbines are built in lands. Since 1991, the offshore wind turbine capacity has been increasing. While onshore wind turbines are supported by monopile or jacket like tower which is mostly

tapered hollow cylinder, offshore wind turbines have additional substructure under the sea level. They are subdivided as offshore fixed bottom and offshore floating turbines. Floating platforms are preferred for deep water. Figure 2.5 shows the different options for offshore wind turbine foundations.

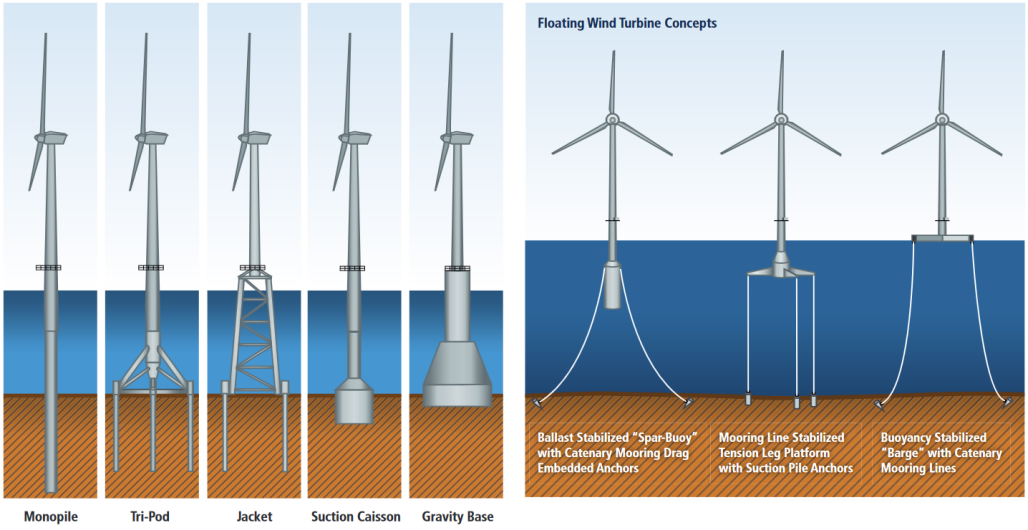

Figure 2.5: Shallow water structure[7]

Besides classifications in terms of working area, wind turbines can be grouped into two categories in terms of the axis of rotation of the blades which are horizontal axis wind turbines (HAWT) and vertical axis wind turbines (VAWT) as depicted in Figure 2.6. For large areas, HAWTs are more widely used since they are more efficient. Under turbulent winds, HAWTs are not efficient. HAWTs are generally installed where wind speed is high, such as sea areas. On the other hand, VAWTs are used in urban areas. VAWTs work efficiently under turbulent wind. They have the capability to generate power from low wind. VAWTs are placed at the ground without a tower. [27, 28, 29].

The main structural parts of wind turbine are blades, tower, nacelle and hub. The blades have an airfoil cross-section and often incorporate twist and taper to have maximum efficiency. Most wind turbine blades are made of fiberglass or carbon fibre reinforced plastics (GRP or CGRP). The tower is generally tapered hollow cylinder, thickness of which is very small and made of steel. The hub provides the connection between blades and the main shaft. It is connected to the nacelle which encloses the drivetrain, electrical generator and other various components. The electrical genera-

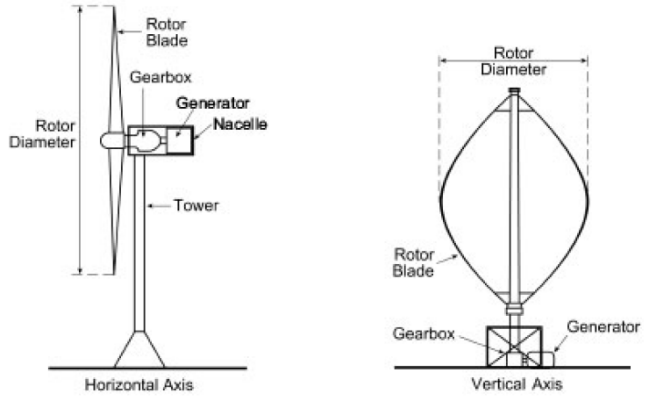

Figure 2.6: Typical examples of HAWT and VAWT (The Scottish Government 2006) [8]

tor converts the mechanical energy to electrical energy. The efficiency is the driving concern for generator and it decreases below its rated wind speed. The gearbox converts the high torque and low speed to high speed and low torque [5]. Figure 2.7 shows a typical wind turbine layout.

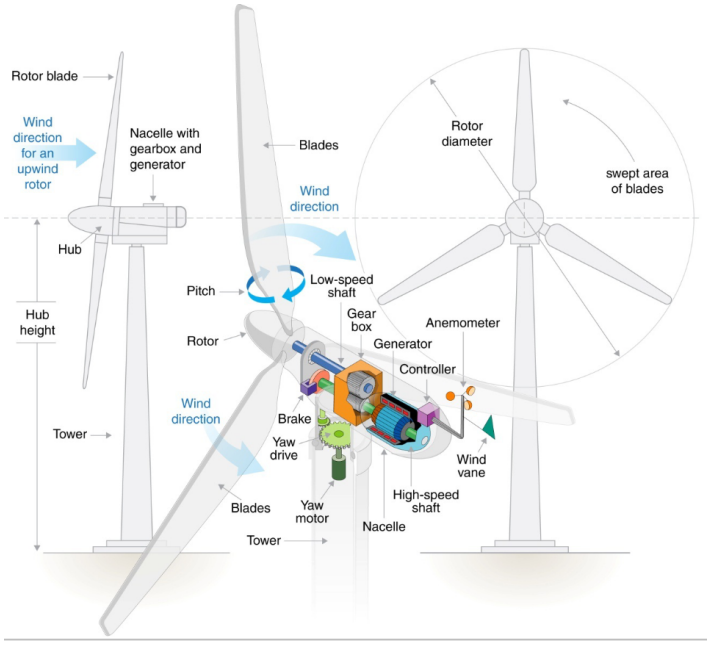

Figure 2.7: Wind turbine layout[9]

Modern wind turbines have complex control and safety systems and mechanisms which are necessary in order to increase efficiency and to provision for harsh environments. Breaking system, either provided by aerodynamic or mechanical brakes,

brings the wind turbine to a safe condition in cases of emergencies such as extreme winds and lightning. Yaw mechanism is another active mechanism which is used to rotate the wind turbine rotor according to the main wind to capture more energy. Yaw motion is achieved by electrical or hydraulic system. Power control is another system used to shut-off the wind turbine when the wind reaches cut-out wind speed, generally above 25 m/s, to ensure safety of the generator and the structure. In addition, power systems of the wind turbines provide maximum power generally below 15 m/s. Figure 2.8 shows the power generated as a function of the mean wind speed, which is specific for each wind turbine. The power control is achieved by adjusting the pitch angle of blades actively according to the wind speed to obtain optimum lift generation below cut out wind speed or parking the wind turbine under harsh environment. In some of the wind turbines, stall control is used to control the generated power by which blades are designed to ensure that the stall conditions occur at higher wind speed.

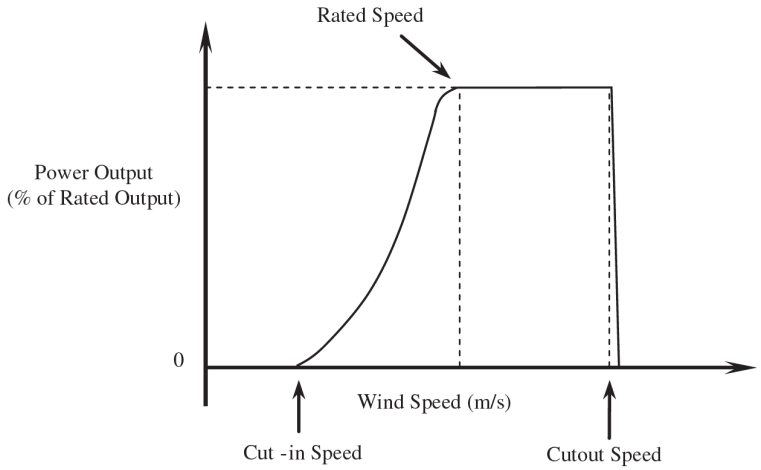

Figure 2.8: Typical wind turbine power curve[10]

2.4 Environmental Loads

2.4.1 Wind Modeling

Wind turbine is an aeroelastic system in which aerodynamic load due to unsteady turbulent wind causes significant vibrations which then affect the dynamic flow around

the structure continuously. In other words, there is a coupling between structural and aerodynamic characteristics of the system. Therefore, both turbulence modeling and aerodynamic load calculation carry important role in wind turbine design procedure.

Wind is a random phenomena and statistical approaches are used to model turbulent wind characteristics. In general, for a 10 minute wind measurement, Gaussian probability distribution is valid with a mean value U_{10} and standard deviation σ_U [30]. By using two parameters, turbulence intensity $I_U(z)$ is defined as in Equation 2.1,

$$I_U(z) = \frac{\sigma_U(z)}{U_{10}(z)} \tag{2.1}$$

It is worth noting that turbulence intensity is dependent on z which is the height above ground. With higher roughness of the terrain and at lower heights, turbulence intensity increases. In addition, the wind is affected by the friction on land which is known as wind shear. Figure 2.9 shows a mean wind speed profile affected by turbulence and wind shear. To take into account the wind shear, two common wind speed profiles are existed. The logarithmic profile is described in Eq. 2.2.

$$U(z) = U_{10}(z_r) ln \frac{z}{z_0} \tag{2.2}$$

Where z_0 is the roughness parameter varying between 0.0001 m to 0.01 m. Another commonly used wind speed profile is the power law as given in Eq. 2.3,

$$U(z) = U_{10}(z_r) \left(\frac{z}{z_r} \right)^{\alpha} \tag{2.3}$$

Where α depends on the surface roughness and z_r is mean reference height, usually taken as hub height. A comparison of power law and logarithmic profile is shown in Figure 2.10 for $z_r = 90m$, corresponding to the hub height of the NREL 5 MW wind turbine, $z_0 = 0.001$, $\alpha = 0.14$ and $U_{10}(z_r) = 12m/s$.

Besides mean wind speed profile, the energy distribution of the ambient turbulence is represented by power spectral density (PSD) function. Several turbulence spectra exist and are mostly based on land or offshore measurements. Von Karman [31],

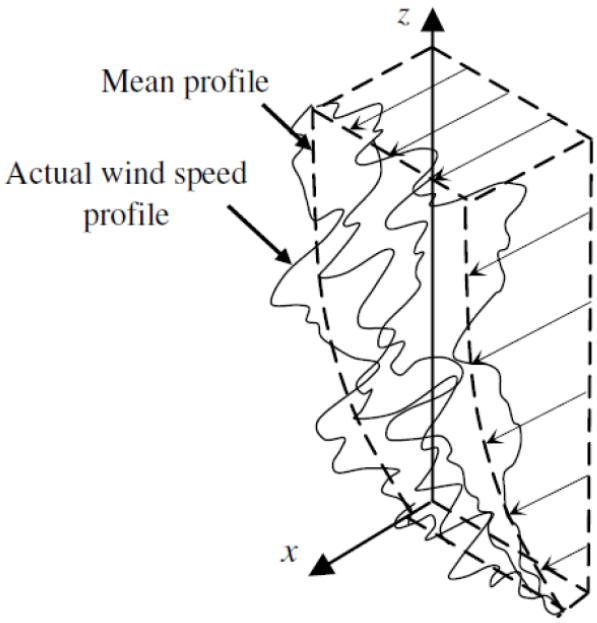

Figure 2.9: Wind speed profile[11]

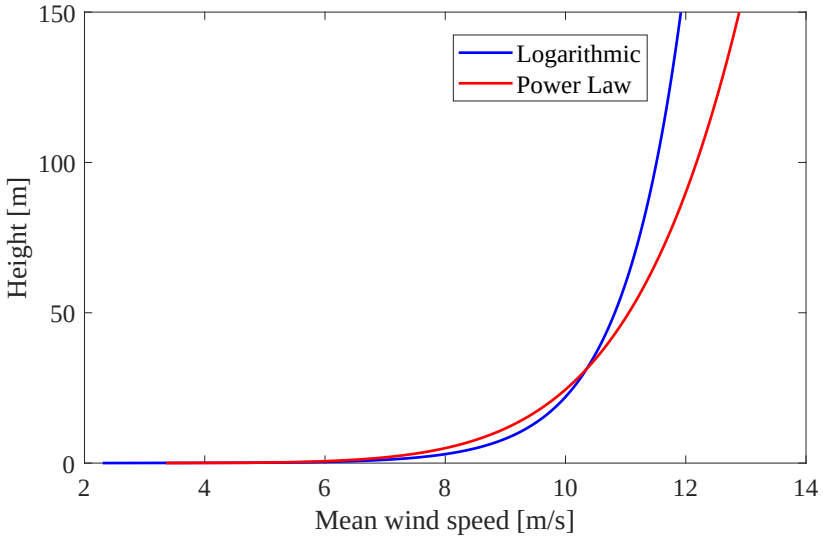

Figure 2.10: Comparison of wind profiles for logarithmic and power laws

Davenport [32] and Kaimal [33] spectrum are the well known spectra used in wind turbine analyses. Figure 2.11 shows the comparison between these spectra for a mean wind speed 12 m/s.

There are some other approaches in turbulence modeling especially for frequency do-

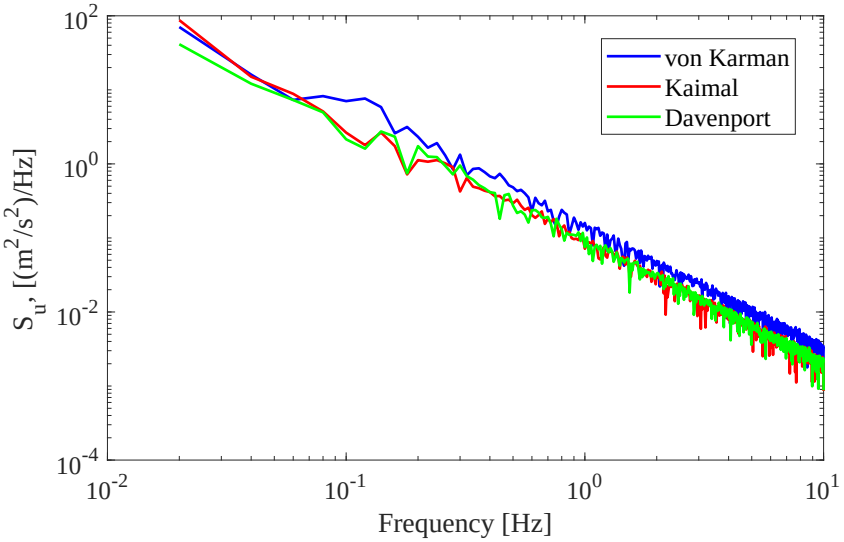

Figure 2.11: Various turbulence models

main analyses. Connell [34] reported that when the blades rotate, they are subjected to a fluctuating wind spectrum. Therefore, the turbulence spectrum appears with peaks which indicate the harmonics of rotating blade frequencies. The analysis is made by first creating rotationally sampled spectrum and converting it to time domain via inverse Fourier transform. Beskhyroun et al. [35] used a similar type of 3-D rotationally sampled spectrum. They included the Taylor's hypothesis for the turbulence. Zuo [36] decomposed the mean wind load into a constant plus fluctuating component. While constant component indicate the mean wind speed, Kaimal spectrum is used for the fluctuating component of the wind along the tower. They are converted to time domain by using Inverse Fourier Transform.

IEC 61400-1 [3] defines wind conditions in terms of the wind turbine classes as shown in Table 2.3. The normal and extreme turbulence conditions are considered for design according to the wind turbine classes. In Table 2.3, V_{ref} is the reference mean wind speed for 10 minutes; A, B and C indicates the category for high, medium and low turbulence characteristics, respectively. I_{ref} is the turbulence intensity.

According to IEC 61400-1, the design lifetime for the wind turbine classes indicated as I, II and III shall be at least 20 years [3]. The wind turbines shall be designed so that they can withstand the load conditions defined by selected wind turbine class. Normal

Table 2.3: Wind turbine classes in IEC61400-1[3]

Wind turbine class		I	II	III	S
V_{ref}	(m/s)	50	42,5	37,5	Values
A	I_{ref} (-)	0,16			specified
B	I_{ref} (-)	0,14			by the
C	I_{ref} (-)	0,12			designer

and extreme wind conditions are defined according to their frequency of occurrence. While normal wind conditions occur frequently, extreme wind conditions are defined as 1-year and 50-year occurrence period. The wind is consisted of a constant mean wind speed which is combined with turbulence or gust.

In this thesis, Kaimal spectrum is used as a turbulence model for the analyses since it is expressed in IEC 61400-1. The component PSD of Kaimal spectrum is given by equation,

$$S_U(f) = \sigma_U^2 \frac{4\frac{L_k}{U_{10}}}{\left(1 + 6\frac{fL_k}{U_{10}}\right)^{3/5}} \tag{2.4}$$

Where L_k is integral length scale parameter expressed as,

$$L_k = \begin{cases} 5.67m, & for \quad z < 60\ m \\ 340.2m, & for \quad z \geq 60\ m. \end{cases} \tag{2.5}$$

The turbulence spectra with a certain mean wind speed is valid for the short-term stationary wind conditions. In long term, according to Det Norske Veritas [30], a Weibull probability distribution function indicating the probability of the mean wind speed can be assumed unless measured data indicate otherwise.

2.4.2 Aerodynamics Modeling

There are several approaches for aerodynamic loads calculation. A steady aerodynamics model can be sufficient for energy estimation of the wind turbine with a

known wind distribution. However, due to the unsteadiness of the wind, tower wake and wind shear, unsteady aerodynamics model is used to estimate the fatigue loads properly [37].

The unsteady aerodynamic loads for the wind turbine blade are generally calculated by Blade Element Momentum Theory accompanied by Dynamic Stall [38, 39, 40]. In this model, as blade approaches to its static stall angle, vortices are occurred at leading edge rather than trailing edge and lift further increases up to a certain angle and then dynamic stall phenomena occurs [12]. Leading edge separation is the fundamental characteristics of the dynamic stall of an airfoil. In fact, trailing edge separation starts in a quasi-steady stall. Figure 2.12 represents the flow morphology and the unsteady air flow during the dynamic stall progress.

In the literature, Murtagh et al. [41, 42, 43] consider a rotationally sampled turbulence caused by the blade rotation. In addition, the lift is not considered because of the hollow cross section of blade models. Aerodynamic loads along the tower are calculated by a joint acceptance function approach.

Caterino [44] uses a 1/20 scaled wind turbine model which is connected to a shaker table from bottom of the tower in lab environment. The input accelerations are given such that the dynamic responses of the structure become equivalent as if it is excited by the wind. Wind buffeting and operating gust, which is a sudden increase in the wind speed are considered.

Iijima [45] and Lackner [46] model the aerodynamic loads by using open source FAST code. AeroDyn submodule of FAST uses unsteady Blade Element Momentum theory which involves dynamic stall. It also involves axial and tangential induction, as well as hub and tip losses. In this thesis, AeroDyn submodule of FAST is used to calculate aerodynamic loads.

2.4.3 Seismic Loads

Seismic loads are earthquake loads that are modeled by ground acceleration time histories and studied in several papers [36, 47, 48, 49, 50]. Earthquake is represented with peak ground acceleration parameter which defines the earthquake severity. The

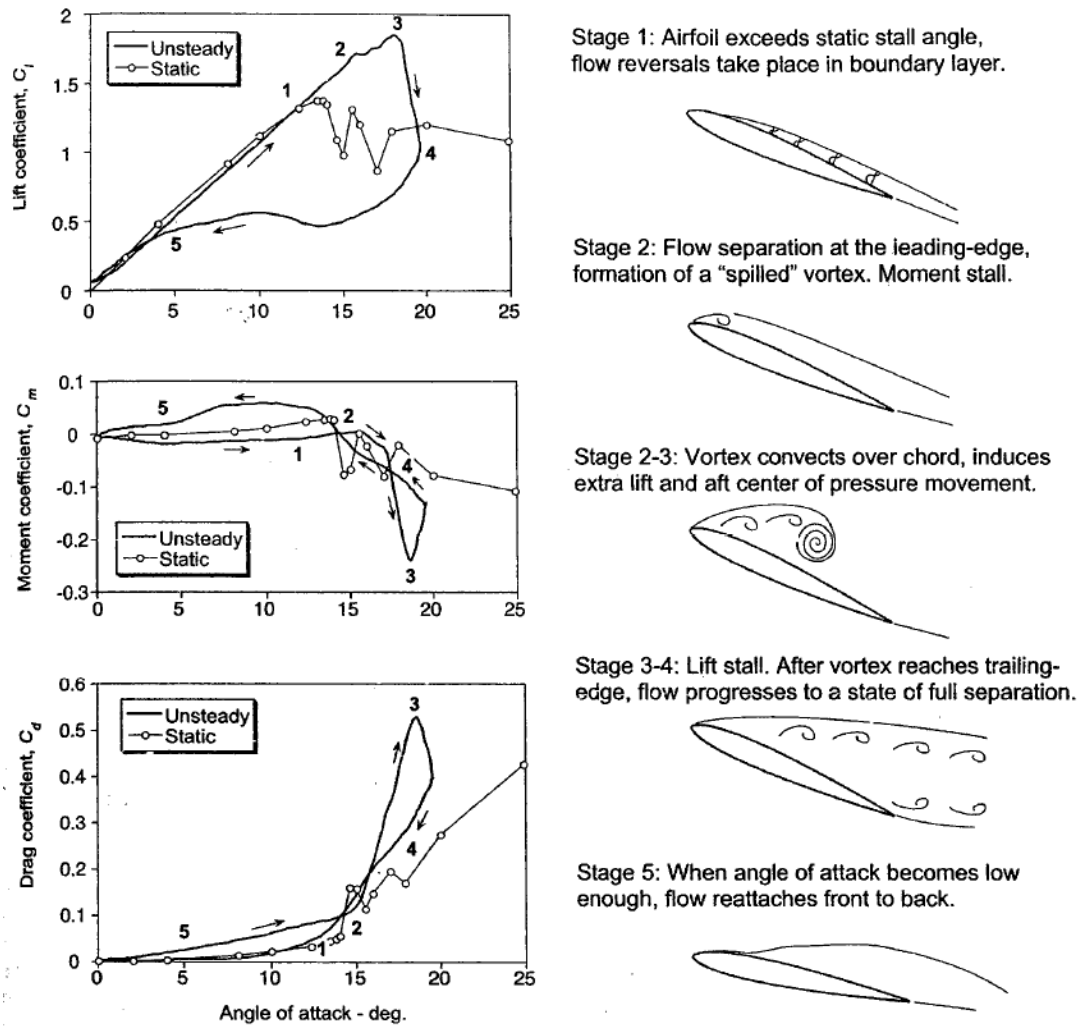

Figure 2.12: Dynamic Stall progression [12]

acceleration is applied in the three translational direction [47]. In some researches, the ground motion is three dimensional [50].

An earthquake can excite the higher frequency modes since its energy is within a broader frequency range with respect to the wind and wave [36]. Due to excitation of higher modes, the maximum displacement can occur at different points along the tower and not at the top.

As output, usually the maximum bending moment at the tower base, upper joint, lower joint and the top of the tower are taken into account. The blades are not critical in seismic excitation.

The stability of the wind turbines under earthquake conditions has to be proved according to Eurocode 8 [51]. In Eurocode 8, a certain spectra of the earthquake input is represented.

2.4.4 Wave Loads

Wave loads are valid for offshore wind turbines. Waves are expressed by stochastic or deterministic models. For low wind speeds and deep water, waves are deterministic. The waves are stochastic when the wind speed is high. Stochastic waves are represented by a PSD function which is dependent on parameters, significant wave height H_s and spectral peak period T_p. Moskowitz [52] proposed a wave spectra which is based on 460 wave records between 10.3 m/s to 20.6 m/s wind speed. It shows that range of critical frequencies of sea lay are between 0.04 and 0.12 Hz. JONSWAP is also a well known spectrum, a modified version of the Moskowitz spectrum and developed in the Joint North Sea Wave Project [53]. The spectrum of JONSWAP model is represented by,

$$S\left(f\right) = \frac{\alpha g^2}{\left(2\pi\right)^4} f^{-5} \exp\left(-\frac{5}{4}\left(\frac{f}{f_p}\right)^{-4}\right) \gamma^{\exp\left(-0.5\left(\frac{f-f_p}{\sigma f_p}\right)^2\right)} \tag{2.6}$$

where,

$$\alpha = 5\left(\frac{H_s^2 f_p^4}{g^2}\right)\left(1 - 0.287\ln\gamma\right)\pi^4 \tag{2.7}$$

f is the frequency of wave, f_p is the spectral peak frequency, g gravity acceleration, γ is the peak-shape factor and is dependent on T_p and H_s. σ is the spectral width parameter. For $\gamma = 1$, the JONSWAP and Pierson-Moskowitz spectra are identical. As in the case of wind, the long-term probability distributions for the waves can be described by Weibull distribution indicating the probability of H_s and T_p.

For offshore wind turbines, the coupling of wind and wave loads may excite both fore-aft and side-side modes of the tower. Especially waves acting on the monopile with a relative angle to the mean wind direction cause large fatigue damage due to the

absence of aeroelastic damping in the direction lateral to the mean wind [54, 55, 56]. For offshore wind turbines, as monopile length increases, the structure becomes more slender which decreases the frequency of tower modes. Thus, they will be move closer to the primary excitation frequency of the waves and vibrations increase due to low damping in the lateral direction. In addition, as monopile becomes slender, the diameter of monopile should be increased correspondingly, which will consequently increase wave loading.

IEC61400-3 [57] defines the wave models in terms of both stochastic sea state representations and regular design waves. The stochastic models shall be based on a wave spectrum appropriate to the site. It is recommended that for a fully developed sea, Pierson-Moskowitz and for a developing sea JONSWAP spectrum can be used.

2.5 Modeling of Wind Turbines

2.5.1 Mathematical Modeling

In the literature, several approaches are valid and useful for modeling wind turbine system. The maturity of modeling approach determines the quality and uncertainty of the outputs. In some modeling approaches, the phenomena such as dynamic stall, unsteady aerodynamics, centrifugal stiffening, structure soil interaction or the effects of servo system are neglected to simplify the system.

The simplest model of a wind turbine is a cantilever beam with a tip mass where the beam corresponds to the tower; the remaining parts such as blades, nacelle, drivetrain, generator and hub correspond to the tip mass. In Figure 2.13, a typical example of cantilever beam model is shown.

It may be merely useful to determine the first natural frequency of the tower by using equation,

$$f_{nat}^2 \cong \frac{3.04}{4\pi^2} \frac{EI}{(m_{top} + 0.227\mu L)\, L^3} \tag{2.8}$$

Where f_{nat} is the fundamental natural frequency, m_{top} is the tower top mass, μ is

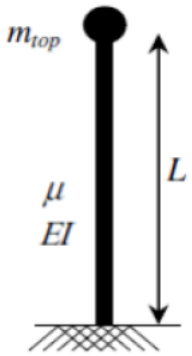

Figure 2.13: Cantilever beam model of a wind turbine [12]

the tower mass per unit length, L is the tower length and EI is the tower bending stiffness. Cantilever beam model ignores the taper of the tower and variable wall thickness. It also neglects the structure soil interaction.

Adhikari and Bhattacharyta [58] use a flexible model including foundation. The Equation 2.8 is not offered since it does not consider the flexibility of the foundation and stiffness softening effect due to the axial load. Instead, the tower is considered as Euler-Bernoulli beam with a base connected to soil by axial and rotational springs. These two springs constrain the system at the bottom. It has a top mass used to idealize the nacelle and blades. Then, the equation of motion of the system is written by using non-dimensional parameters and foundation model is validated with experiment.

Murtagh et al. [59] model wind turbine system by employing the lumped mass method which is a model order reduction technique. They demonstrate that modal characteristics of the wind turbine obtained by lumped mass method and finite element method are in close agreement. Moreover, a further simplified modeling using the approximate cantilever system, a cantilever beam with a mass at the top, provide accurate estimates for modal frequencies and mode shapes of the lattice tower.

Zhao and Maiber [50] construct the wind turbine model by using joint beam elements which are used along the tower. They are consisted of joints and springs. Equations of motion are derived by Lagrange formulation including Lagrange multipliers. The structure soil interaction (SSI) is modeled as spring damper system at the foundation.

For the SSI, two translational components in the horizontal plane and one rotational motion are modeled. The tower is modeled as a tapered beam which consists of several conical sections.

Hanler [48] creates a code called SIWEC by considering that SSI and ground base acceleration input are allowed. The wind turbine is described by a flexible multi-body system. He describes the system with a total of 28 DOF, in which foundation has 6 DOF, tower bending have 2 DOF N modes, tower torsion has 1 DOF, nacelle tilt motion has 1 DOF, drive train rotation and torsion motion have 2 DOF, blades flapwise and edgewise motions have N modes.

Krenk et al. [60] model the wind turbine with accurate representation of the centrifugal forces. Finite element approach is used to model the rotor and blades with 46 sections in each blade. The shaft is modeled as a lumped element. The collective, backward whirling and forward whirling modes are included in the equation of motion.

Staino and Basu [61] formulate the wind turbine by using a Lagrangian-Eulerian formulation with centrifugal stiffening and gravity effects involved. The coupling between structure and aerodynamics is achieved by Blade Element Momentum Theory. The blade is cantilever beam with with N modes in edgewise direction. The tower is modeled as a single degree of freedom system.

Martynowicz [62] reduce the turbine components to mass and mass moments of inertia while aerodynamic forces are applied to the nacelle or to the tower. Simulink is used in order to represent the equations of motion. In addition, Comsol Multiphysics is used to develop tower-nacelle system. The tower-nacelle model was built as a cantilever beam with an additional mass and mass moments of inertia at its top. The beam is Euler beam with three modes.

Enevoldsen and Mørk [63] construct a tower model with Euler-Bernoulli beam formulation. The longitudinal and lateral axes are decoupled and torsion motion is neglected. In addition, they model the nacelle as a point mass. The blades are also formulated by Euler-Bernoulli beam formulation.

Iijima [45] develop a simulation tool for floating offshore wind turbines which cou-

ples hydrodynamic analysis and aerodynamic analysis codes. Most of the researches in the literature considers floater as a rigid body. In their study, floater is flexible and the difference between flexible foundation and rigid foundation is clarified. The floater can be modeled by using beam elements via DYNABEAM.

Fitzgerald and Basu [64] investigate the effect of structure soil interaction in the wind turbine structural control. Both flapwise and edgewise blade vibrations are considered by using an Euler-Lagrangian model which is based on energy formulation. The wind load that the wind turbine is subjected is simulated by using Blade Element Momentum (BEM) theory with a turbulence of rotationally sampled spectra. The effect of centrifugal stiffening is also considered. The developed model is benchmarked against FAST. In addition, the foundation is modeled and analyzed as 3-D in geotechnical Plaxis FEM code. The rotations in bi-axial way which are obtained from dynamic FEM analysis are used to calculate rotational spring constants that describe the structure soil interaction. It is worth pointing out that structural damping coefficients are modeled as stiffness proportional. It is concluded that uncertainties due to the soil stiffness can make the passive vibration control schemes ineffective. To avoid this ineffectiveness, they propose an active vibration control scheme.

Thauvin et al. [65] experimentally study the breaking and steep sea waves which produce high loads for offshore wind turbines. In the experiment, 1:48 scaled SDOF model which is composed of a stiff cylinder is exposed to extreme wave conditions in a wave flume. The structure is hit by many steep and breaking waves and time record is obtained. The main frequency of wave load usually excite the first mode of the structure. Firstly decay test is performed and found that the system has a damping ratio of 2.4%. The turbine is in idling condition, thus no aerodynamic modeling is implemented. The response of the experiment is compared with the mathematical simulations which is obtained using Faltinsen-Newman-Vinje (FNV) model.

2.5.2 FAST Approaches

In the literature, besides various mathematical modeling approaches, there are several studies in which the system is modeled by using NREL's code FAST. Matha et al. [66] consider a 10 MW DTU Reference Wind Turbine in FAST. The structural model is

based on multi-body formulation with linearized response shape representation. This is achieved by ElastoDyn with sixth-order polynomials to a subset of the modes of the blades and tower. For the tower, the first two fore-aft and side-side modes are considered. The first edgewise and the first two flapwise modes are considered for the blades. The drivetrain is modeled as one elastic degree of freedom between the hub and the generator.

Prowell et al. [47] construct an experimentally validated wind turbine system both in FAST and OpenSees [67]. Results from the two models show the capability of FAST to simulate earthquake excitations.

Roderick [68] uses FAST in order to model an offshore 5 MW NREL wind turbine. A tuned liquid damper is implemented to reduce vibrations as well as fatigue loads.

2.5.3 Vibration Control Approaches in Wind Turbines

Recently, a significant interest has arised for research and development in wind turbine technology to overcome vibration related problems. These endeavors come up with active, semi-active and passive vibration control devices [69]. The active vibration control systems consist of actuators, sensors and data processors. The actuators provide forces to reduce the vibrations in accordance with measured and processed vibration data in real-time. The passive vibration control does not need any external force and sophisticated feedback systems [70]. It includes damping layer treatments in which a viscoelastic material is attached to the system to convert mechanical energy into strain energy. Another conventional vibration control technique is consisted of mass, spring and damper to transmit and absorb vibration energy or loading. Semi-active control method is the mixture of passive and active control in which controllable forces are provided by external mechanisms.

In the literature, several passive control methods have been investigated for wind turbines. One of the most popular vibration control device is Tuned Mass Damper (TMD) which was presented by Den Hartog [71]. It has a mass and damper which make it an external system with a specific natural frequency. Thus, it provides an additional damping at its natural frequency to the main structure to which it is con-

nected. Figure 2.14 shows a typical frequency response function (FRF) of a structure with and without TMD. TMDs can be used as passive, semi-active and active device. They are mainly used in civil engineering structures and also used in wind turbine systems to provide more efficient power generation by mitigation of vibration. An example of a TMD connected to the wind turbine nacelle is shown in Figure 2.15.

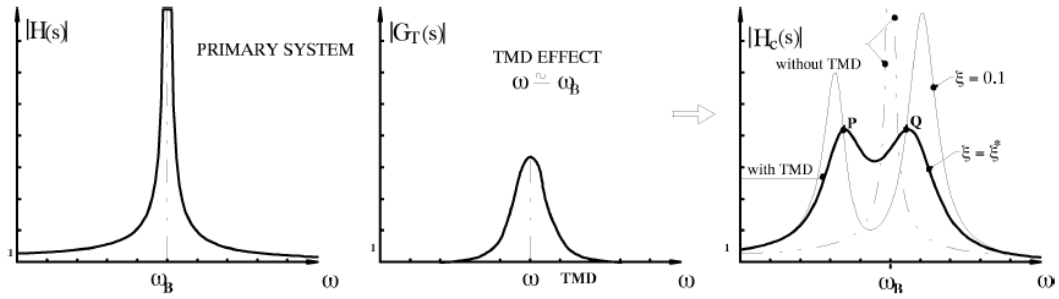

Figure 2.14: TMD effect on a system

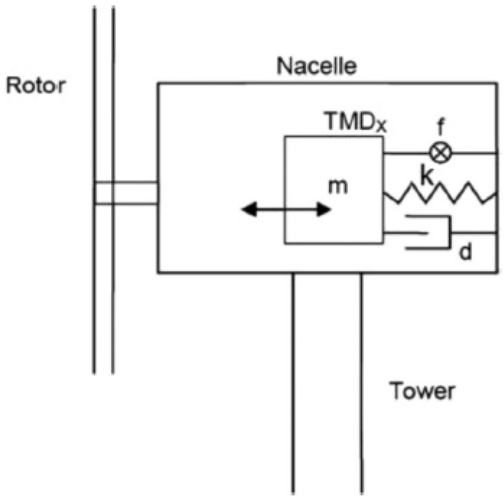

Figure 2.15: Construction of TMD in wind turbine[13]

Recently, use of TMD in wind turbine systems have been investigated in several studies. Stewart and Lackner [56] deal with the effect of wind and wave misalignment which causes excessive vibrations in lateral direction since side-side modes are less likely to be damped by aerodynamic forces. The impact of wind-wave misalignment is observed on a 5 MW NREL offshore wind turbine monopile in terms of damage equivalent loads, then the effect of varying mass and orientation of TMDs are investigated. A normal turbulence model defined in IEC 61400-1 is considered with all

three turbulence categories A, B and C. Optimized tuned mass dampers are able to achieve reductions in tower fore-aft and side-side damage equivalent loads by approximately 5% and 40%, respectively. Stewart and Lackner [72] also make optimization for offshore wind turbines with a parametric approach. The determined parameters are applied to a series of wind turbine by using FAST. Results present that up to 20% fatigue damage reductions can be provided.

Lackner and Rodeo [46] investigate the effect of TMD inside the nacelle. TMD moves in the fore-aft direction. FAST-SC, the new modified version of FAST for structural control is used. Up to 8% reduction is provided at the tower base damage equivalent moment under turbulence with mean a wind speed of 18 m/s and waves with 3.7m significant wave height.

Murtagh et al. [43] investigate the use of TMDs for mitigation of tower fore-aft vibrations. The free vibration analysis is firstly done by separating blades and the tower. The nacelle has a single element at the top of the tower. The centrifugal stiffening is taken into account for the blades. The motions of the tower and nacelle are coupled with the blades. Maximum tower tip displacement can be reduced approximately 20% with the damper attached at the nacelle.

Shzu et al. [73] study a model of the tower by using beam, shell and mass elements distributed along the tower. The modal characteristics of the model is obtained by modal analysis, followed by transient and harmonic analysis to determine the response in time and frequency domain. A pendulum TMD is modeled with ANSYS. The wind turbine model is a beam with a tip mass attachment which reflects the nacelle and blades. The tower is modeled by Timoshenko beam theory with BEAM188 elements and there is a MASS21 on the top representing the nacelle. The TMD is represented by COMBIN14 at the top of the structure. With this model, it is assumed that the contribution of the wind rotor is the centrifugal forces due to rotor rotation.

In almost all studies, the vibration control device is installed at the tower top with the aim of mitigating the vibrations coming from the fundamental bending mode. However, there may be other loading cases such as earthquakes that excite the higher structural modes as well especially for offshore wind turbines since they are more prone to seismic excitations. In such cases, it may be necessary to use multiple tuned

mass dampers. Zuo et al. [36] investigate the effect of multiple TMDs for wind turbines to control vibrations under combined wave, wind load and earthquake excitations. Structure soil interaction is neglected to provide simplicity. For the monopile in the water, the water-monopile interaction is modeled by the added mass method [74]. The detailed finite element model of wind turbine is modeled with shell elements (S4) in ABAQUS. The study aims to investigate the effectiveness of multiple TMDs on reducing tower vibrations and the system is assumed to be at parked condition. Thus, geometry of the rotor and the centrifugal stiffness effect that increase modal frequencies of the blades is neglected. Only lumped mass element is located at the top of the tower to represent nacelle and three blades. The TMDs are modeled by mass spring and damper elements in ABAQUS. The damping of the tower is considered by Rayleigh damping and 2% is assumed. It is concluded that the use of multiple TMDs is effective in reducing peak displacements when both wind, wave and earthquake excitations are considered.

In some studies, semi-active and active tuned mass dampers are developed. Arrigan et al. [75] observe the effect of semi-active tuned mass dampers on vibration reduction. A semi-active control scheme is presented to take into account the change in the natural frequencies of the blades by centrifugal stiffening. The blades are modeled by Euler-Bernoulli beam formulation and they are connected to the nacelle which is point mass. Blade and tower coupling is considered. A semi-active tuned mass damper is connected to the each blade tip and to the nacelle. The natural frequency of the semi-active damper is matched with the dominant frequency of displacements by applying short time Fourier transform to a moving window of 40 seconds. A noticeable amount of vibration reduction is achieved in flapwise direction.

Fitzgerald et al. [76] investigate active TMDs for mitigation of edgewise vibrations of the blades. NREL 5 MW offshore wind turbine is used for the simulation and TMDs are located at a location 75% along the blade length. Under 0.30 turbulence intensity and 12 m/s mean wind speed, the actively controlled TMDs provide 53% reduction in peak-to-peak in-plane blade displacements compared with the uncontrolled blade and 42% reduction when compared with the passively controlled blade. The active TMDs can also reduce the peak displacement by 24% compared to the uncontrolled blade. In the another study of Fitzgerald and Basu [14], the effect of a cable connected

active tuned mass dampers for edgewise blade vibrations is observed. Compared to traditional actively controlled damper, cable connected damper is placed at a certain distance from the blade tip as well but connected to the tip with a cable, thus tensile force is applied. When the active TMD moves, the cable makes an inclined angle with respect to the radial axis of the blade, thus in-plane vibrations are mitigated. A schematic of a cable connected damper is represented in Figure 2.16. Interactions between in-plane and out-of-plane vibrations, blades, tower and tuned mass dampers are also included. Results show that cable connected TMDs are able to mitigate in-plane vibrations up to 41% under 12 m/s wind conditions. This control approach also provides 67% reduction for in-plane vibrations under highly turbulent cases with a mean speed of 18 m/s.

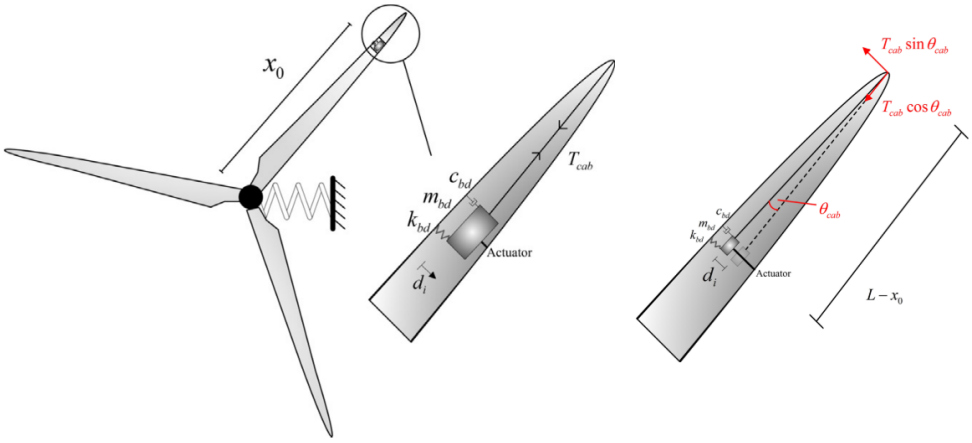

Figure 2.16: Cable connected ATMD inside the blade and cable arrangement[14]

Another commonly used passive control device is tuned liquid column damper (TLCD), generally a U-Shaped tube which is filled with liquid which stands for mass of the damper. When the main structure oscillates, the liquid of TLCD sloshes inside the tube and provides counter force to re-establish the system to equilibrium. An example of a TLCD is shown in Figure 2.17.

There are several papers investigating the efficiency of TLCD in mitigating wind turbine vibrations. Zhang et al. [77] observe the performances of TLCD for mitigating lateral tower vibrations in a multi-megawatt wind turbine model by using real-time hybrid testing. In the experiment, TLCD is tested as a full-scale and physical substructure while the wind turbine is mathematically modeled using a 13-DOF aeroe-

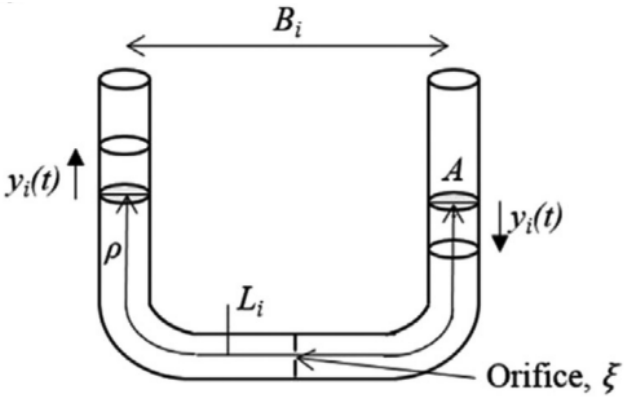

Figure 2.17: Tuned liquid column damper[13]

lastic model. 3 MW and 2 MW wind turbines are established in Matlab and different water levels are provided for frequency tuning of TLCD. It is concluded that the overall control effect of the TLCD is slightly worse for the 3 MW wind turbine due to the less amount of water and thus the mass ratio of the damper. For both wind turbines, the best performance is obtained when the tuning ratio is 1.0 and damping screens, which are used to increase sloshing motion and consequently damping, are equipped.

Colwell and Basu [78] study the use of TLCDs for offshore wind turbines. The wind turbine is modeled as a MDOF system. The blades are modeled as a lumped mass at the nacelle. The fatigue life of the structure is estimated by using rain-flow calculation method.

Another commonly used passive control device is ball vibration absorber, which has heavy ball in a curvilinear path sliding on it to establish equilibrium state when the main structure vibrates.

Zhang et al. [79] investigate the effectiveness of roller dampers for in-plane blade vibrations which are lightly damped when the blades rotate. The optimization of the damper parameters are performed on a 2-DOF wind turbine blade model with a roller damper. The edgewise vibrations on the blade are calculated from 13-DOF aeroelastic model with couplings, turbulence and the aerodynamic damping. In addition, it is used to verify the 2-DOF optimization model. The properties of NREL 5 MW wind turbine is used. The effectiveness criteria is edgewise tip displacement. It is revealed that as mass ratio increases and the damper is closer to the blade tip, higher vibration

mitigation can be achieved. It is also shown that optimized damper is effective in both 13-DOF and 2-DOF models.

Gentils et al. [80] deal with the optimization of offshore wind turbines' supporting structures in order to reduce the high cost. By using coupled parametric finite element model of NREL 5 MW offshore wind turbine monopile and genetic algorithm, mass of the wind turbine is tried to be minimized. The outer diameters and section thicknesses are chosen as design variables for optimization process. Since assumption of rigid soil may cause high deviations in the dynamic characteristics, in this study, SSI is considered by using brick elements (SOLID185) in the finite element model. A bias factor of 15 is used for the mesh on the contact surfaces between monopile and soil. Since NREL 5 MW offshore wind turbine is designed to operate with Class I turbulence, the load case is applied as input with respect to the classifications specified in IEC 61400-1. A Pierson-Moskowitz wave spectrum is used in this study. Results show 19.8% mitigation is achieved in the global mass of the support structure corresponding to 182.7 tonnes.

Bottasso et al. [81] study a different concept by implementing a flap moving passively opposed to the blade motion in order to mitigate blade vibrations. An aeroservoelastic multibody model of the 10 MW wind turbine is considered. In the study, flaps are implemented at 75% of the span for each blade. 3D aeroservoelastic model created in C_p lambda code and a 2D typical section model are loosely coupled. While 2D model transfers the aero loads to the 3D model, 3D model is used for generating realistic flow conditions at the blade. The effect of normal turbulence and extreme operating gust are investigated while defining the wind loading. Fatigue load reduction is very noticeable after flaps are added to blades.

2.5.4 Fatigue Life Consideration in Wind Turbines

Wind turbines encounter many different sources of loads during their lifetime. They are mainly stochastic in nature such as wind, wave, earthquake; as well as transient loads such as gusts, lighting strike; and cyclic loads due to the rotation of the blade. The loads are important in two primary areas: fatigue and ultimate strength. According to IEC 61400-1, the design lifetime for wind turbines shall be at least 20 years

and both failure issues shall be considered during design process.

It has been very recently realized that fatigue should be an important concern for wind turbines and thus the design of their components is dictated not only by ultimate strength, but also fatigue considerations. There are some adversities in fatigue analyses of wind turbines. Firstly, it is not practical to estimate the wind speed distribution of a wind farm since wind is highly stochastic and non-stationary in nature. Thus, for a wind farm under different environmental conditions, the load estimation procedure is the same and taken from the standards which makes the design conservative and contains high uncertainties. Secondly, the blades are made of composite materials thus fatigue lifetime estimation necessitates very sophisticated and experimental methods. In addition, their structural and geometric properties vary along the length, making necessary to use detailed finite element model to obtain confidential stress values. Thirdly, for the tower that experiences the highest stresses at the base, modeling of structure soil interaction plays a crucial importance.

In the literature, the studies rather focus on time domain responses and mitigation in responses if control approach is applied, or statistical aspects of these measured responses such as root mean square and maxima. These measurements can be loads such as shear force and bending moment, or accelerations and displacements. Usually, critical regions of wind turbine are determined to monitor the measurements. For the tower, since the highest stresses are experienced at the base, the forces and moments at the base are monitored. The displacement and acceleration at the tower top are also considered [44]. Considering the blades, in general root of the blades exhibit the highest shear force and bending moment. In addition, the transition region between root zone and aerodynamic zone of the blade carries special importance in terms of fatigue due to the sharp cross section change [82, 83].

In this thesis, the concept of Damage Equivalent Load (DEL) is used which is developed by NREL and detailed in [84]. DEL is a constant load range causing the same damage with N cycle as the original stochastic load series. In other words, it is a projected equivalent load of the whole simulated loads that the wind turbine encounters. If N is specified as 1, DEL will represent the equivalent load of 1 cycle.

While estimating the DELs of the wind turbine, it is assumed that the fatigue damage

is accumulated linearly with contribution of each load cycles. This assumption is called Miner's rule and is mainly utilized for the evaluation of fatigue loads of the wind turbine for time domain simulations [19].

With this aspect, the fatigue tool used in this thesis is MLife [85], theory is further explained in Chapter 3.1.6.

2.5.5 Viscoelastic Link Treatment

Viscoelastic materials are polymers in which strain energy can be stored. The damping mechanism arises from the polymer chain after they are deformed. Mathematically, they can be represented by a complex stiffness which means the stress lags the associated strain and composed of storage and loss modulus corresponding to elastic and dissipative characteristics, as in Equation 2.9 [86, 87].

$$E(f) = E(f) + iE(f)^* = E(f)(1 + i\eta(f)) \tag{2.9}$$

Equation 2.9 is also applicable for shear modulus, G. The properties of viscoelastic materials are frequency and temperature dependent. Therefore, for each temperature, a different frequency dependent complex modulus function can be defined.

In the literature, there is a deficiency in using viscoelastic materials for wind turbine vibration control. In fact, viscoelastic damping treatment is widely utilized in structures and machines. Johnson and Kienholzt [88] developed an efficient technique for modeling laminate with a viscoelastic layer in the middle by finite element approach. Barone et al. [89] studied the effectiveness of elastomeric rubber bearings connected to the base structure with a viscoelastic link. Adams [90] modeled the viscoelastic layer by using a set of Kelvin equivalent springs and dashpots which connect the nodes of two adjacent layers composed of shell elements. The nodes of the shell elements are offset to the edges of the viscoelastic layer.

Viscoelastic link is a type of viscoelastic damping treatment through which two parts of a structure can be connected with a viscoelastic material to dissipate mechanical energy by converting it to strain energy using the relative motion between connected parts.

CHAPTER 3

THE AEROSERVOELASTIC WIND TURBINE MODELING TOOL: FAST

For the development of wind energy technology, reliable and accurate computational tools are essential. Throughout this thesis, the software used to create aeroservoelastic wind turbine model is called FAST, which means Fatigue, Aerodynamics, Structures and Turbulence [16]. It is used for simulating horizontal axis wind turbines and developed by United States' National Renewable Energy Laboratory (NREL). It is able to model onshore and offshore wind turbines. It is open source and written in Fortran v90 and certified by Germanischer Lloyd WindEnergie for the calculation of wind turbine loads for design and certification [91]. FAST combines modal and multibody dynamics approaches. It employs fully coupled simulations consisting of structural dynamics, aerodynamics, hydrodynamics and control system dynamics. The simulations are employed in time domain. For each of these simulations, different callable submodules of FAST are employed and assembled in the main FAST code. The input and source files of submodules are created separately.

FAST is used in modeling for 2 and 3 bladed horizontal axis wind turbines; and for onshore or offshore wind turbines. While it models the blades and tower with modal approach, the base platform, generator, nacelle, hub, gearbox and tail are modeled with multi-body systems of equations. Kane's method is used for the derivation of equations of motion. In FAST, the tower and the blade mode shapes are specified as input in the form of 6th order polynomial as FAST utilizes assumed modes approach.

Figure 3.1 schematically illustrates the global coordinate axes, which are valid for FAST as well as most of the software used in wind turbine technology [8]. The main wind component blows through positive X direction. In the literature, while pitch and surge motion of the wind turbine system is also called as fore-aft motion, roll and

sway motion is referred as side-side motion. The torsion movement of the tower is called yaw motion.

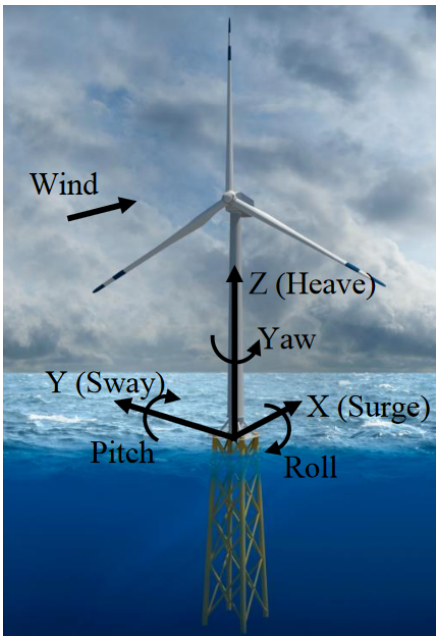

Figure 3.1: Global coordinate axes of FAST [15]

FAST requires 24 DOFs to utilize wind turbine dynamics. These are illustrated in Figure 3.2.

- 6 DOF: 3 translational, 3 rotational platform relative to inertia frame (surge, sway, heave, roll, pitch, yaw)
- 4 DOF: Tower motion: 2 longitudinal modes (fore-aft), 2 lateral modes (side-side)
- 1 DOF: Yawing motion of the nacelle
- 1 DOF: Generator azimuth angle
- 1 DOF: Compliance in the drivetrain between the generator and hub/rotor
- 3 DOF: Flapwise tip motion for the first mode
- 3 DOF: Tip displacement for each blade for the second mode.
- 3 DOF: Edgewise tip displacement for the first mode

- 2 DOF: Rotor and tail furl

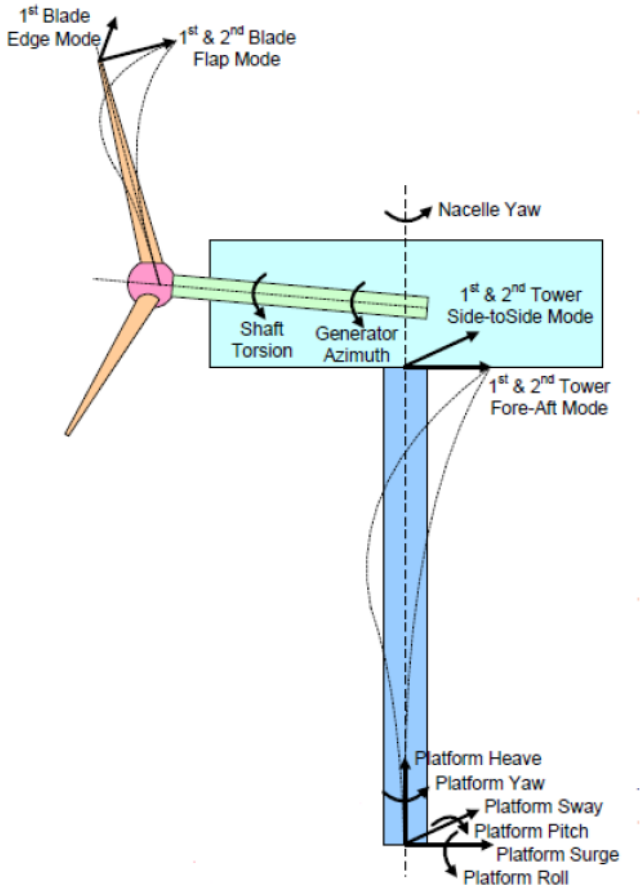

Figure 3.2: DOFs of a wind turbine in FAST model [16]

Tower-ground and blade-hub connection are rigid. The tower, blades and drive shaft are flexible.

3.1 FAST Scheme

FAST contains an archive of different submodules required for performing full capable analyses for wind turbines. The main modules in FAST are ElastoDyn for tower and blade elastic modeling and structural dynamics, SubDyn for modeling structural dynamics of multi-member fixed-bottom substructures, ServoDyn for the power generation and the control system, InflowWind for wind conditions, HydroDyn for wave loads and AeroDyn for aerodynamic loads. In addition, there are also external modules used to support the inputs of submodules. For instance, Turbsim is a stochastic

turbulence generator which feeds InflowWind. The input-output relation between submodules and their purposes are represented in Figure 3.3.

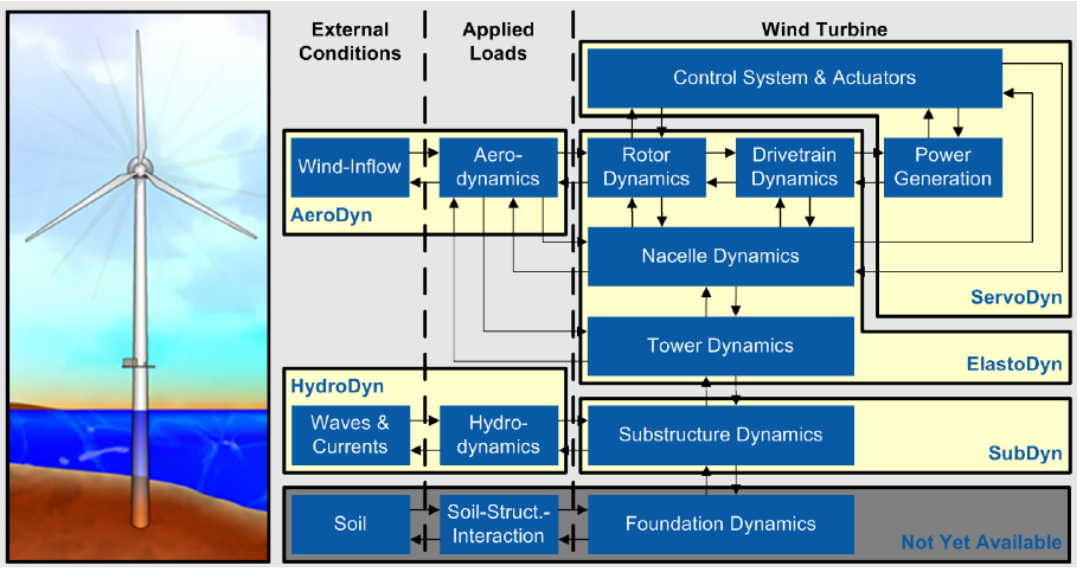

Figure 3.3: Main FAST scheme [17]

Implicit or explicit time integration is achieved with a predictor-corrector approach between each submodule. The main input file of FAST can be found in Appendix A.1.

3.1.1 Structural Dynamics Module: ElastoDyn

ElastoDyn is the fundamental part of FAST, a structural dynamics module used to model the tower, platform, rotor, drivetrain and nacelle. It enables to model horizontal axis, two or three bladed, upwind or downwind, land or offshore based wind turbines. It allows user to chose many parameters, such as which degrees of freedom is enabled or disabled, initial conditions and configuration of the wind turbine. The tower and blade structural properties in sectionwise manner should be included in ElastoDyn input files. As ElastoDyn depends on assumed modes approach, the first and the second fore-aft and side-side mode shapes of the tower, as well as the first and second blade flapwise and the first blade edgewise mode shapes are defined as coefficients of a 6th order polynomial. The mode shapes can be calculated outside of FAST and BModes can be used [92].

Considering the definition of modal damping ratio, the equations of motion for the physical coordinates *x* of the wind turbine in ElastoDyn module can be represented as,

$$[M]\{\ddot{x}\} + [C]\{\dot{x}\} + [K]\{x\} = \{F\} \tag{3.1}$$

where *M* is the mass matrix, *C* is the damping matrix, *K* is the stiffness matrix and *F* represents the external forces. Assuming that the damping is proportional to the mass and stiffness matrices, *C* can be decomposed as,

$$[C] = \alpha[M] + \beta[K] \tag{3.2}$$

where α and β are real positive constants. The equation of motion can be decoupled in terms of generalized coordinates x_r,

$$\{\ddot{x}_r\} + [2\zeta_r\omega_r]\{\dot{x}_r\} + \left[\omega_r^2\right]\{x_r\} = \{F_r\} \quad \text{for } r = 1, 2, \ldots n \tag{3.3}$$

Equation 3.3 consists of *n* uncoupled equations. ω_r and ζ_r are the modal frequency and modal damping ratio for mode *r*. ζ_r can also be expressed as [93],

$$\zeta_r = \frac{\alpha}{2\omega_r} + \frac{\beta\omega_r}{2} \tag{3.4}$$

In modal approach, the total harmonic response of a MDOF system is composed of the summation of each mode's contribution as shown in Equation 3.5,

$$\{x\} = \sum_{r=1}^{n} \frac{\{\phi_r\}\{\phi_r\}^T}{(\omega_r^2 - \omega^2 + i2\zeta_r\omega_r\omega)}\{F\}e^{i\omega t} \tag{3.5}$$

where ϕ_r is the modal matrix containing eigenvector of mode *r*.

ElastoDyn enables to set the modal damping ratio ζ_r for each tower and blade modes. It utilizes stiffness-proportional damping, which means $\alpha = 0$ in Equation 3.2 and 3.4. In this thesis, the effect of modal damping ratio for the critical modes are investigated. For the selected modes of the tower and blades, the modal damping ratios are iterated for 1.0%, 5.0%, 10%, 20% and 30%.

In ElastoDyn, the nonlinear equations of motion are governed by using Kane's dynamics [94] which is not an energy based method. Time integration is done using

one of the several options; 4th order Runge-Kutta (RK4) explicit, 4th order Adams-Bashforth (AB4) multi-step explicit and 4th order Adams-Bashforth-Moulton multi-step predictor-corrector are applicable.

ElastoDyn models the tower and the blades according to Euler-Bernoulli beam approach in which axial and torsional degree of freedoms are neglected and no shear deformation occurs. In addition, bending assumes small strains and small angel approximations are done with nonlinear corrections for coordinate system orthogonality. An example of ElastoDyn file is in Appendix A.2.

3.1.2 Turbulence Modules: InflowWind and Turbsim

Turbsim [95] is a turbulence code which develops statistical model to numerically simulate stochastic 3D turbulence in time series at a two dimensional rectangular grid.

It requires specifications for spectral models such as Kaimal and von Karman spectrum, turbulence intensity, mean wind speed and wind profile parameters. In addition, the user selects a seed number to create random phases for the wind velocity time series. Turbulence intensity can be specified by IE61400-1 standard categories A, B, C, or by percentage. InflowWind submodule of FAST processes time series wind data generated by Turbsim. Examples of InflowWind and Turbsim input files are in Appendix A.3 and A.4 respectively.

3.1.3 Unsteady Aerodynamics Module: AeroDyn

AeroDyn [96] is the unsteady aerodynamics module of FAST. It obtains undisturbed wind data from InflowWind and calculate aerodynamic forces, which are drag, lift and pitching moments on both the blades and tower in time domain. It can be used either coupled with FAST or standalone code by neglecting aero-structural coupling effects. The aerodynamic calculations are based on approximating the three dimensional flow around the wind turbine as two-dimensional flow at discretized elements of the blade and tower. The calculated two-dimensional lift, drag and pitching mo-

ments are lumped at the nodes of the elements.

For calculating the influence of the wake on the turbine, AeroDyn employs a quasi-steady Blade Element Momentum (BEM) theory which is combination of blade element theory and the momentum theory and requires an iterative nonlinear solver [97]. AeroDyn considers the dynamic stall based on Beddoes-Leishman formulation, hub and tip losses, and the axial and tangential induction. An example of an AeroDyn input file is in Appendix A.5.

3.1.4 Control System Module: ServoDyn

ServoDyn is one of the main submodules of the FAST used to model electrical drive and control system for blade pitch, nacelle yaw, generator torque, blade-tip brakes and high-speed shaft brake. The pitch control system of the NREL 5 MW reference wind turbine is embedded in ServoDyn as dynamic link library (DLL). Yaw and pitch control of the wind turbine increase the efficiency in generating power. Above cut-out wind speed, the blades are feathered by pitch control system and wind turbine is parked. The nacelle yaw control steers the rotor plane angle so that it is perpendicular to the mean wind direction. A typical ServoDyn input file is given in Appendix A.6.

3.1.5 Hydrodynamics Module: HydroDyn

HydroDyn [98] is a hydrodynamics submodule of FAST to provide aero-hydro-servo-elastic simulation of offshore wind turbines. It can be used for both fixed-bottom and floating offshore platforms to calculate hydrodynamic loads, including linear hydrostatic restoring contributions obtained from buoyancy and waterplane area, viscous drag calculated using Morison's equation, added mass and damping contributions from linear wave radiation, free surface memory effect and the incident wave excitation from diffraction. In HydroDyn, the waves can be generated as regular (periodic), irregular (stochastic with JONSWAP and white noise spectrum), long-crested (unidirectional) or short-crested (range of different directions) models [99].

3.1.6 Fatigue Tool: MLife

MLife [85] is a Matlab code used for post-processing the time-series data obtained from wind turbine simulations. The statistics and fatigue load estimations are performed for the simulation results. The statistical outputs include minimum and maximum value, mean, standard deviation, skewness, kurtosis and maximum range. The fatigue calculations comprise short-term DELs and damage rates based on single time-series; lifetime DELs based on set of time-series, the total damage and the time until failure for the component.

MLife performs Rainflow Cycle Counting, algorithm of which is firstly presented by Downing and Socie [100], for converting time series into cycle count matrices. It is achieved by breaking whole time series into the individual similar set of half-cycles. The half-cycles are obtained with the rotation of whole time series by 90 degrees as illustrated in Figure 3.4 [8].

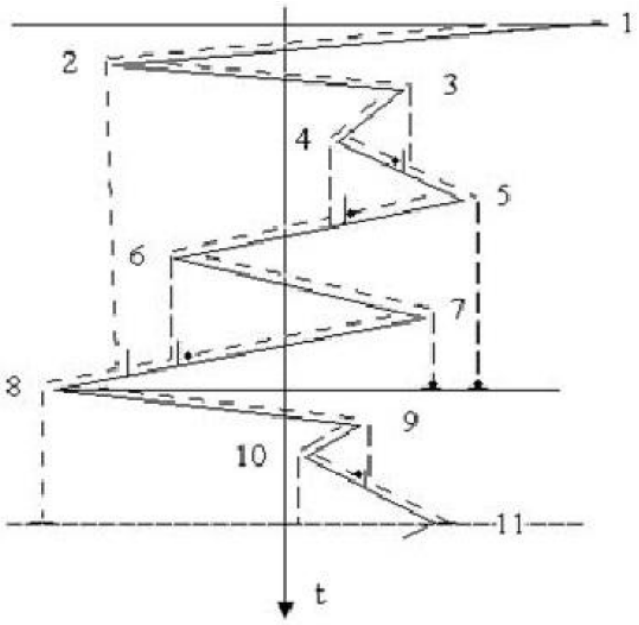

Figure 3.4: Rainflow counting [18]

In rainflow counting, a half cycle is counted when a rainflow dropping down encounters with a higher or lower peak value. These identified half-cycles construct a matrix according to their load mean and range. In Figure 3.5, a typical matrix of a rainflow counted time series data is shown. As suggested in IEC61400-1 Annex G [3], the

damage at a given location accumulates linearly with these half-cycles. In this case, the total damage caused by all counted cycles will be,

$$D = \sum_i \frac{n_i}{N_i\left(L_i^{RF}\right)} \tag{3.6}$$

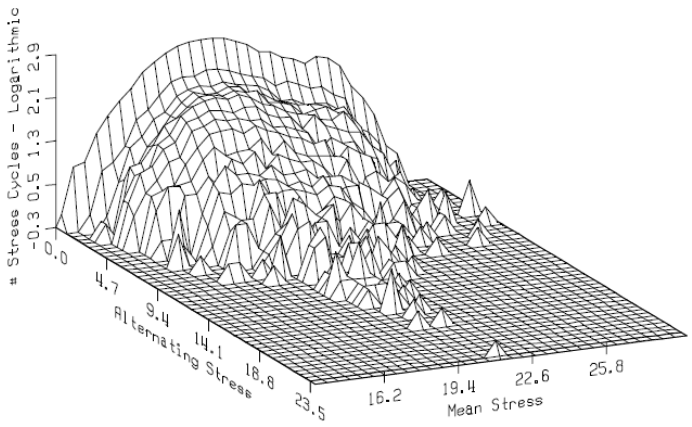

Figure 3.5: Rainflow counted stress data [19]

Where N_i is the number of cycles to failure for a load case i according to the S-N curve, n_i the cycle count, and L_i^{RF} is the cycle's load range and D is the accumulated damage for given time series.

To express the above equation with respect to the S-N curve parameters N_i can be written as,

$$N_i = \left(\frac{L^{ult} - \left|L^{MF}\right|}{\frac{1}{2}L_{\mathrm{i}}^{RF}}\right)^m \tag{3.7}$$

Where L^{ult} is the ultimate load of the component, L^{MF} is the fixed load mean and m is the Wöhler exponent. Wöhler exponent is specific to the material under consideration. It is worth noting that for steel tower, m is taken as 3. For Glass-reinforced composites, m is 10.

The equations assume fatigue load cycles occur over a constant load mean. However, mean of each load cycle will vary in reality. In order to compensate this, it is assumed that the loads have varying range around a fixed mean value and Goodman correction

is made as below,

$$L_i^{RF} = L_i^R \left(\frac{L^{ult} - \left| L^{MF} \right|}{L^{ult} - |L_i^m|} \right) \tag{3.8}$$

Above equation is for a Goodman exponent which is one. L_i^R is the i^{th} cycle's range about a load mean of L_i^m.

In practice, while estimating the lifetime damage of a wind turbine, short time simulation data is extrapolated over the lifetime of the wind turbine. In order to extrapolate short time series over design lifetime, Weibull distribution is used since main wind speed exhibits Weibull probability of occurence. f_j^{Life} is the extrapolation factor for the time series j corresponding to a certain wind speed. It is multiplied with n_{ji} which is the count of load cycles for load block i and time series j. Then, the extrapolated damage count for cycle i and time-series j can be obtained as,

$$n_{ji}^{Life} = f_j^{Life} n_{ji} \tag{3.9}$$

The total accumulated lifetime damage becomes,

$$D^{Life} = \sum_J \sum_{\text{i}} \frac{n_{ji}^{Life}}{N_{ji}} \tag{3.10}$$

Where N_{ji} is the number of cycles to failure for block i in time series j. The condition $D^{Life} \geq 1.0$ means failure. This implies that the ratio of the design lifetime over the accumulated damage gives the time until failure,

$$T^{Fail} = \frac{T^{Life}}{D^{Life}} \tag{3.11}$$

MLife estimates Damage Equivalent Loads (DELs) which are estimation of fatigue loads for wind turbines and first developed by NREL [84]. DEL can be characterized as short-term and lifetime. Short-term DEL represents fatigue load based on a single time series, while lifetime DEL is extrapolated load according to the probability dis-

tribution. DEL is a constant amplitude load with specific frequency which causes the same damage as the time-series,

$$D_j^{ST} = \sum_i \frac{n_{ji}}{N_{ji}} = \frac{n_j^{STeq}}{N_j^{eq}} \tag{3.12}$$

Where D_j^{ST} is the short term damage from time series j. N_j^{STeq} is the total equivalent number of load cycles for time j,

$$n_j^{STeq} = f^{eq} T_j \tag{3.13}$$

Where f^{eq} is the equivalent frequency of DEL for time series j. N_j^{eq} is the equivalent number of cycles until failure for time series j,

$$N_j^{eq} = \left(\frac{L^{ult} - \left| L^{MF} \right|}{\frac{1}{2} DEL_j^{ST}} \right)^m \tag{3.14}$$

Where DEL_j^{ST} is the short-term DEL for series j. From above equation, short-term DEL can be estimated as,

$$DEL_j^{ST} = \left(\frac{\sum_i \left(n_{ji} \left(L_{ji}^{RF} \right)^m \right)}{n_j^{ST,eq}} \right)^{\frac{1}{m}} \tag{3.15}$$

Lifetime DEL can be estimated by considering all times series j. About a fixed load mean, lifetime DEL is calculated as follows,

$$DEL^{Life} = \left(\frac{\sum_i \sum_j \left(n_{ji}^{Life} \left(L_{ji}^{RF} \right)^m \right)}{n^{Life,eq}} \right)^{\frac{1}{m}} \tag{3.16}$$

Where $n^{Life,eq}$ is,

$$n^{Life,eq} = \sum_j f_j^{Life} n_j^{ST,eq} \tag{3.17}$$

In Appendix A.8, example of an MLife file used in this thesis is given. If short-term DELs are considered for a given wind speed; there is no point in specifying shape factors and scale of the Weibull distribution of the wind. In this thesis, the short-term and lifetime DELs are considered for the tower base and blade root as explained in Chapter 2.5.4.

To estimate the DELs, ultimate design load L^{ult} is needed to be specified for each load type. To define ultimate load, finite element model of the component or experimental data specified for the wind turbine is needed. As no finite element model or data are available, the ultimate load factors for the tower base and blade root are given as $7.46 \times 10^8 N.m$. It is usually recommended that L^{ult} should be selected such that any further increase in L^{ult} does not change the resultant DELs. These are fairly rough estimations and not too important since different cases are compared relative to each other. Thus, relative magnitudes carry more importance.

CHAPTER 4

DEFINITION OF NREL 5 MW WIND TURBINE

NREL 5 MW wind turbine model was developed for engineering studies for large onshore and offshore wind turbines and one of the most widely used wind turbine model as it represents the current and future state of the art in an HAWT system. It is a three-bladed upwind wind turbine with a rated wind speed of 11.4 m/s. It means that the wind turbine generates 5 MW power when the mean wind speed reaches to 11.4 m/s. Between rated and cut-out wind speeds, the blades are pitched according to the wind speed to regulate the generator speed and to reduce excessive loads. Above cut-out wind speed, which is 25.0 m/s, the wind turbine is shut down and blades are pitched to 90 degrees to set up parked condition.

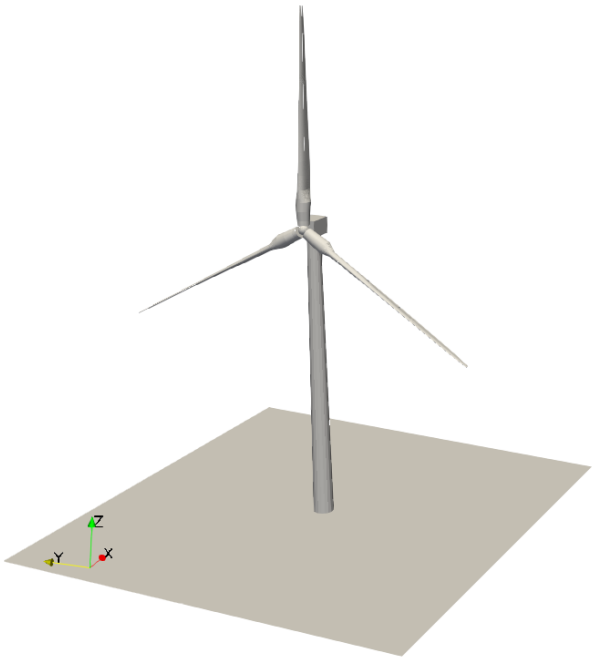

Figure 4.1: NREL 5MW Wind Turbine model

Since it is heavy and long structure, the natural frequencies of the blades and tower are very low and this causes wind turbine subject to high loads due to the fact that the ambient turbulence that excites lower frequency modes. The 3D representative model of the wind turbine is shown in Figure 4.1. The properties of the wind turbine is represented in Table 4.1.

Table 4.1: NREL 5 MW Wind Turbine properties [4]

	Max. rated power	5 MW
Basic Description	Rotor orientation, configuration	Upwind, 3 blades
	Rotor diameter	126 m
	Hub height	90 m
	Cut-in, rated, cut-out wind speed	3 m/s, 11.4 m/s, 25 m/s
	Cut-in, rated rotor speed	6.9 rpm, 12.1 rpm
Blade (LM 61.5 P)	Length	61.5 m
	Overall mass	11740 kg
	Second mass moment of inertia	11746 kgm^2
	1st in-plane mode natural frequency	1.0606 Hz
	1st out-of-plane mode natural frequency	0.6767 Hz
	Structural damping ratio (all modes)	0.48%
Hub + Nacelle	Hub diameter	3 m
	Hub mass	56780 kg
	Nacelle mass	240000 kg
Tower	Height above ground	87.6 m
	Overall mass	347460 kg
	1st fore-aft mode natural frequency	0.324 Hz
	1st side-side mode natural frequency	0.312 Hz
	Structural damping ratio (all modes)	1.0%

For a wind turbine tower, FAST requires sectional mass density per unit length, fore-aft stiffness and side-side stiffness. For blades, structural twist, blade mass density, flapwise and edgewise stiffness are necessarily given as input. For both tower and

blades, mode shapes are required as a 6th degree as FAST uses assumed-mode approach.

Although there is only mathematical model developed by NREL, in the literature, there are several attempts to design the finite element model by using the structural and geometrical properties of the mathematical model [101].

In Figure 4.2, the sectional stiffness for the blade and tower are represented through the length. It is worth noting that the flapwise and edgewise stiffness of the tower are the same and they decrease exponentially since the tower is tapered hollow cylinder with decreasing diameter through the top. Considering the blade stiffness, at the root, it first increases then sharply decreases after transition region where structural and aerodynamic parts intersect. The structural part is cylindrical hollow shaped region from where it is connected to the hub, and the aerodynamic part has airfoil cross section where torque is generated. The design of a transition part of the blade carries crucial importance since the abrupt change in cross section causes higher stress concentration which decreases fatigue life [82, 102].

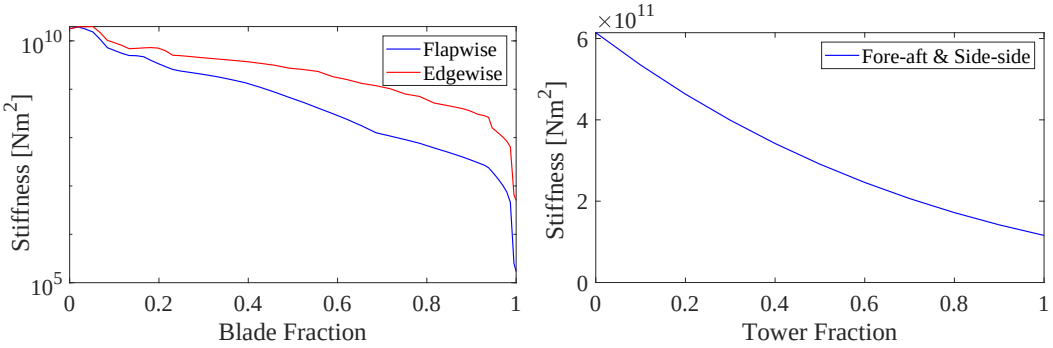

Figure 4.2: Stiffness for the blade and tower (left: blade, right: tower)

Figure 4.3 shows the mass densities per unit length of the blade and tower along the length. While mass of the blade shows a sharp decrease around transition region and then gradual decrease, mass per unit length of the tower decreases exponentially due to the tapered shape.

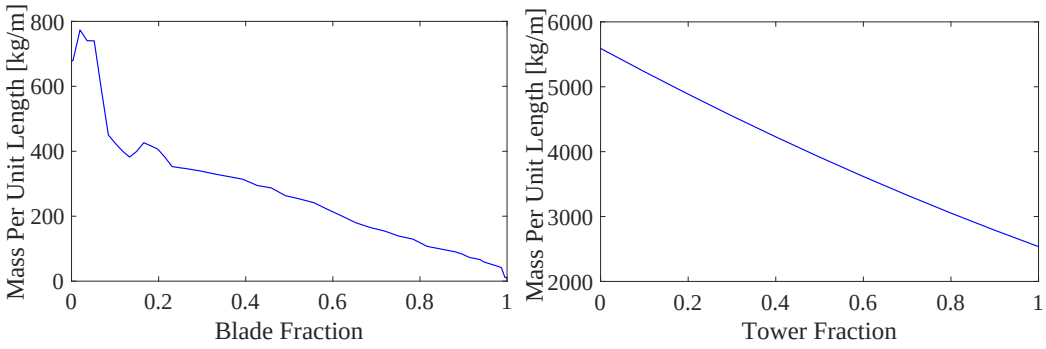

Figure 4.3: Mass density for the blade and tower (left: blade, right: tower)

In Figure 4.4, NREL 5MW wind turbine blade, known as LM 61.5 blade, is designed by using NUMAD [103], which is an efficient tool to create wind turbine blade geometry with specified cross sections and mesh parameters for further finite element processing.

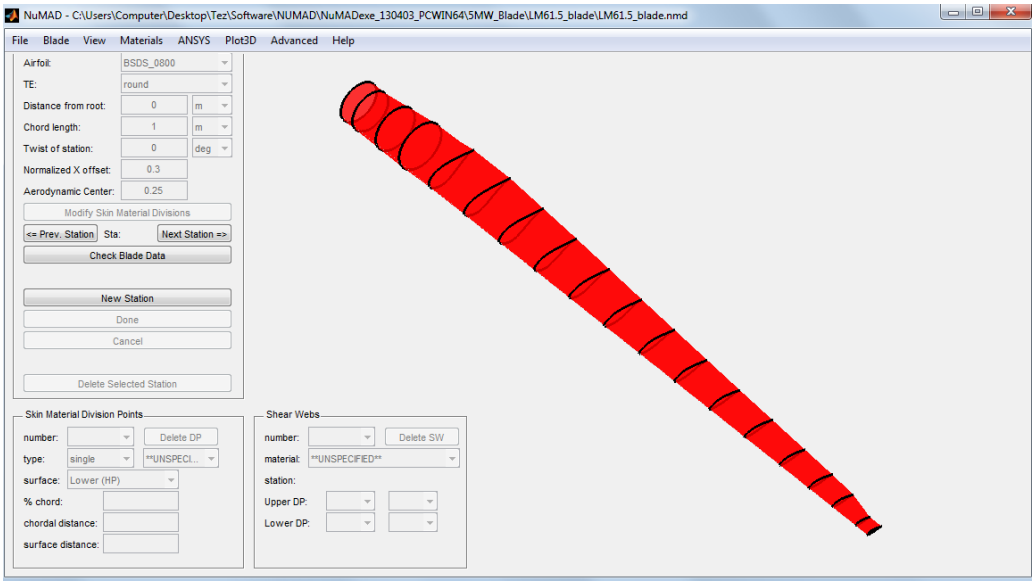

Figure 4.4: LM 61.5 Blade for NREL 5MW Wind Turbine

The mode shapes of the blade and tower are determined by using BModes [92] as FAST requires them as input. Figure 4.5 shows the blade and tower mode shapes in terms of normalized length. They are shown graphically in Figure 4.6 and 4.7.

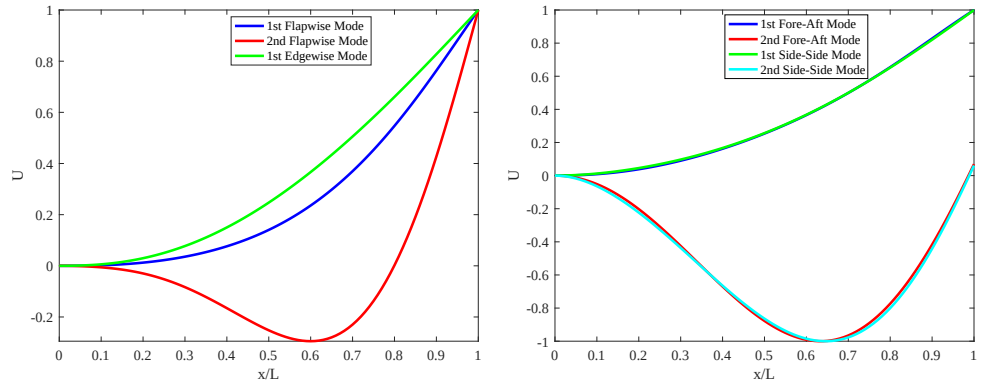

Figure 4.5: Mode shapes (left: blade, right: tower)

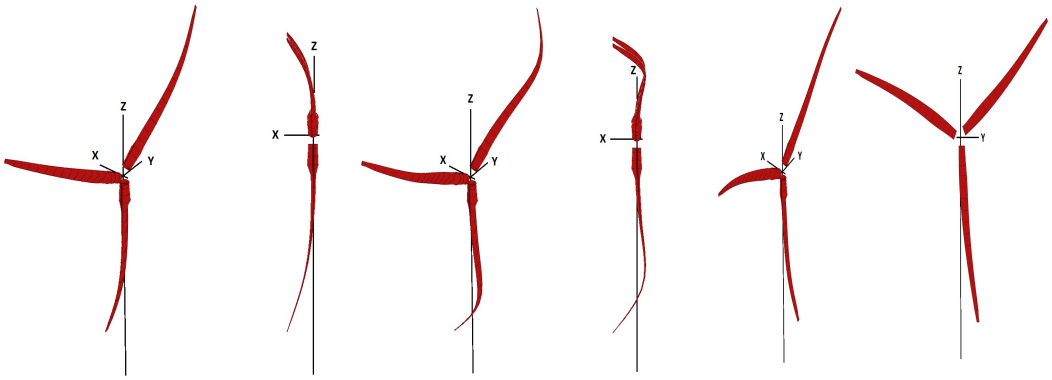

1 2 3

Figure 4.6: Mode shapes of the blade (1: first flapwise, 2: second flapwise, 3: first edgewise)

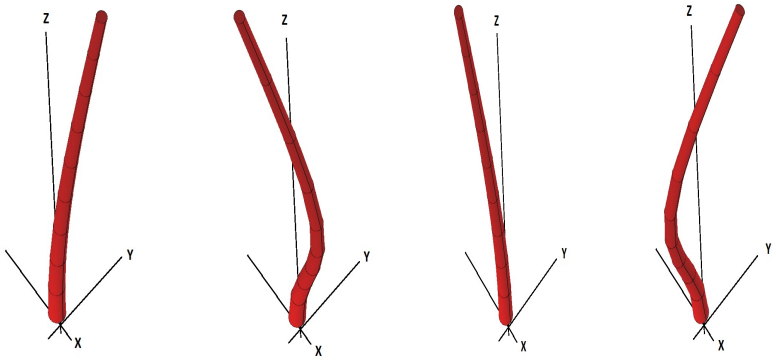

1 2 3 4

Figure 4.7: Mode shapes of the tower (1: first fore-aft, 2: second fore-aft, 3: first side-side, 4: second side-side)

CHAPTER 5

VIBRATION RESPONSE AND FATIGUE LOAD SIMULATIONS

In this thesis, aeroservoelastic simulations are made by FAST to observe the effect of structural damping of both wind turbine tower and blade modes to vibration response and fatigue loads. As an effectivity measurement for fatigue load, damage equivalent load (DEL), the theory of which is explained in detail in Section 3.1.6, is used. Both short-term and lifetime DELs of tower base and blade root are specifically examined. For each configuration, the structural damping of the tower and blade modes and wind speed are iterated. For short-term DELs, 3D surface plots are preferred for clear representation. In some cases, the sectional shear and bending loads are investigated and plotted with respect to the length of the tower or blade. Moreover, for different structural damping ratios, lifetime DEL calculation is performed and tabulated.

In Section 5.1.1, before going into detailed simulations, in order to identify the critical modes, firstly preliminary analysis is made in operating condition and acceleration power spectral densities for the tower and the blades are observed. In Section 5.1.2, sectional load analyses are performed to see where the highest loads are observed along the tower and blades. After that, the effect of pitch control to the wind turbine fatigue life is observed by considering different blade pitch angles in Section 5.2. In addition, in Section 5.3, parking condition in which wind turbine does not generate power and blades are feathered is considered under different mean wind speeds. In Section 5.4, operating condition in which both power generation and control systems are active is studied. In Section 5.5, lifetime DELs are calculated by extrapolating the short-term DELs to the wind turbine lifetime.

5.1 Preliminary Response and Fatigue Load Analyses

5.1.1 Modal Identification of the Wind Turbine

The reference system used throughout the study is illustrated in Figure 5.1. The in-plane and out-of-plane loads of the blade are defined as edgewise and flapwise loads, respectively. For the tower, loads coming through the main wind in X direction is called as fore-aft loads, while the lateral loads are defined as side-side loads.

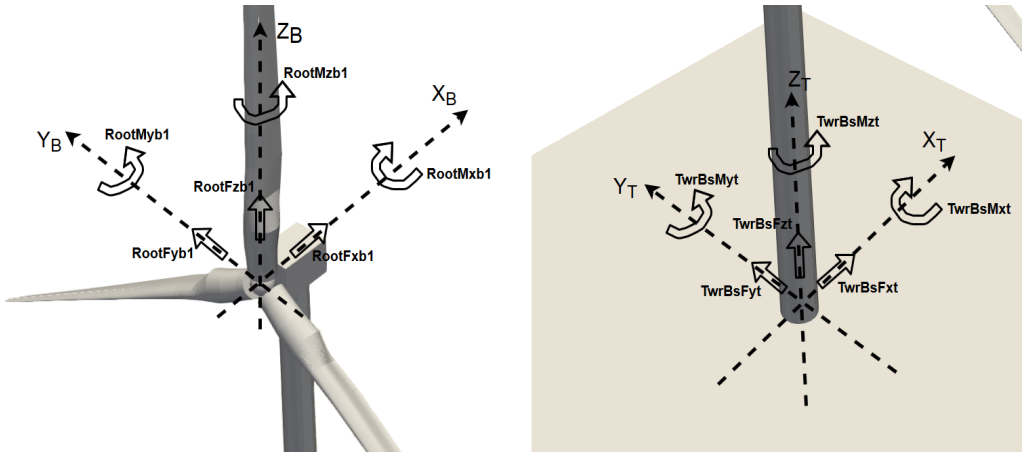

Figure 5.1: Coordinate systems [20]

In order to make a preliminary observation in terms of dynamic response and to identify the excitation levels of the tower and blade modes, the wind turbine model is exposed to normal turbulence model for 600 seconds with mean speed of 8 m/s, 12 m/s and 25 m/s. During each simulation, the pitch and yaw controls are active and the generator is enabled in order to produce energy. Figure 5.2 and 5.3 show the blade tip and tower top acceleration spectra for each wind speed simulation. It is worth noting that the highest acceleration values are seen at the top of the tower and the blade tip as they are cantilever connected. According to the PSDs, at frequencies higher than 6 Hz, no mode is excited significantly and acceleration values are in decreasing trend above 6 Hz. The reason is due to the turbulence characteristics which tends to excite lower frequencies more intensively. Considering the energy distribution, the highest acceleration values are observed in Z direction since Z acceleration also includes centrifugal acceleration value coming from the rotation of the blades. The centrifugal part of the acceleration is more dominant in Z direction and directly related with the

square of the angular rotation of the blade and the radius. However, compared to X and Y acceleration at the blade tip, Z acceleration is more steady and exhibits less fluctuations in time domain.

Considering Figure 5.2, in all directions, the first, second and the third harmonics of the blade can be observed at 0.2, 0.4 and 0.6 Hz, respectively. It is due to the blade angular rotational speed which is around 12 rpm, thus giving 12/60 = 0.2 Hz fundamental peak and its harmonics. The first flapwise mode of the blade is not appeared as a clean spike at 0.68 Hz in X direction in Figure 5.2a. Since it is highly damped and closely spaced peaks are existed in that region, first flapwise mode is not easily understood. However, the first edgewise blade mode is appeared as sharp spike at around 1.07 Hz in Y direction as depicted in Figure 5.2b. The clear appearance is due to the low aerodynamic damping in edgewise direction. At around 1.97 Hz, vibration levels are significantly high which may be due to the drive train modes effecting the blade in X and Y directions. Around 4 Hz, there are also high levels of vibration in Y direction but the mode that contributes to this vibration is vague.

Considering the tower top accelerations in Figure 5.3, above 6 Hz, no mode is excited as expected. Considering X direction, the first tower fore-aft mode is appeared around 0.32 Hz which is the highest spike in Figure 5.3a. The blade first flapwise mode affects the tower top fore-aft response around 0.67 Hz but is buried under turbulence noise. The second tower fore-aft mode which is around 2.90 Hz also contributes to the total response but with a lesser amount compared to the first fore-aft mode. The pitch and yaw motion of the nacelle are observable around 1.97 Hz. For the fore-aft response, the frequencies between 0.25 Hz and 0.75 Hz are very dominant in terms of acceleration responses. The fundamental peak and related harmonics of the blade rotation are not observed in tower response. It is interesting to note that for 8 m/s mean wind speed, the excitation is higher than that for 12 m/s wind speed. In addition, the highest blade-tower coupled responses are observable around 0.60 Hz for 12 m/s as represented in Figure 5.3a. It is due to the aerodynamic and structural coupling which affects the modal frequencies and modal damping ratios of the modes especially in fore-aft direction, which may alter the responses in fore-aft modes. In Figure 5.3b, considering the lateral direction Y, which is also referred as side-side direction, at the first look, it may be stated that the peaks are more clearly distinguishable since the

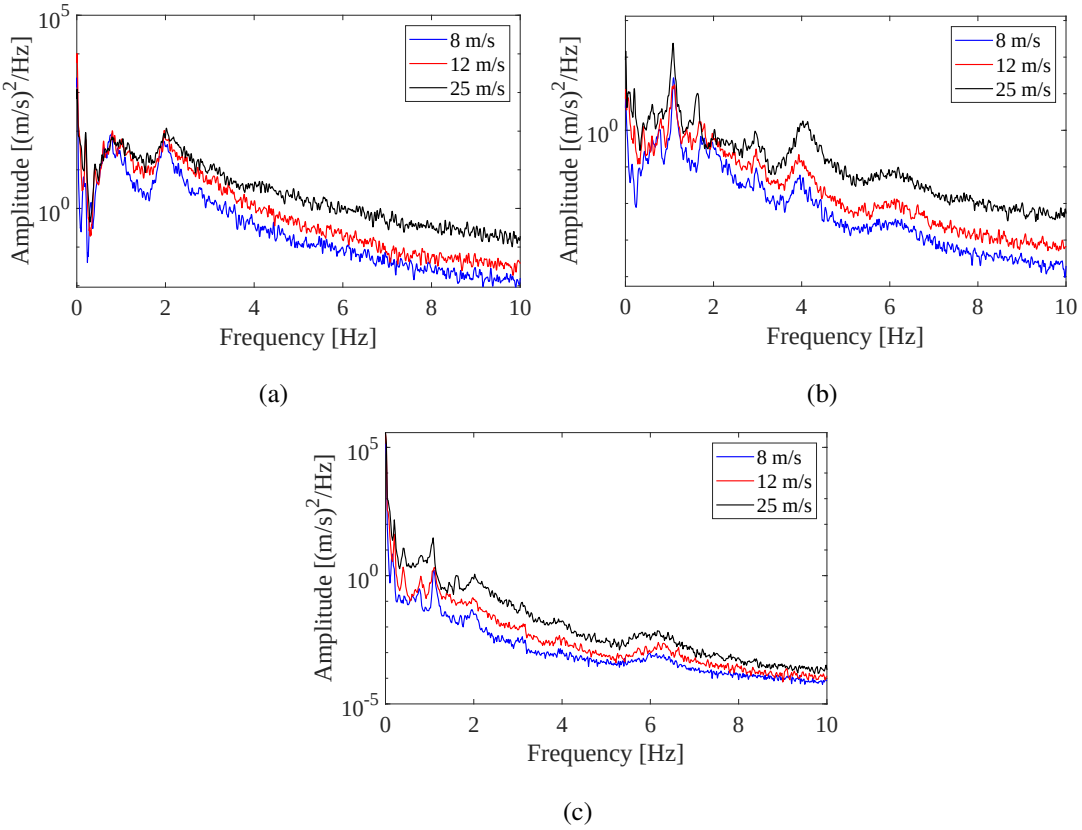

Figure 5.2: Blade tip acceleration PSDs ((a): X, (b): Y, (c): Z)

aerodynamic damping in lateral direction is very low compared to that in longitudinal direction. The first side-side tower mode exhibits the highest responses around 0.31 Hz and the tower-blade coupled mode around 0.60 Hz is the latter as in the case of fore-aft accelerations. In addition, there is a spike around 1.26 Hz which may be another coupled tower-blade mode. At 2.93 Hz, the tower second side-side mod is distinguishable with a lesser amount of excitation. According to Figure 5.3c, the acceleration responses in Z direction is low but around 2.9 Hz, there is a significant level of vibration which may be due to the drivetrain motion or pitch and yaw control system of the wind turbine. The effect of the tower modes and the coupled blade-tower modes are also distinguishable but the overall vibration level of Z direction is very low compared to X and Y at the tower top.

To observe the effect of structural damping ratio to the blade and tower loads in spectral aspects, a normal Kaimal turbulence model with 12 m/s mean wind speed is generated and simulations are made for 1800 seconds in operating condition. Since

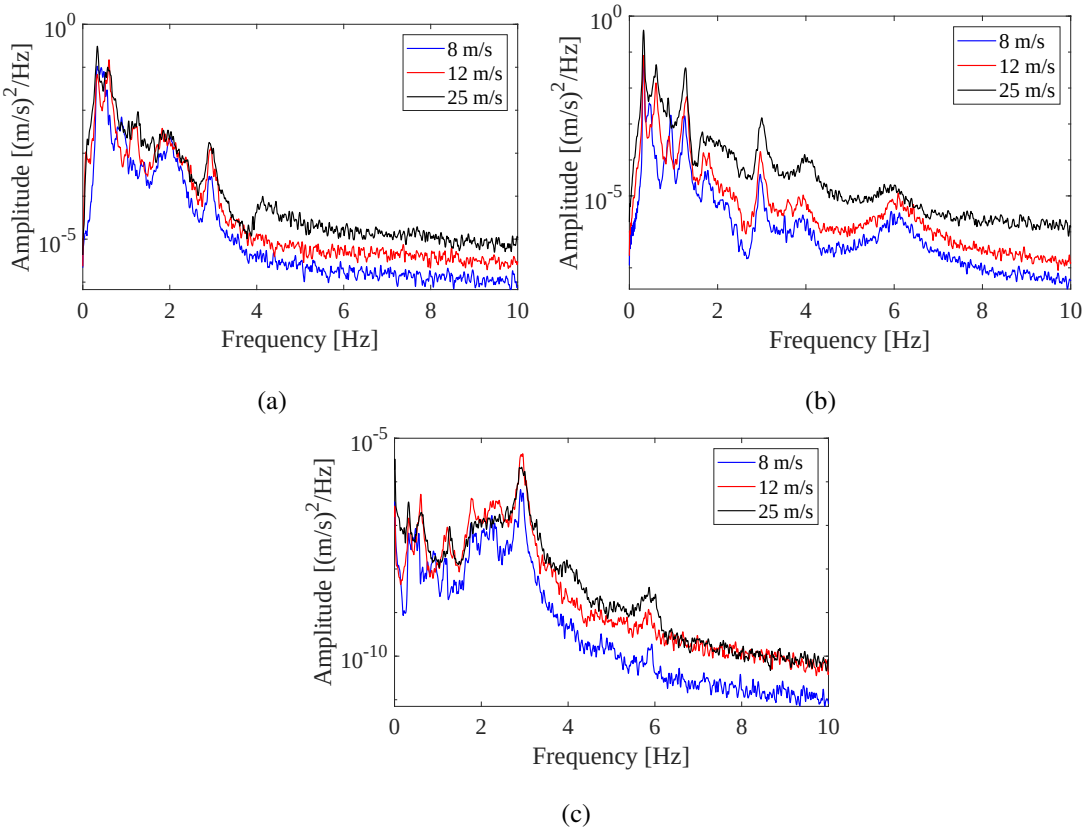

Figure 5.3: Tower top acceleration PSDs ((a): X, (b): Y, (c): Z)

the highest sectional shear forces and bending moments are expected at the tower base and blade root, the spectra of these loads are calculated for all directions. Figure 5.4 illustrates the load spectra for different tower modal damping ratios. It is worth noting that both the first and second fore-aft and side-side modes are considered when increasing the tower modal damping ratios. According to Figure 5.4, it is shown that above 6 Hz, no mode causes significant load levels. The first fore-aft and side-side tower modes are what contribute most to the total tower loads at 0.32 and 0.31 Hz in longitudinal and lateral directions, respectively. Increasing the tower modal damping ratios has an enormous effect on reducing the tower base loads caused by the first and second fore-aft and side-side tower bending modes, as illustrated in Figure 5.4g, 5.4h, 5.4j and 5.4k. It can be also stated that while reduction in tower fore-aft shear force and bending moment is due to the increase in modal damping ratios in fore-aft mode, the reduction in tower side-side shear force and bending moment is due to the additional modal damping in side-side mode. In addition, around 2.92 Hz, the fore-aft and

side-side shear and bending moments at the tower base are mitigated by increasing the modal damping ratio of the second fore-aft and side-side modes, respectively. It is also worth pointing out that blade root shear force and bending moments are not mitigated much with additional tower modal damping ratios except the mode around 3 Hz which is tower and blade coupled bending mode and thus increasing tower damping ratios mitigates the blade loads around 3 Hz yet it has negligible effect when total stress at the blade root is considered. The fundamental blade passage frequency due to 12 rpm rotor rotation is appeared as a spike at 0.20 Hz in both X and Y directions at the blade root. Its related harmonics appear until 1.0 Hz with decreasing amplitudes.

Figure 5.5 shows the PSDs of shear forces and bending moments of the tower base and blade root for different blade modal damping ratios between 1% and 30%. The first and second blade flapwise and the first blade edgewise modes are considered while iterating the modal damping ratios. The increase in blade modal damping ratios provides load mitigation in wider frequency range but with a lower amount compared to the mitigation with increase in tower modal damping. While the flapwise modal damping of the blade does not have crucial mitigation on blade root and tower base loads, the edgewise modal damping provides significant reduction in edgewise blade root loads since edgewise vibrations are less damped by the aerodynamic forces. In addition, blade flapwise mode provides slight load mitigation for side-side shear forces and bending moments at the tower base. It is worth noting that there is no remarkable load mitigation at the tower base for frequencies smaller than 1.0 Hz but a remarkable reduction is provided between 1.0 Hz and 6.0 Hz at the tower base by increase in blade modal damping. Moreover, it can be stated that the blade edgewise mode is more effective on reducing tower base side-side loads.

It is worth noting that the load spectra can only give clue about the frequency characteristics of the load mitigation. For a detailed investigation, DELs are calculated in the following sections.

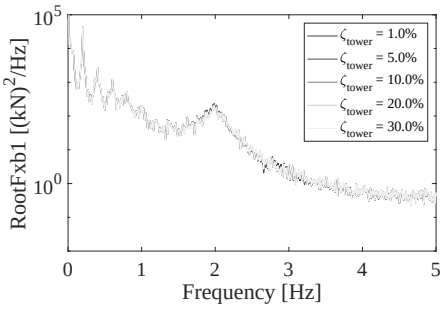
RootFxb1 [(kN)^2/Hz]
10^5
10^0
0 1 2 3 4 5
Frequency [Hz]
ζ_{tower} = 1.0%
ζ_{tower} = 5.0%
ζ_{tower} = 10.0%
ζ_{tower} = 20.0%
ζ_{tower} = 30.0%

(a)

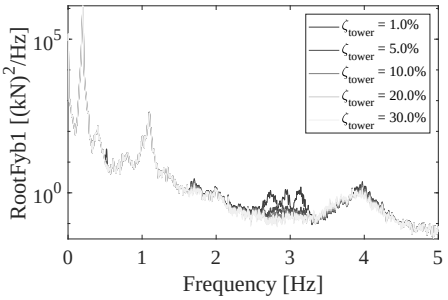
RootFyb1 [(kN)^2/Hz]
10^5
10^0
0 1 2 3 4 5
Frequency [Hz]
ζ_{tower} = 1.0%
ζ_{tower} = 5.0%
ζ_{tower} = 10.0%
ζ_{tower} = 20.0%
ζ_{tower} = 30.0%

(b)

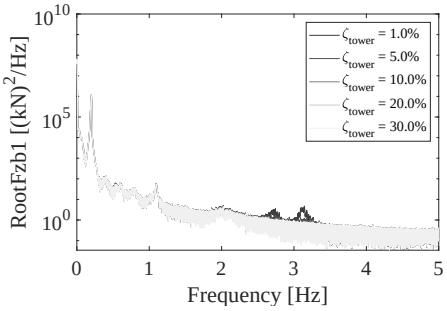
RootFzb1 [(kN)^2/Hz]
10^{10}
10^5
10^0
0 1 2 3 4 5
Frequency [Hz]
ζ_{tower} = 1.0%
ζ_{tower} = 5.0%
ζ_{tower} = 10.0%
ζ_{tower} = 20.0%
ζ_{tower} = 30.0%

(c)

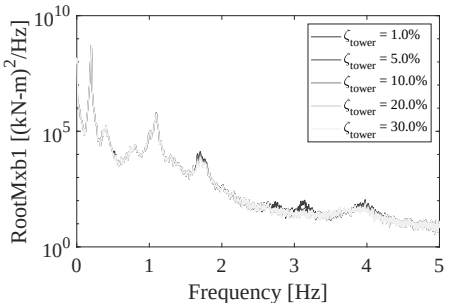
RootMxb1 [(kN-m)^2/Hz]
10^{10}
10^5
10^0
0 1 2 3 4 5
Frequency [Hz]
ζ_{tower} = 1.0%
ζ_{tower} = 5.0%
ζ_{tower} = 10.0%
ζ_{tower} = 20.0%
ζ_{tower} = 30.0%

(d)

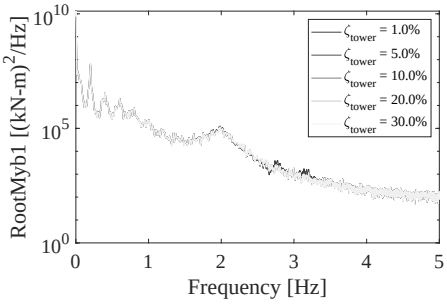
RootMyb1 [(kN-m)^2/Hz]
10^{10}
10^5
10^0
0 1 2 3 4 5
Frequency [Hz]
ζ_{tower} = 1.0%
ζ_{tower} = 5.0%
ζ_{tower} = 10.0%
ζ_{tower} = 20.0%
ζ_{tower} = 30.0%

(e)

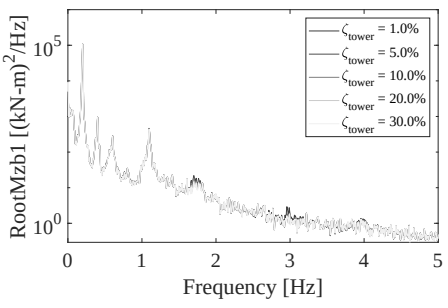
RootMzb1 [(kN-m)^2/Hz]
10^5
10^0
0 1 2 3 4 5
Frequency [Hz]
ζ_{tower} = 1.0%
ζ_{tower} = 5.0%
ζ_{tower} = 10.0%
ζ_{tower} = 20.0%
ζ_{tower} = 30.0%

(f)

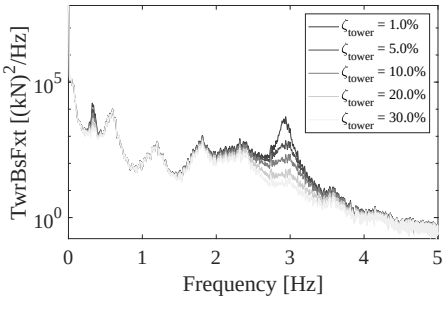
TwrBsFxt [(kN)^2/Hz]
10^5
10^0
0 1 2 3 4 5
Frequency [Hz]
ζ_{tower} = 1.0%
ζ_{tower} = 5.0%
ζ_{tower} = 10.0%
ζ_{tower} = 20.0%
ζ_{tower} = 30.0%

(g)

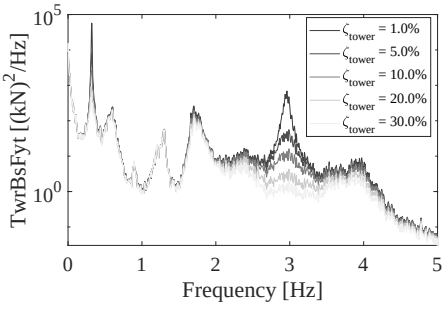
TwrBsFyt [(kN)^2/Hz]
10^5
10^0
0 1 2 3 4 5
Frequency [Hz]
ζ_{tower} = 1.0%
ζ_{tower} = 5.0%
ζ_{tower} = 10.0%
ζ_{tower} = 20.0%
ζ_{tower} = 30.0%

(h)

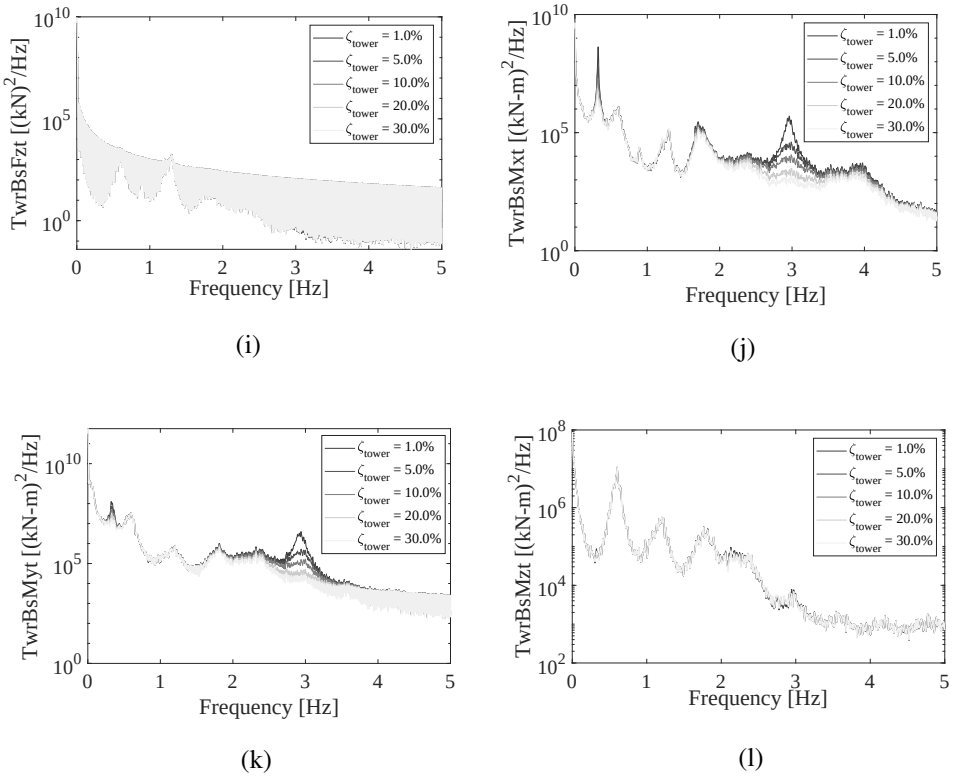

Figure 5.4: PSDs of loads for different tower modal damping ratios

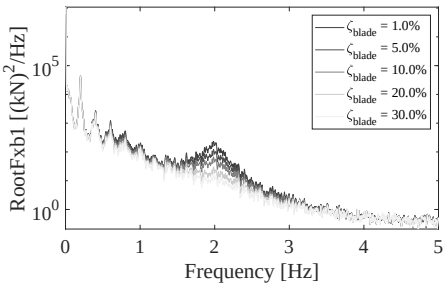
RootFxb1 [(kN)^2/Hz]
10^5
10^0
0 1 2 3 4 5
Frequency [Hz]
ζ_{blade} = 1.0%
ζ_{blade} = 5.0%
ζ_{blade} = 10.0%
ζ_{blade} = 20.0%
ζ_{blade} = 30.0%

(a)

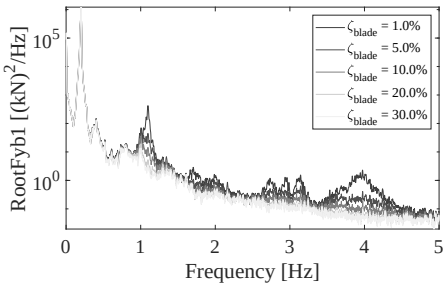
RootFyb1 [(kN)^2/Hz]
10^5
10^0
0 1 2 3 4 5
Frequency [Hz]
ζ_{blade} = 1.0%
ζ_{blade} = 5.0%
ζ_{blade} = 10.0%
ζ_{blade} = 20.0%
ζ_{blade} = 30.0%

(b)

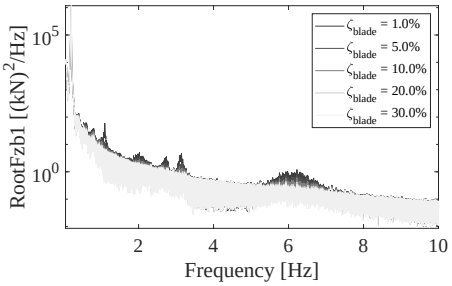
RootFzb1 [(kN)^2/Hz]
10^5
10^0
2 4 6 8 10
Frequency [Hz]
ζ_{blade} = 1.0%
ζ_{blade} = 5.0%
ζ_{blade} = 10.0%
ζ_{blade} = 20.0%
ζ_{blade} = 30.0%

(c)

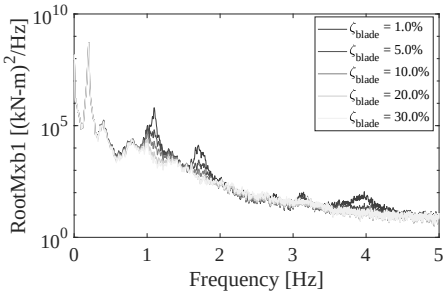
RootMxb1 [(kN-m)^2/Hz]
10^{10}
10^5
10^0
0 1 2 3 4 5
Frequency [Hz]
ζ_{blade} = 1.0%
ζ_{blade} = 5.0%
ζ_{blade} = 10.0%
ζ_{blade} = 20.0%
ζ_{blade} = 30.0%

(d)

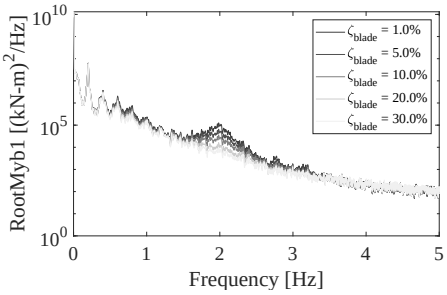
RootMyb1 [(kN-m)^2/Hz]
10^{10}
10^5
10^0
0 1 2 3 4 5
Frequency [Hz]
ζ_{blade} = 1.0%
ζ_{blade} = 5.0%
ζ_{blade} = 10.0%
ζ_{blade} = 20.0%
ζ_{blade} = 30.0%

(e)

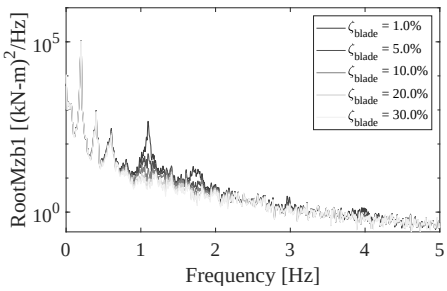
RootMzb1 [(kN-m)^2/Hz]
10^5
10^0
0 1 2 3 4 5
Frequency [Hz]
ζ_{blade} = 1.0%
ζ_{blade} = 5.0%
ζ_{blade} = 10.0%
ζ_{blade} = 20.0%
ζ_{blade} = 30.0%

(f)

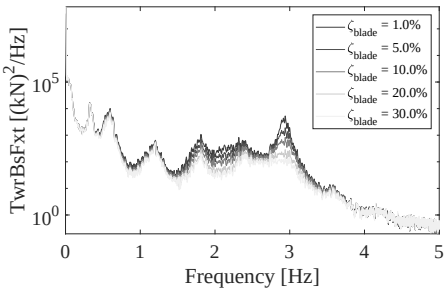
TwrBsFxt [(kN)^2/Hz]
10^5
10^0
0 1 2 3 4 5
Frequency [Hz]
ζ_{blade} = 1.0%
ζ_{blade} = 5.0%
ζ_{blade} = 10.0%
ζ_{blade} = 20.0%
ζ_{blade} = 30.0%

(g)

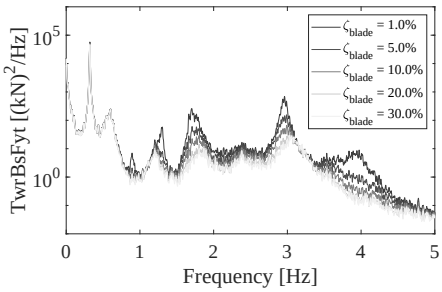
TwrBsFyt [(kN)^2/Hz]
10^5
10^0
0 1 2 3 4 5
Frequency [Hz]
ζ_{blade} = 1.0%
ζ_{blade} = 5.0%
ζ_{blade} = 10.0%
ζ_{blade} = 20.0%
ζ_{blade} = 30.0%

(h)

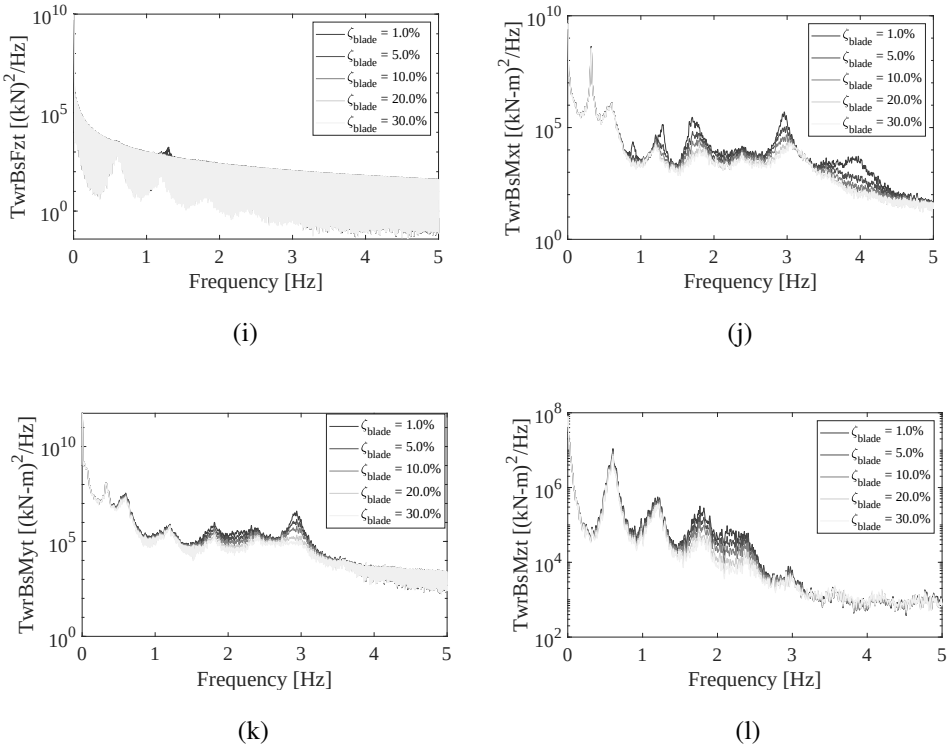

Figure 5.5: PSDs of loads for different blade modal damping ratios

5.1.2 Sectional Short-term Damage Equivalent Loads

The tower and blades have cantilever connection to the ground and hub, respectively. Although they do not have perfect rigid connection, it is expected to have the maximum stress measured at connection zones. It is almost correct for the tower; for the blade however, since the geometry and the structural properties change along the length, a detailed finite element model is necessarily needed in order to figure out where excessive stresses are observed. In this chapter, a detailed stress analysis is not made. Nevertheless, sectional loads along the tower and the blade are calculated. Shear and bending diagrams are plotted in terms of short-term damage equivalent loads for different mean wind speeds, as represented in Figure 5.6 and 5.7.

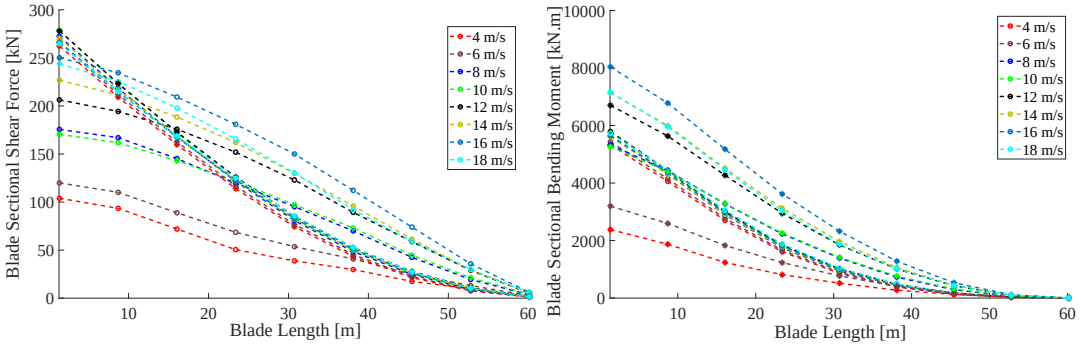

(a) (b)

Figure 5.6: Sectional loads along the blade length ($--\text{o}-- : X$ / $- - * - - : Y$)

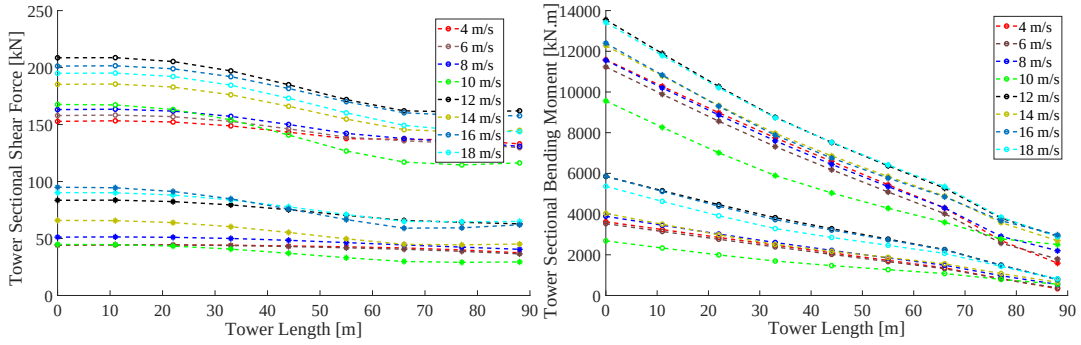

(a) (b)

Figure 5.7: Sectional loads along the tower length ($--\text{o}-- : X$ / $- - * - - : Y$)

It is observed that although the highest loads are measured at the blade root and tower base, there is no linear relationship between loads and mean wind speed due to the

aeroelastic characteristics of the wind turbine and active pitch control system of the blades. To be more precise, as wind speed changes, the total damping consisted of structural damping and aerodynamic damping changes. In addition, pitch angle of the blades is highly effective on reducing blade loads above the rated wind speed. It is worth pointing out that the shear forces in the tower slightly increase through the base due to the increase in diameter of the cross section of the tower causing aerodynamic forces to increase, as represented in Figure 5.7a. It is also valid for the blades that both in-plane (Y direction) and out-of-plane (X direction) forces are in increasing trend through the root due to the increase in generated lift and drag, as illustrated in Figure 5.6a.

In order to measure the effect of structural damping on lifetime DELs along the tower and blade length, analyses are made from 4 m/s wind speed which is cut-in wind speed to 25 m/s which is cut-out wind speed of the NREL 5 MW reference wind turbine. For each wind speed, 1 hour simulation is performed. By assuming that the wind speed has Weibull probability distribution in the site where wind turbine is placed, Weibull weighted lifetime DELs are estimated.

Figure 5.8 and 5.9 shows the effect of tower and blade structural damping ratios to the sectional tower and blade lifetime damage equivalent loads, respectively. All the tower and blade modal damping ratios are increased by equal amounts. Considering the blade loads, as they are highly damped due to aerodynamic forces, the additional structural damping does not contribute to reduction of shear forces and bending moments remarkably. With additional 30% structural damping for all blade modes, 5.6% and 4.9% reductions can be achieved in flapwise damage equivalent shear forces and bending moments at the blade root. In addition, 1.4% and 3.2% reductions are observed in edgewise shear force and bending moment loads, respectively when the structural damping ratio of the blade modes are 30%. For the tower loads, with additional 30% structural damping ratio to all tower modes, 25% and 17.7% mitigation are provided for tower base fore-aft shear forces and bending moments. For side-side direction, 59.9% and 60.9% load reductions are achievable for shear forces and bending moments at the tower base, respectively. It is worth noting that higher reductions are provided at the tower loads when compared to the blade loads which is due to the fact that the blades are highly damped by aerodynamic forces. As expected, the

highest reduction is achieved at the side-side loads of the tower, which are less likely to be damped by aerodynamic forces.

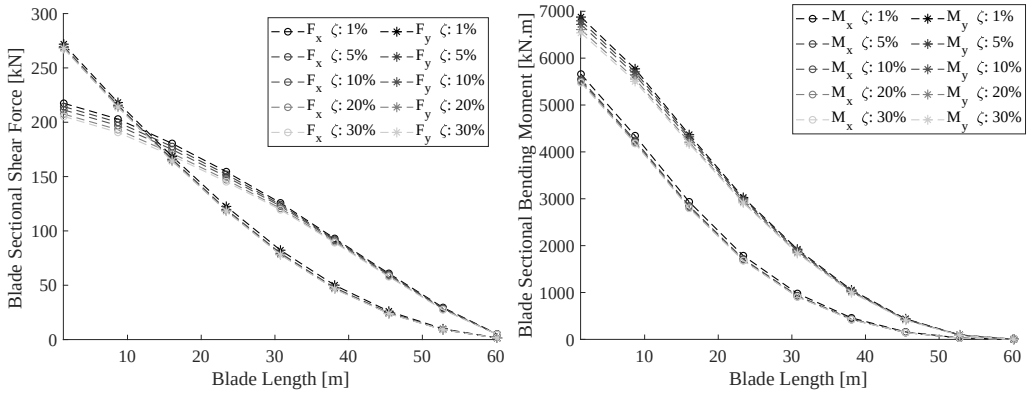

(a) (b)

Figure 5.8: Sectional Lifetime Damage Equivalent Loads along the blade length ($--\text{o}--: X$ / $- - * - - : Y$)

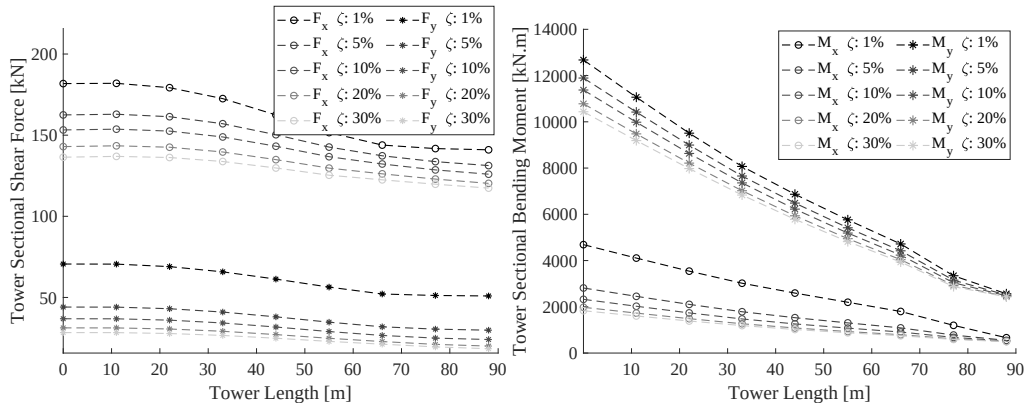

(a) (b)

Figure 5.9: Sectional Lifetime Damage Equivalent Loads along the tower length($--\text{o}--: X$ / $- - * - - : Y$)

5.2 The Effect of Blade Pitch Angle on Damage Equivalent Loads

For a pitch controlled wind turbine, the power output is controlled by an active control system. When the wind speed and the power generation become too high, it controls the blade pitch mechanism to pitch (turn) the blades out of the wind. Conversely, when the wind speed drops, the blades are turned back to generate more energy. At very higher wind speeds, the blades are feathered, which means they are pitched to 90 degrees, and the wind turbine is parked to regulate the loads in order not to exceed the design limits. In other words, pitched blades behave as a brake system by decreasing angle of attack which results in decrease in aerodynamic loads. In aeroelasticity point of view, blade pitch angle is highly effective on the response as it determines the angle of attack thus aerodynamic structural coupling.

Although NREL 5 MW wind turbine has an active pitch control system, in this section, it is assumed that the blade pitch angle does not change with varying wind speed due to the turbulence. The effect of blade pitch angle under extreme turbulence model with a mean wind speed of 20 m/s is observed. For each tower and the blade mode, the effect of structural damping ratio to the tower base and blade root forces and moments is investigated for different blade pitch angles. Figure 5.10, 5.11, 5.12 and 5.13 illustrate the effect of blade pitch angle and structural damping ratio of the tower fore-aft, side-side; blade flapwise and edgewise modes, respectively. The short-term DELs are plotted for different blade pitch angles and damping ratios and represented as a surface graph.

The effect of the first tower fore-aft modal structural damping ratio for different blade pitch angles is illustrated in Figure 5.10. It is observed that a considerable load reduction is provided in fore-aft direction. According to Figure 5.10a and 5.10e, fore-aft shear forces and bending moments can be decreased up to 10% and 15% with 30% structural damping in fore-aft mode. These decreases are highly crucial when considering tower fatigue life since the highest stresses at the tower base are mostly contributed from fore-aft shear forces and bending moments, as represented in Figure 5.6, 5.7. Although fore-aft mode of the tower is highly damped by the aerodynamic forces, the amount of structural damping has considerable effect on mitigation of fore-aft structural loads. On the other hand, increase in fore-aft structural damping

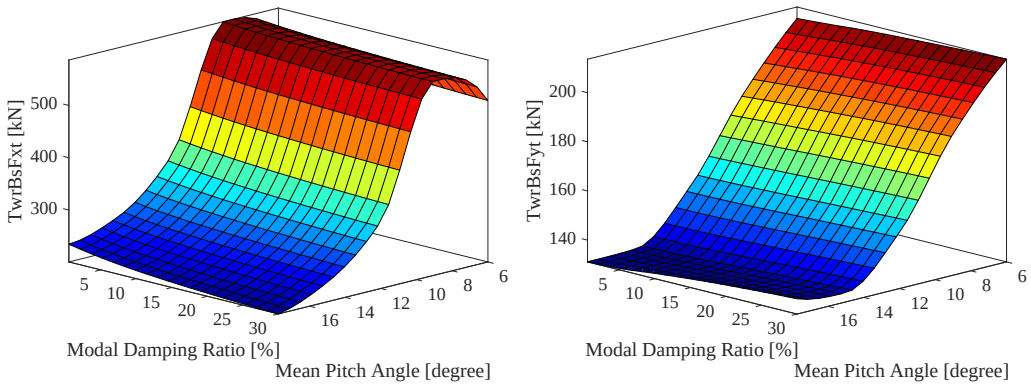

(a)

(b)

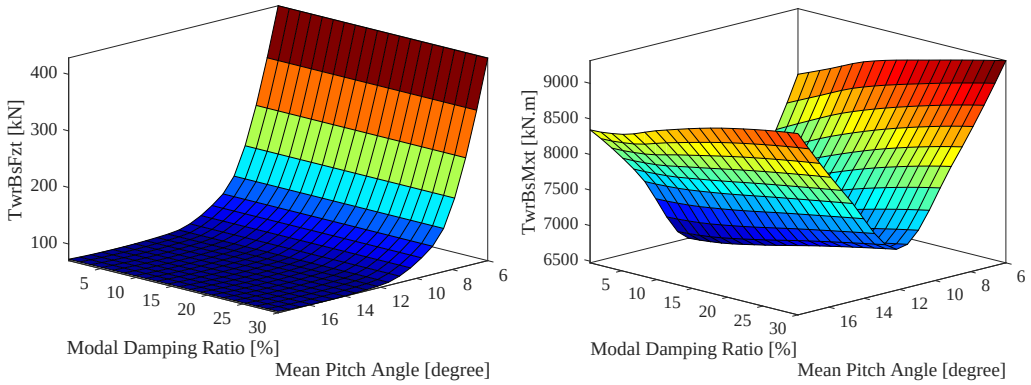

(c)

(d)

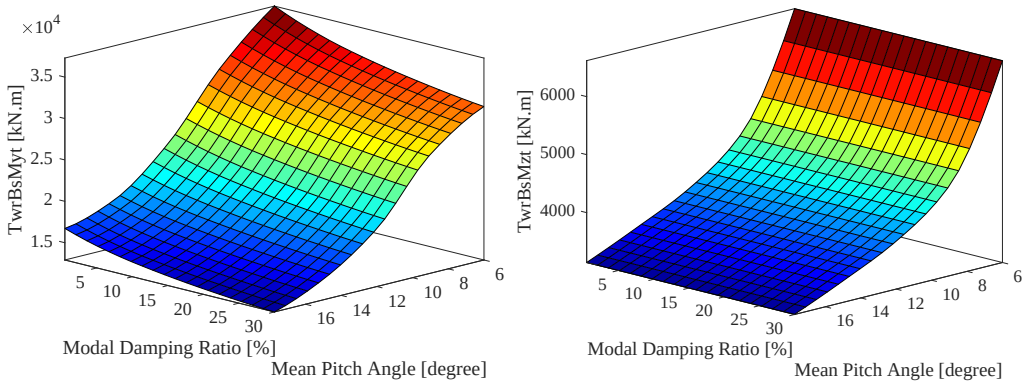

(e)

(f)

Figure 5.10: Damage Equivalent Loads for pitch cases with additional tower fore-aft modal damping

ratio has reverse effect in side-side loads of the tower as in Figure 5.10b and 5.10d due to the fact that the modal frequencies of the first fore-aft and side-side modes are very close to each other and thus modal responses of each mode are very close which

necessitate the optimization procedure between fore-aft and side-side loads to obtain minimum base stresses. In addition, it is worth noting that the first fore-aft tower mode is the fundamental mode with the lowest frequency at 0.32 Hz and thus able to be excited easily with ambient turbulence. Therefore, careful attention is needed to apply a vibration control approach.

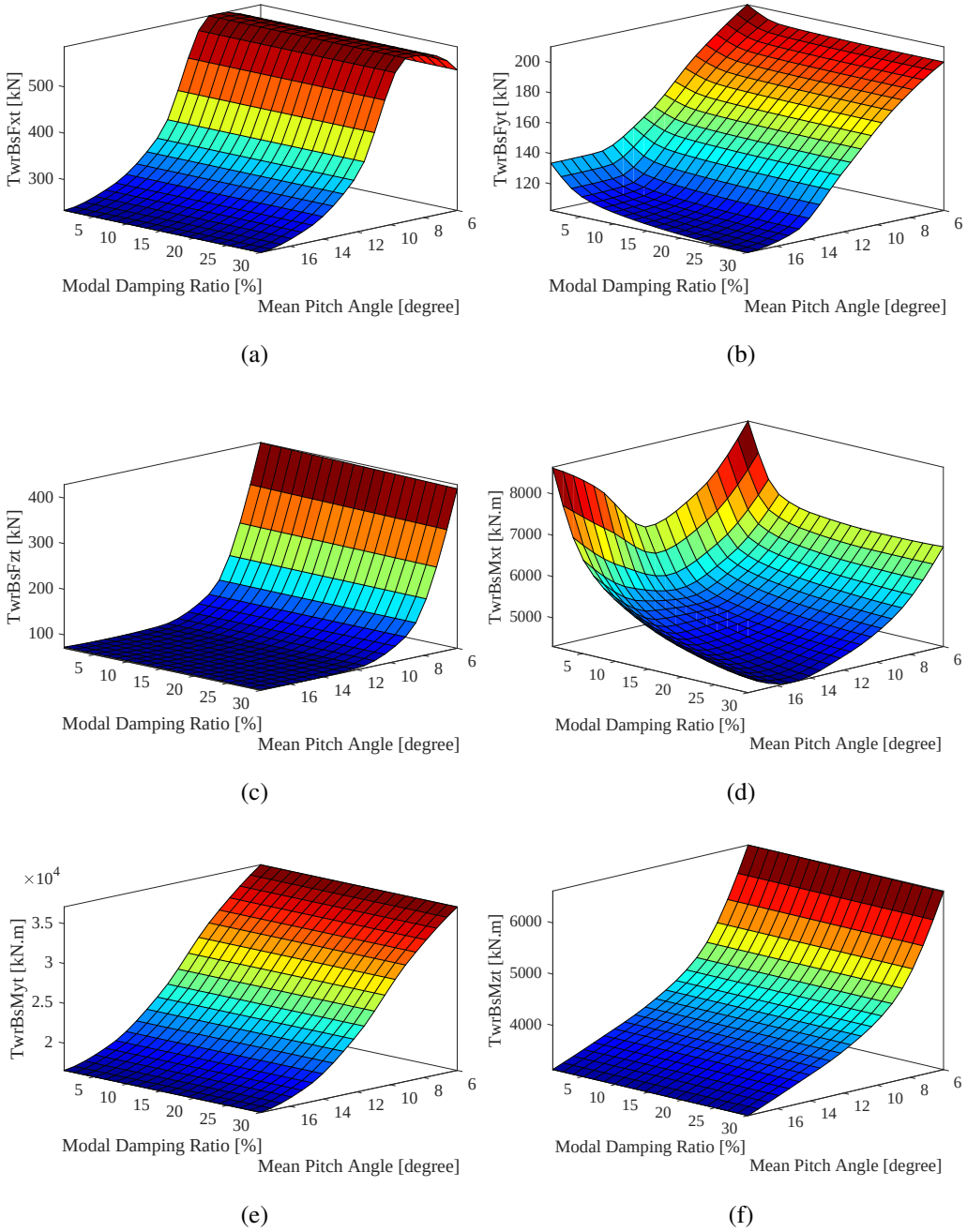

Figure 5.11: Damage Equivalent Loads for pitch cases with additional tower side-side modal damping

Figure 5.11 reveals the effect of structural damping for the first tower side-side mode and blade pitch angle to the short-term DELs. Generally speaking, modal structural damping ratio increase in tower side-side mode has a dominant effect on the reduction of tower side-side shear force and bending moment. According to Figure 5.11b and 5.11d, 15% reduction in side-side shear force and 28% reduction in side-side bending moment are possible for the tower base with additional structural damping ratio up to 30%. The side-side loads at the tower base converge to their final reduction after 10% structural damping ratio which means further damping might be unnecessary to mitigate side-side bending moment which has serious contribution to the tower base stresses. It is worth noting that at higher pitch angles where forces and moments are decreased in fore-aft and axial direction, the side-side bending moment reaches to its minimum value at 15 degree mean pitch angle and then starts to increase with increase in pitch angle as shown in Figure 5.11d. This increase is overcame by increasing structural damping ratio of the first side-side mode, which decreases side-side loads with a significant amount for all pitch angles. The effect of second side-side modal damping ratio shows similar trend but the effect of structural damping of the tower first side-side mode is low compared to that of the second side-side mode since it is less likely to be excited. Thus, contribution of the tower second side-side mode to the total response is lower and results are not investigated in this study.

For all loads except side-side loads, increase in pitch angle decreases the loads with similar exponential trends. On the other hand, considering Figure 5.10d and 5.11d, the effect of pitch angle is somewhat different and increase in pitch angle results in increase in side-side bending moments after a specific pitch angle that minimizes side-side bending moment.

Considering blades, the structural damping ratios of two modes are iterated which are the first flapwise and edgewise blade modes with mode shapes shown in Figure 4.5. The effectivity measurements are selected as short-term DELs of blade root shear force and bending moment. According to Figure 5.12, there are 4% and 8% reductions in edgewise shear force and bending moment at the blade root with 30% structural damping ratio of the blade first flapwise mode. The flapwise mode of the blade is already damped by the aerodynamic forces on the blade, thus the effect of additional structural damping to the flapwise loads is lower. Since blade second flapwise

mode has higher frequency and less likely to be excited by the ambient turbulence, the increase in the second flapwise mode damping does not have a remarkable reduction on the blade root loads and thus results are not needed to be further explained.

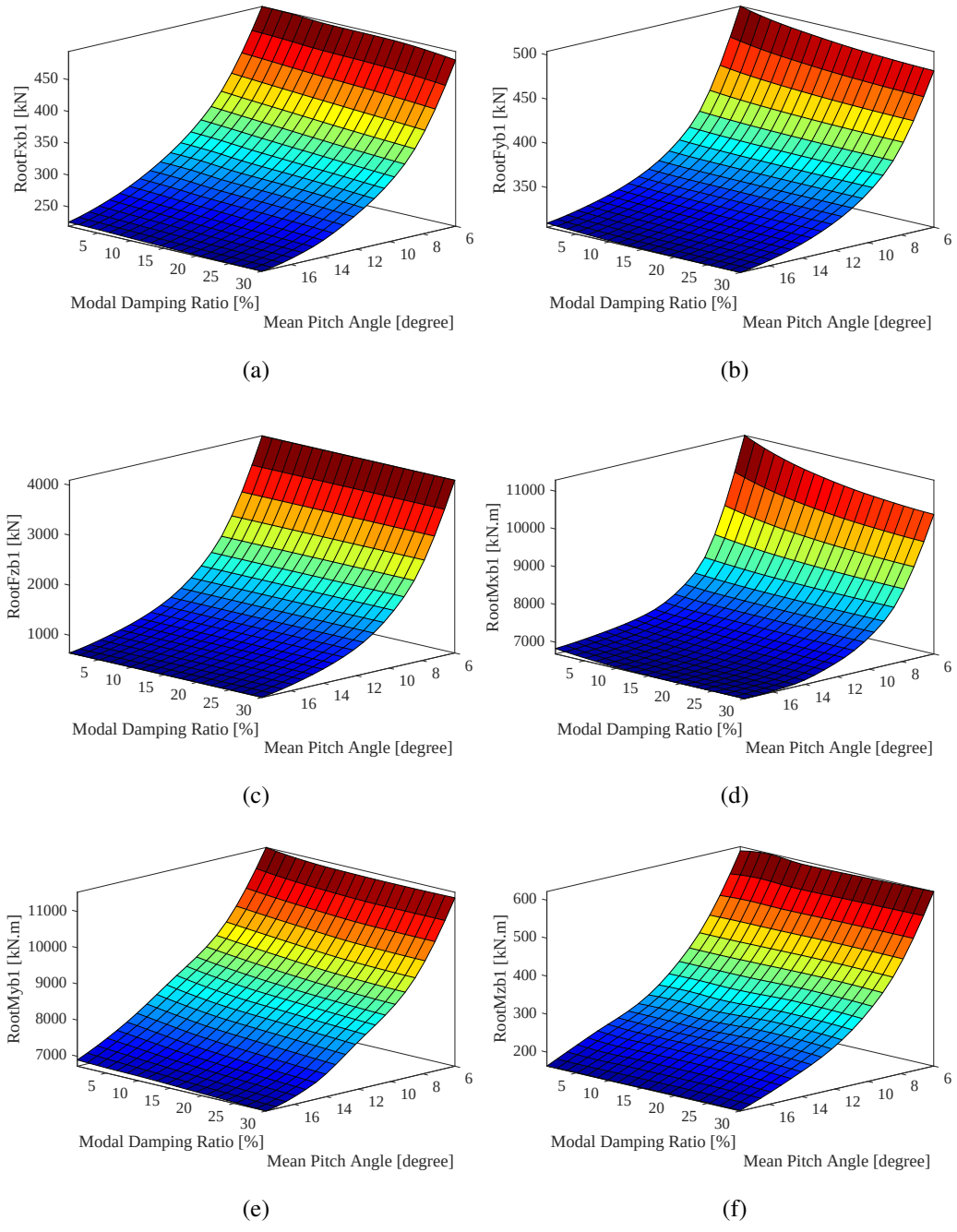

Figure 5.12: Damage Equivalent Loads for pitch cases with additional blade flapwise modal damping

Considering the effect of the structural damping of the first blade edgewise mode, the

short-term DELs of side-side shear force and bending moment at the blade root are reduced up to 9% and 11%, respectively for low pitch angles as shown in Figure 5.13b and 5.13d. However, there is no load mitigation in flapwise direction with additional structural damping in blade edgewise mode according to Figure 5.13a and 5.13e.

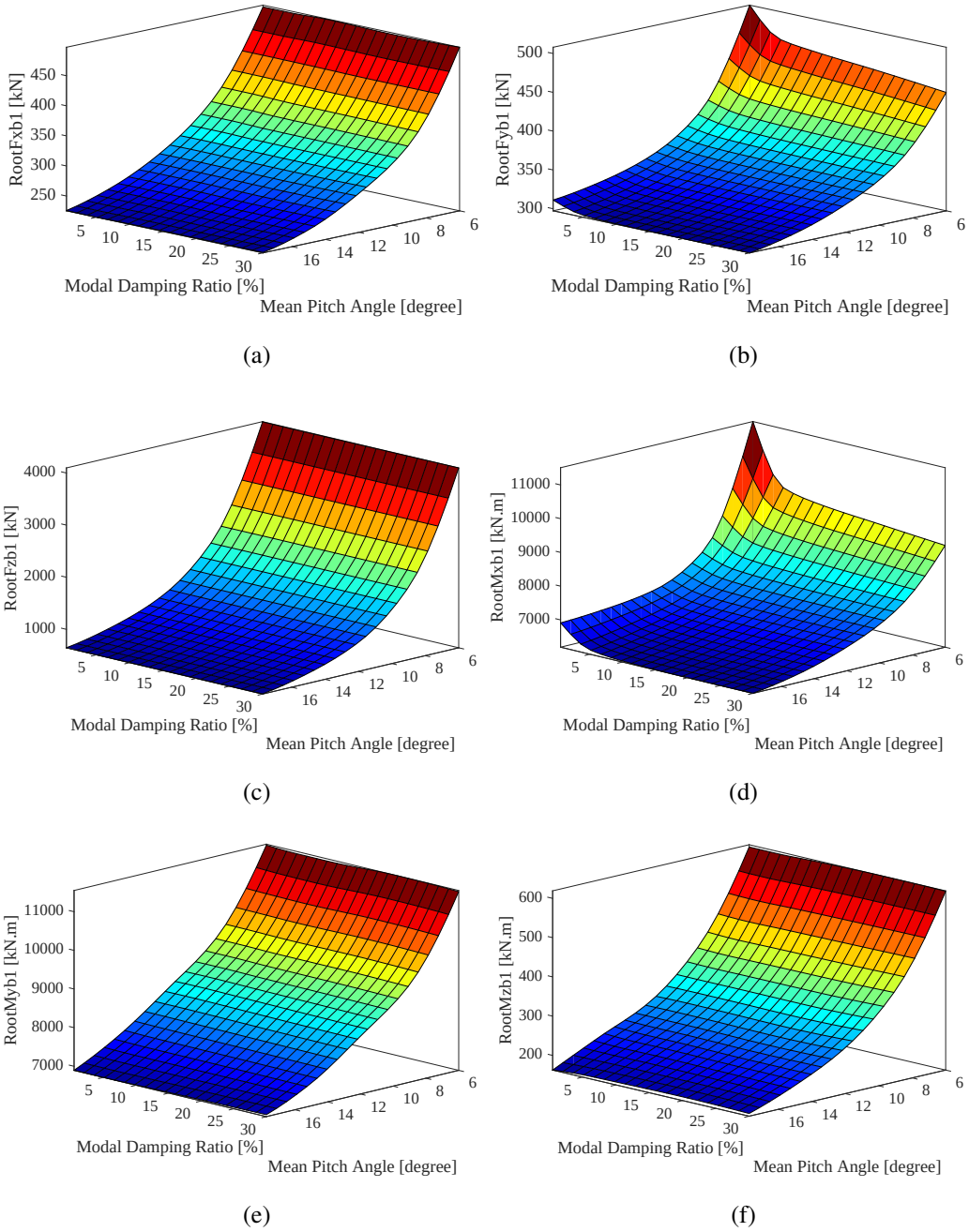

Figure 5.13: Damage Equivalent Loads for pitch cases with additional blade edgewise modal damping

In general, the edgewise vibrations are more prone to be damped with the additional structural damping as shown in Figure 5.12 and 5.13 that the structural damping ratio increase has significant effect on the mitigation of edgewise shear force and moment at the blade root no matter structural damping of which mode is increased. The reason is that although blade flapwise vibrations are highly damped due to aerodynamic forces, edgewise vibrations have low aerodynamic damping thus additional structural damping to the edgewise modes are more effective in terms of mitigating damage equivalent loads.

In the literature, since aerodynamic damping is low in edgewise direction, aeroelastic stability problems arise which were first noticed in the early 1990s [104]. Several attempts are tried in order to mitigate the vibrations in wind turbine blades in edgewise direction [76, 105].

Besides, preceding results highlight that axial force and torsional moment at the tower base and blade root are independent of the structural damping, yet they are dependent on the blade pitch angle. With decrease in pitch angle, the axial force and torsional moment increases exponentially according to the Figure 5.12c, 5.12f, 5.13c and 5.13f.

5.3 Damage Equivalent Loads in Parked Condition

To make a wind turbine last for the design period, situations like maintenance or extreme wind speed must be taken into consideration according to IEC61400-1 load cases [3]. In IEC 61400-1, the extreme wind conditions are characterized by a period: for instance a 1 year extreme turbulence model which is so severe that it is expected to occur only once in 1 year. For these types of extreme situations, wind turbine system is usually set to parked or idling condition in which blades are fully stopped or rotates at very low speed without power generation. For parking, the brake system is used. In the standard of Germanischer Lloyd, it is required two independent braking systems one of which is aerodynamic brake and the other of which is on the drive train [20]. Most of the wind turbines employ a mechanical brake on the drive train to keep the rotor from turning for parking. In idling condition, the blades keep rotating in low wind speeds and high-wind shut downs. It helps to reduce the frequency of imposition

of braking loads on the drive train.

In this section, to simulate parked condition, the blades are pitched to 90 degrees in order to minimize the aerodynamic loads and the generator is stopped. Figure 5.14, 5.15, 5.16 and 5.17 present the short-term DELs at the blade root and the tower base for different structural damping ratios and mean wind speeds.

Figure 5.14 represents the effect of the tower first fore-aft mode structural damping ratio on the DELs at the tower base when the wind turbine is in parking condition. It can be stated that fore-aft DELs of shear forces and bending moments are reduced by 42% and 69% around rated wind speed as shown in Figure 5.14a and 5.14e. These reductions are considerably high and a damping treatment to fore-aft mode could be useful when the wind turbine is under harsh environment or in maintenance. On the other hand, there is no DEL mitigation in side-side shear force and moment with the additional structural damping in fore-aft direction according to Figure 5.14b and 5.14d. Considering axial force and torsional DELs, there is also no vibration mitigating with increase in tower fore-aft structural damping.

Figure 5.15 shows DEL for shear force and bending moment of the tower base with respect to the structural damping ratio of the first tower side-side mode. The side-side shear forces and bending moments mitigate by 40% and 42% respectively, as shown in Figure 5.15b and 5.15d. It is worth noting that additional damping up to 30% causes significant amount of vibration mitigation around cut-out wind speed which is 25 m/s. Moreover, side-side loads have more contribution to the total stresses in parked condition compared to operating condition while fore-aft loads are more dominant for total stresses in operating condition.

Figure 5.16 reveals the effect of blade first flapwise mode's structural damping ratio on the DELs in parking condition. Additional structural damping provides 9% and 14% DEL reduction in edgewise shear forces and bending moments according to Figure 5.16b and 5.16d, respectively. In general, load mitigation increases in percentage with increase in mean wind speed. It is worth pointing out that a slight amount of DEL reduction is achievable for blade torsional moment and axial force at the blade root as shown in Figure 5.16c and 5.16f. On the contrary to the effect of flapwise structural damping, the effect of edgewise modal damping on the blade root load mit-

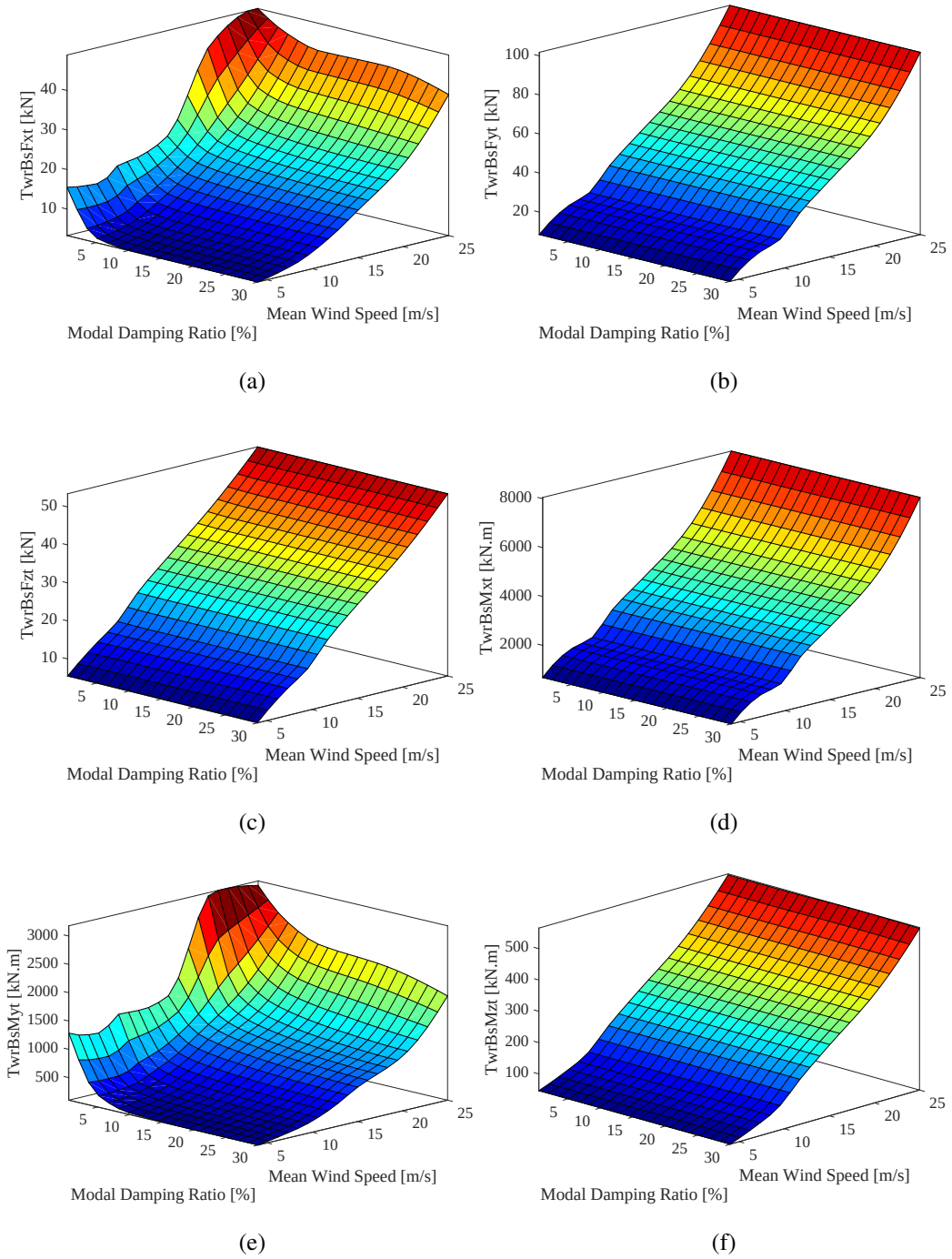

Figure 5.14: Damage Equivalent Loads for parked cases with additional tower fore-aft modal damping

igation is higher. According to Figure 5.17b and 5.17d, 28% and 42% reductions can be possible in edgewise shear force and bending moment with 30% structural damping ratio at cut-out wind speed. In general, it can be said that flapwise modes are

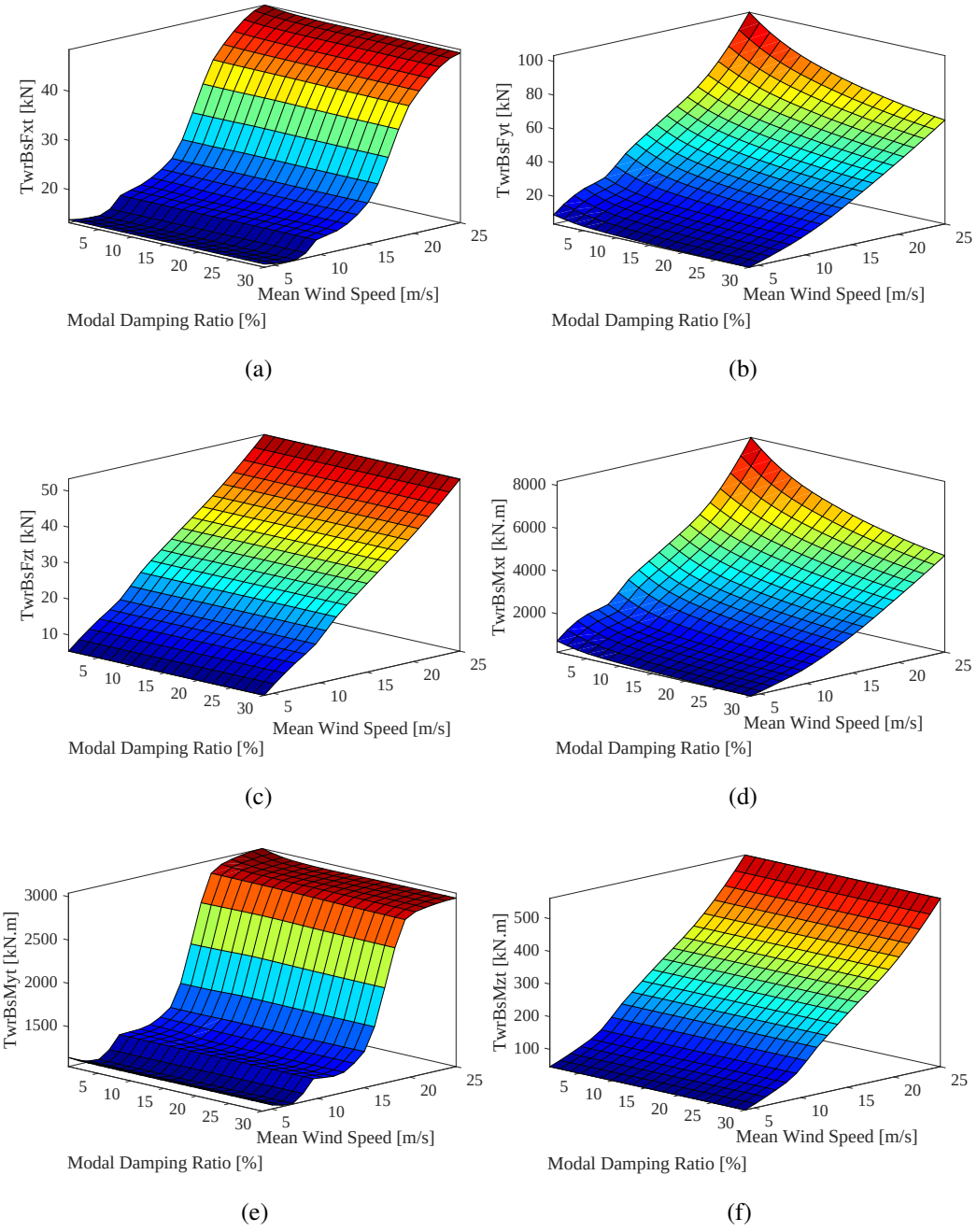

Figure 5.15: Damage Equivalent Loads for parked cases with additional tower side-side modal damping

highly damped due to aerodynamic forces, thus the effect of flapwise and edgewise damping to the flapwise loads is very low.

In summary remarkable DEL reduction is possible for both tower base and blade root in parking condition. Results emphasize that damping treatment could be very

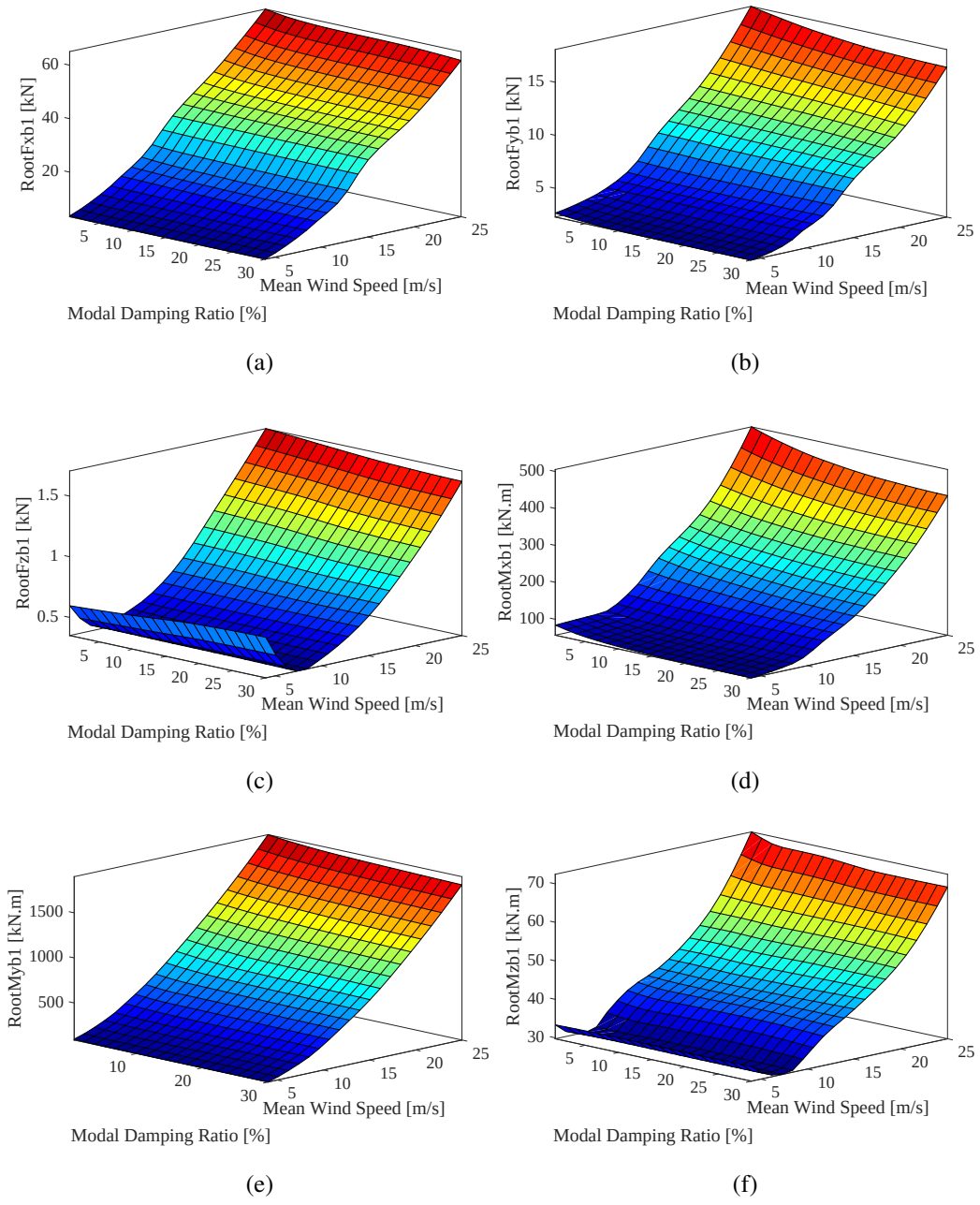

Figure 5.16: Damage Equivalent Loads for parked cases with additional blade flap-wise modal damping

effective in terms of fatigue life provided that the wind turbine system parks under harsh conditions or for maintenance issues during their lifetime.

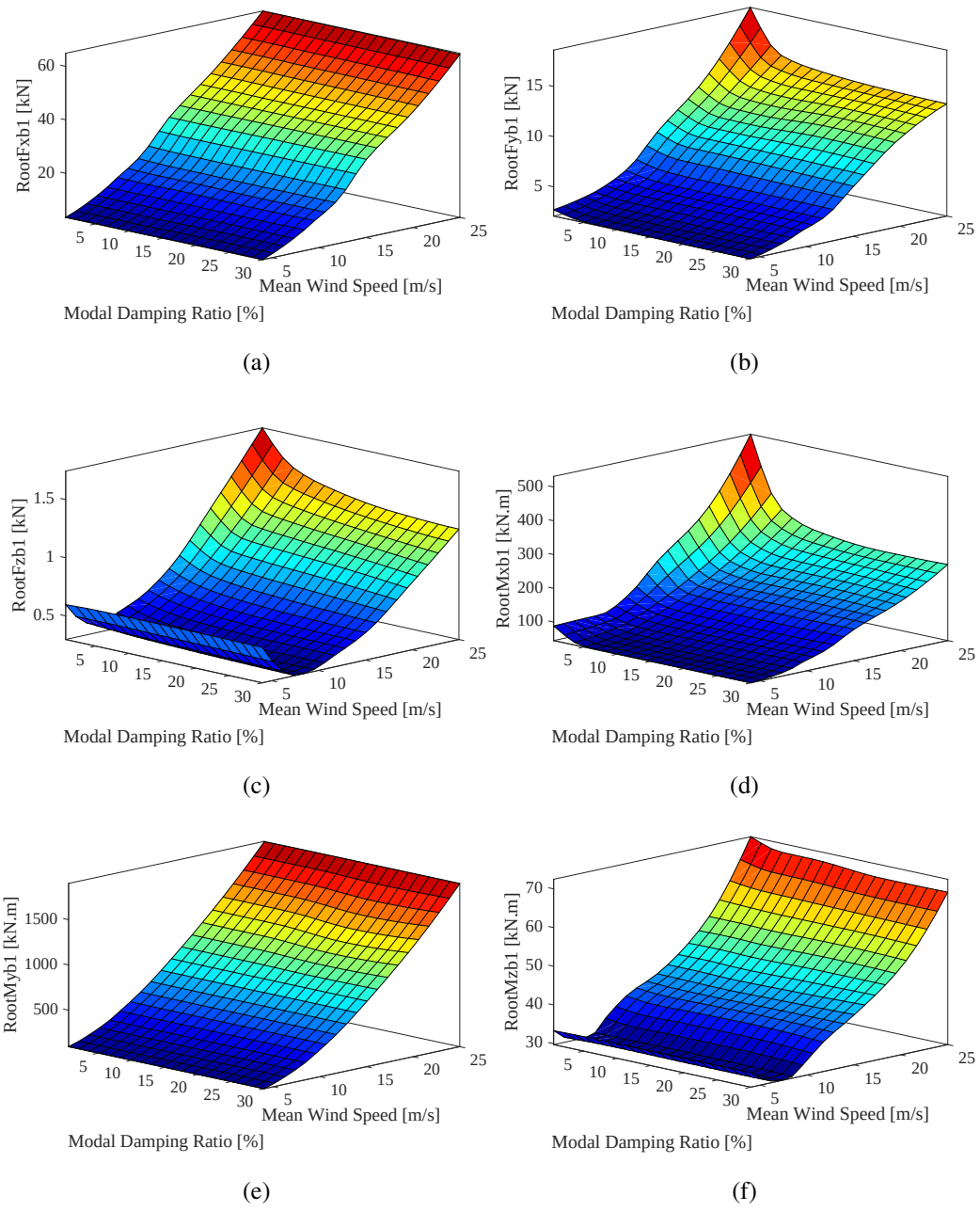

Figure 5.17: Damage Equivalent Loads for parked cases with additional blade edge-wise modal damping

5.4 Damage Equivalent Loads in Operating Condition

In order to observe the fatigue loads when the wind turbine is operating for different modal structural damping ratios and mean wind speeds, a series of analyses are made for 600 seconds under normal turbulence level with a mean wind speed varying from

4 m/s to 24 m/s with 2 m/s equal spacing. In order to increase reliability, turbulence fields are generated with 6 different random seeds for each wind speed and results are averaged. In other words, 1 hour simulation is made for each wind speed. In operating condition, the blades are actively pitch controlled. In addition, the yaw control system is active. The generator has variable speed controller which is supplied as built-in control system in FAST ServoDyn module. During the simulations, the amount of power generated is checked in order to make sure that the additional damping does not cause any decrease in the generator efficiency.

Figure 5.18 illustrates the effect of structural damping ratio of the tower first fore-aft mode to the tower base short-term DELs. According to Figure 5.18a and 5.18e, DELs of fore-aft shear force and bending moment at the tower base are reduced by 17% and 21% at rated wind speed with 30% fore-aft structural damping. However, side-side tower loads are increased slightly as shown in Figure 5.18b and 5.18d. It is due to the proximity of the fore-aft and side-side modal frequencies and this increase can be neglected since side-side loads are already lower in working condition and a damping treatment in fore-aft direction would compensate the increase in side-side loads. As pitch control system is active in working case, the loads are prone to decrease after rated wind speed due to the fact that pitched blade decreases the overall loads in both tower and blades. Near cut-out wind speed, however; increase in blade pitch angle no longer reduces the loads with increase in wind speed as illustrated in Figure 5.18a and 5.18e. A structural damping treatment to the tower fore-aft mode could be helpful for increasing fatigue life of the tower since it is dominantly excited.

Additional structural damping of the tower side-side mode provides 31% and 54% DEL reduction around rated wind speed for side-side shear force and bending moments respectively as indicated in Figure 5.19b and 5.19d. It is crucial to note that above 10% structural damping, the load mitigation is about to reach an equilibrium value. Thus, in the case of a damping treatment, further increase in structural damping might be unnecessary and expensive. Considering the fore-aft and axial loads and moments, obviously there is no DEL reduction, as shown in Figure 5.19a, 5.19c, 5.19e and 5.19f. It is demonstrated that as side-side modes have less amount of aerodynamic damping, additional side-side modal damping is more effective in mitigating side-side DELs compared to the effectivity of fore-aft modal damping on fore-aft

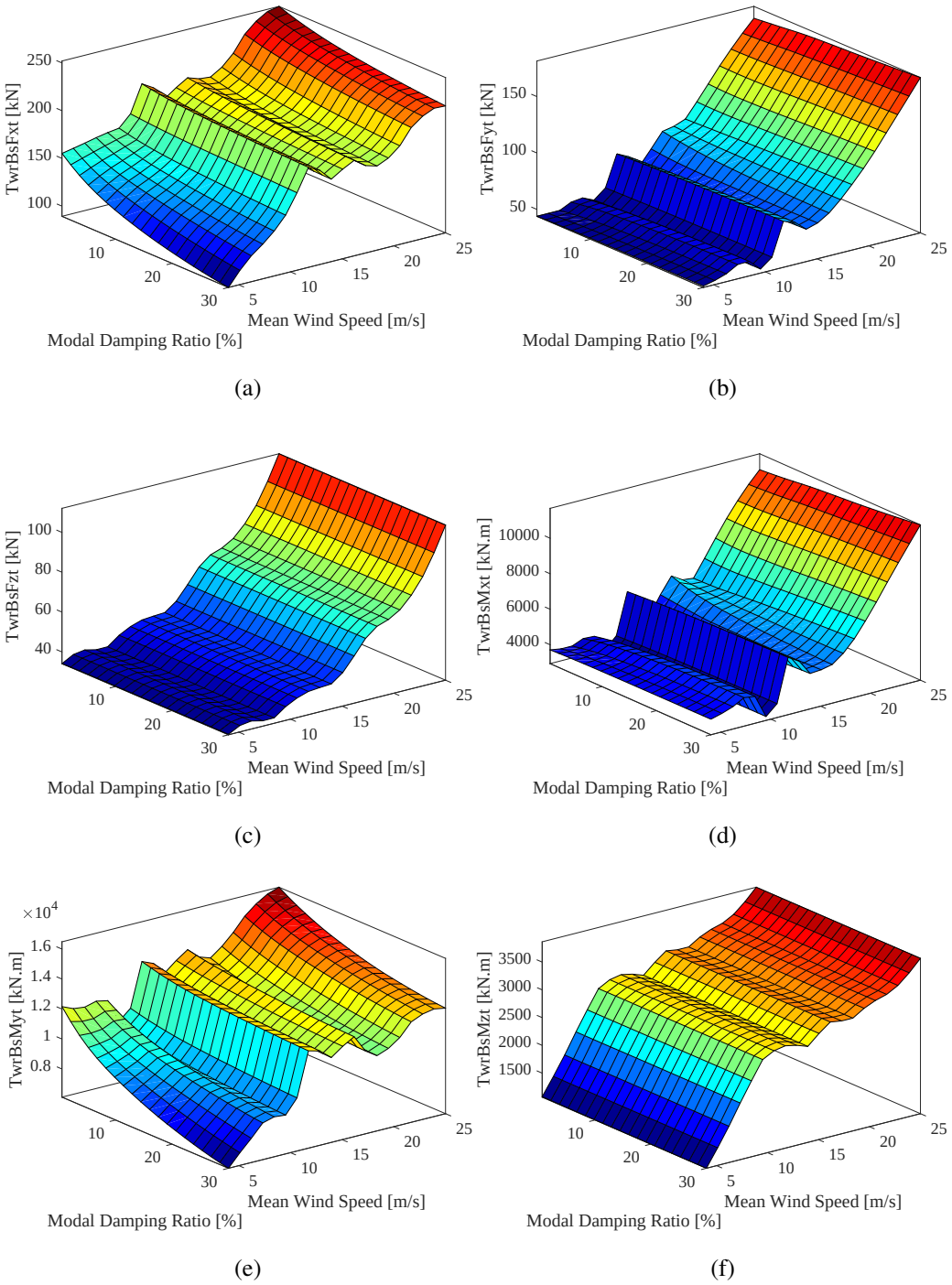

Figure 5.18: Damage Equivalent Loads for operating cases with additional tower fore-aft modal damping

DELs.

From Figure 5.20, it can be seen that blade loads generally show a significant increase

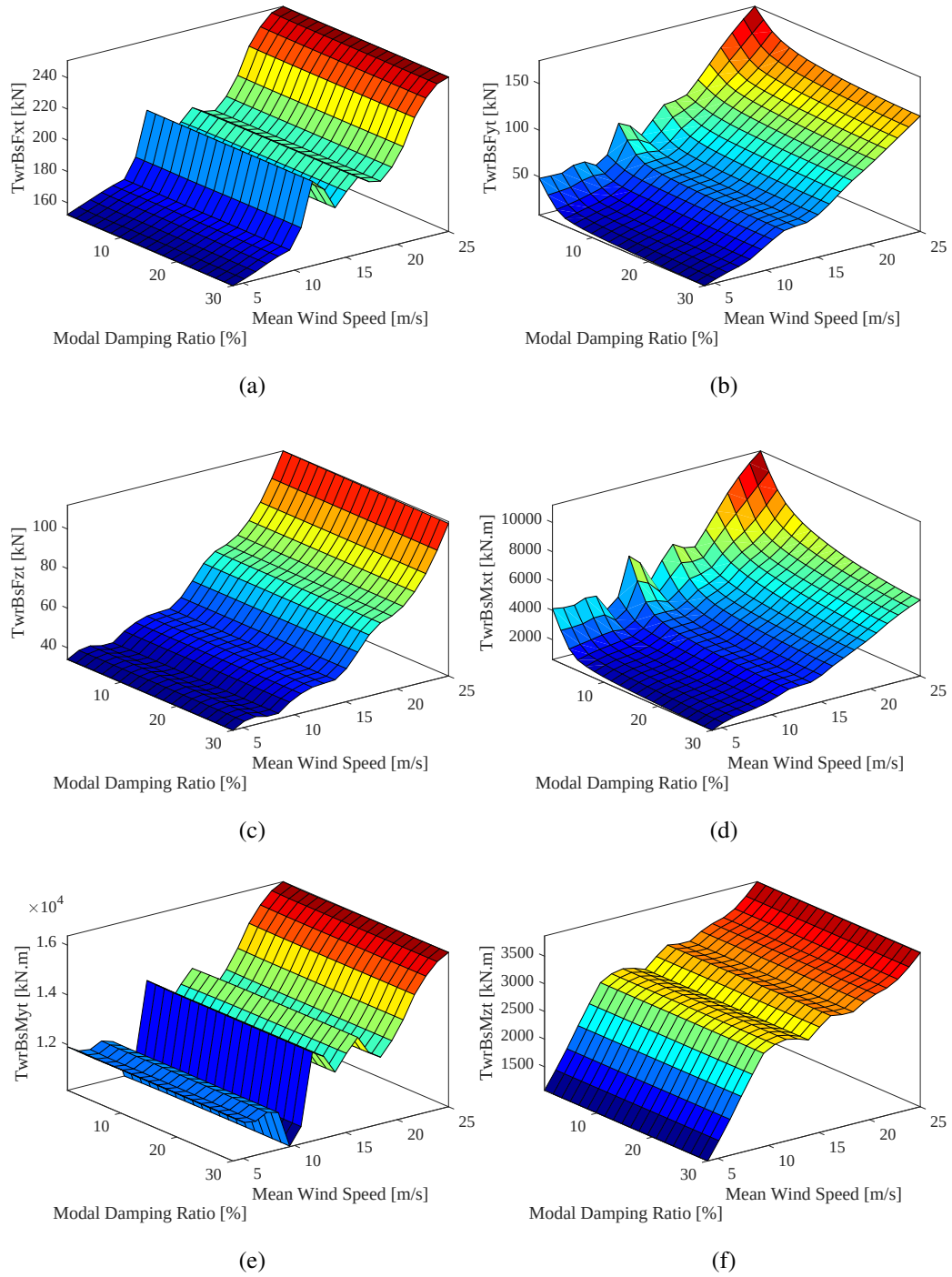

Figure 5.19: Damage Equivalent Loads for operating cases with additional tower side-side modal damping

up to rated wind speed, which is 11.4 m/s and then shows a decreasing trend between cut-out and rated wind speed. Above rated wind speed, the blades are pitched with an angle that increases exponentially with increasing mean wind speed, thus lowers

the flapwise and edgewise bending loads at the blade root. At rated wind speed, no significant load reduction is provided by the additional structural damping ratio in flapwise mode. Remarkably, only 6% reduction is observed for flapwise bending moment of the blade as indicated in Figure 5.20e. Considering the axial force and torsional moment, no remarkable load mitigation is provided as depicted in Figure 5.20c and 5.20f, respectively.

Considering Figure 5.21, the modal structural damping of blade edgewise mode has no effect on mitigation of flapwise loads as they are highly damped by aerodynamic forces. However, it can reduce DEL of edgewise shear force and bending moment at the blade root with 7% and 10% near cut-out wind speed, as shown in Figure 5.21b and 5.21d respectively. At rated wind speed, the edgewise modal structural damping provides 4% reduction for DEL of edgewise bending moment.

Taken as a whole, preceding results suggest that damping treatment to the blade edgewise mode may be unfavorable since at the rated wind speed where the highest amount of blade root loads are seen, no significant load mitigation is provided. Although short-term DEL reduction is considerable at higher wind speeds, damping treatment may not provide significant reduction considering lifetime DELs since higher wind speeds have lower probability of occurrence.

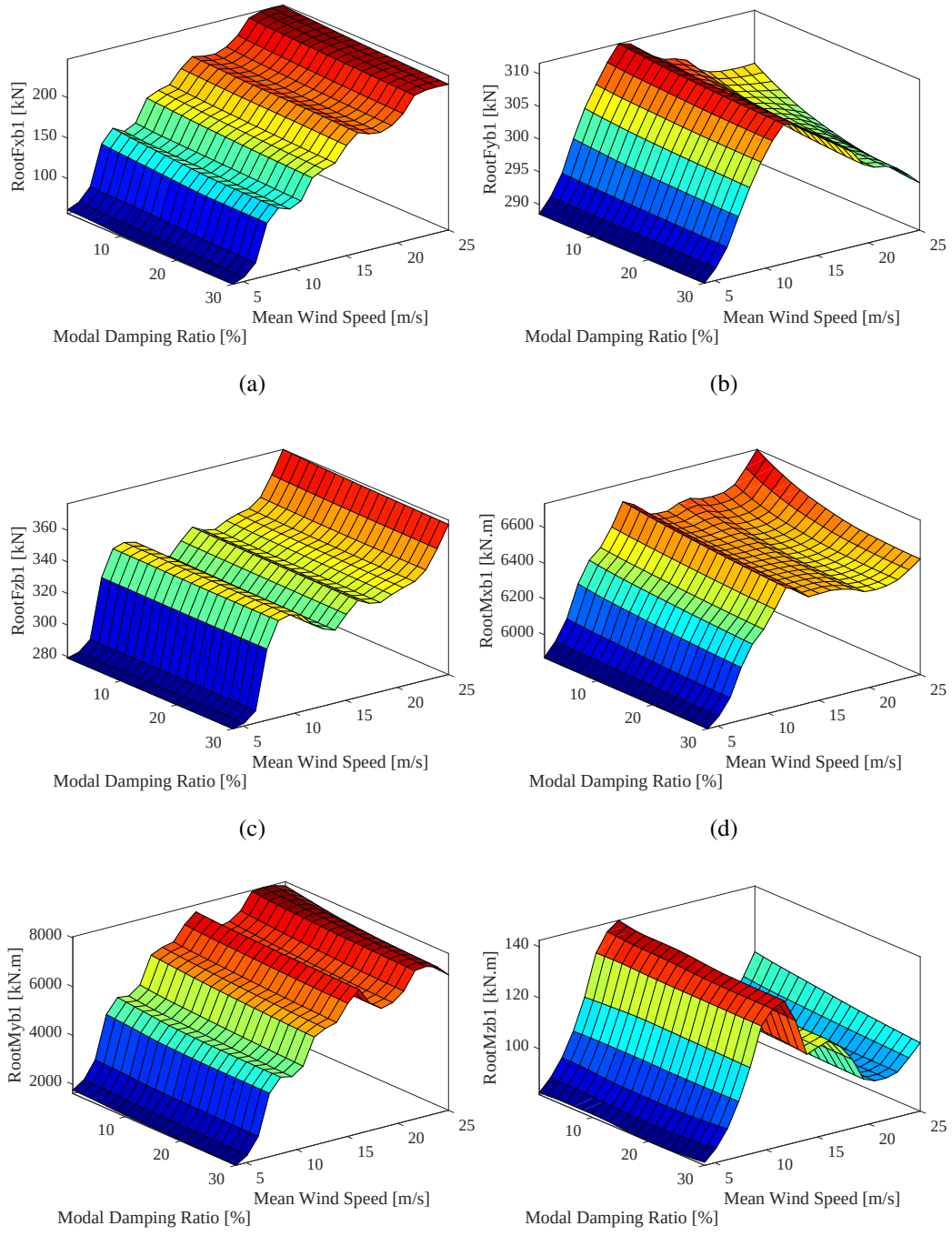

Figure 5.20: Damage Equivalent Loads for operating cases with additional blade flapwise modal damping

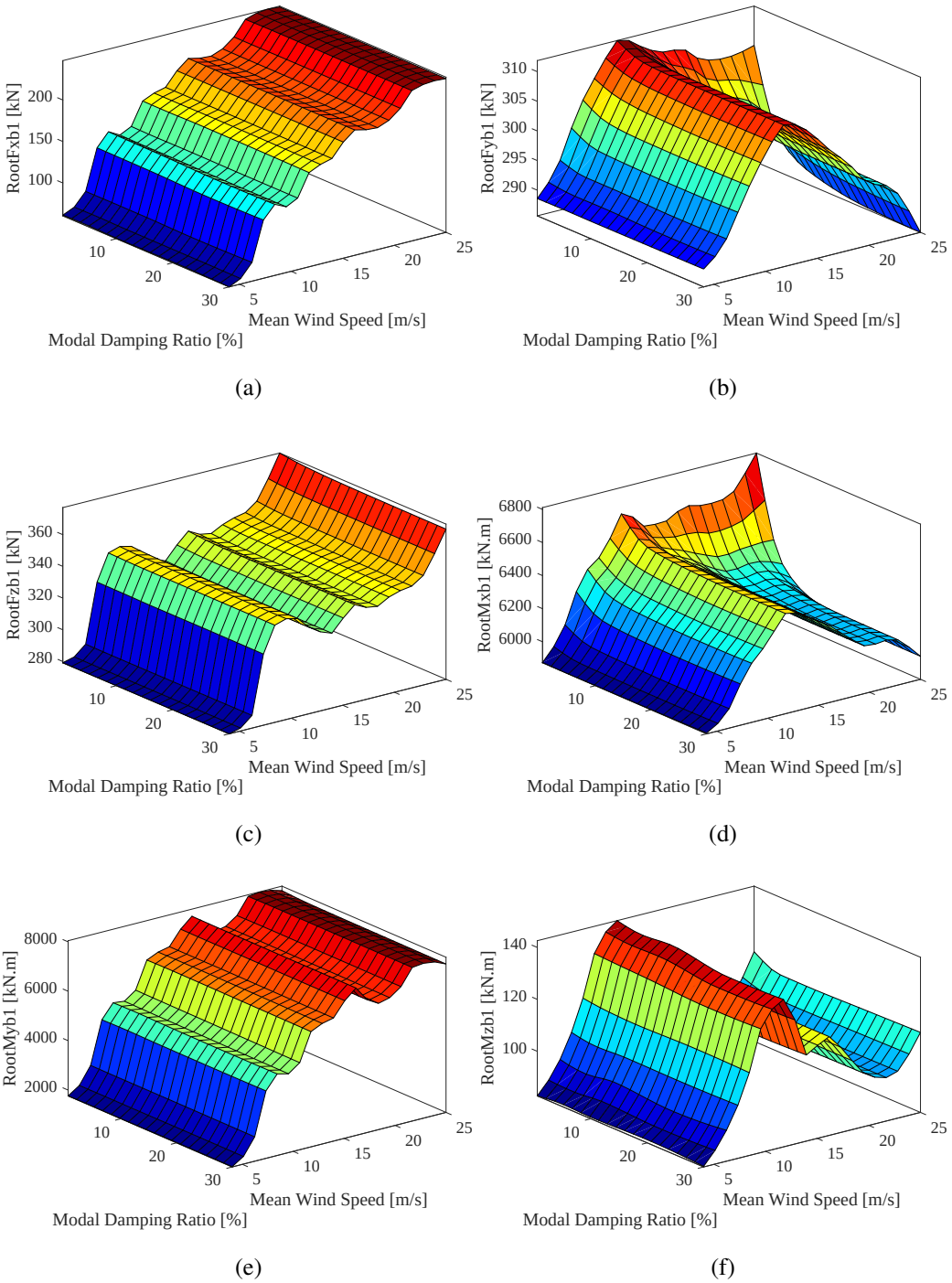

Figure 5.21: Damage Equivalent Loads for operating cases with additional blade edgewise modal damping

5.5 Lifetime Damage Equivalent Loads

In the preceding sections, the short-term DELs represent the loads caused by short-term stationary wind conditions, thus each analysis is unique for each main wind speed and does not represent the lifetime loads. In long-term, since the wind turbine is exposed to different wind speeds during its lifetime, the probability distribution takes into part and can be represented by measured mean wind speed and turbulence intensity parameters with a corresponding probability. In general, Weibull distribution can be assumed for long-term wind speed distribution in a wind turbine site and loads are weighted accordingly in order to estimate lifetime DELs [106, 30]. In other words, short-term DELs for each wind speed is weighted and extrapolated to the wind turbine's lifetime with a Weibull probability distribution. Figure 5.22 illustrates the Weibull wind speed probability distribution which is used for weighting. For Weibull distribution function, shape parameter k is specified as 2.4 for the simulated wind turbine site.

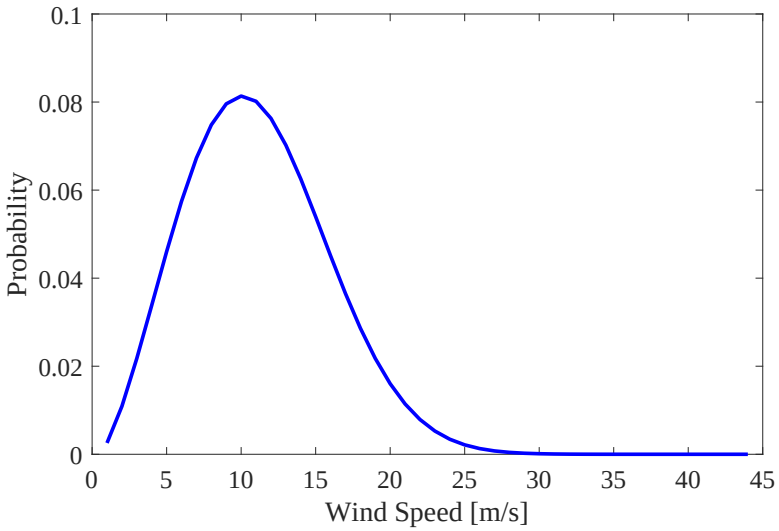

Figure 5.22: Weibull probability distribution function for analysis

In this section, long term analyses are made in order to estimate lifetime DELs. 11 different turbulence models that last 600 seconds, from cut-in wind speed of 4 m/s to 24 m/s with 2m/s increments, with 6 different turbulence seeds are generated by using Turbsim. FAST simulations are performed for each wind speed and turbulence seed.

By using MLife [85], the loads obtained by these simulations are weighted according to the Weibull distribution to evaluate lifetime DELs as explained in Chapter 3.1.6.

Table 5.1, 5.2, 5.3 and 5.4 tabulate the change in lifetime DELs at the tower base and blade root in percentage with the additional tower fore-aft and side-side modal structural damping. According to Table 5.1, up to 11.88% shear force and 17.68% bending moment reductions at the tower base are achievable along the dominant wind direction, which is fore-aft axis. On the other hand, in the lateral direction, side-side axis, the shear forces and bending moments are increased 5.10% and 7.44% with additional damping ratio of 30%. However, the decrease in fore-aft loads compensates the increase in side-side loads since loads along fore-aft direction are comparatively higher. Therefore, a damping treatment to the first fore-aft tower mode can provide significant contribution to lifetime of the structure.

Table 5.1: Lifetime Damage Equivalent Loads for different tower first fore-aft modal damping ratios

Load / Improvement in Percentage	**Baseline Load**	**5%**	**10%**	**20%**	**30%**
TwrBsFxt (kN)	183.33	-3.75	-6.55	-9.83	-11.88
TwrBsFyt (kN)	74.77	1.07	2.27	4.01	5.10
TwrBsFzt (kN)	49.52	0.00	0.01	-0.06	-0.09
TwrBsMxt (kN.m)	5026.92	1.66	3.44	5.93	7.44
TwrBsMyt (kN.m)	12477.63	-5.75	-10.07	-14.92	-17.68
TwrBsMzt (kN.m)	2691.89	0.00	-0.01	-0.02	-0.01
RootFxb1 (kN)	190.36	-0.05	-0.08	-0.10	-0.11
RootFyb1 (kN)	304.82	0.00	0.00	-0.01	-0.02
RootFzb1 (kN)	332.67	0.01	0.01	0.00	0.00
RootMxb1 (kN.m)	6424.65	0.00	-0.01	-0.01	-0.02
RootMyb1 (kN.m)	6675.36	-0.05	-0.09	-0.13	-0.16
RootMzb1 (kN.m)	127.52	0.24	-0.07	0.07	0.44

Considering the effect of the second fore-aft tower modal damping to the lifetime DELs, it is shown that 12.58% reductions are achievable in the fore-aft shear load

TwrBsFxt as tabulated in Table 5.2. In addition, fore-aft bending moment TwrBsMyt decrease by 2.89%. It is worth noting that this decrease in shear load is higher compared to the decrease provided by the modal damping of the first tower fore-aft mode. Moreover, it is worth pointing out that both the first and second fore-aft modes do not have significant contribution in reducing blade root loads. Therefore, it can be stated that tower damping treatment only contribute to the fatigue loads at the tower.

Table 5.2: Lifetime Damage Equivalent Loads for different tower second fore-Aft modal damping ratios

Load / Improvement in Percentage	**Baseline Load**	**5%**	**10%**	**20%**	**30%**
TwrBsFxt (kN)	183.33	-7.10	-9.30	-11.36	-12.58
TwrBsFyt (kN)	74.77	-0.57	-0.60	-0.56	-0.54
TwrBsFzt (kN)	49.52	-0.12	-0.33	-0.62	-0.84
TwrBsMxt (kN.m)	5026.92	-0.10	-0.13	-0.11	-0.11
TwrBsMyt (kN.m)	12477.63	-1.55	-2.07	-2.58	-2.89
TwrBsMzt (kN.m)	2691.89	-0.11	-0.22	-0.36	-0.41
RootFxb1 (kN)	190.36	-0.03	-0.08	-0.13	-0.15
RootFyb1 (kN)	304.82	-0.04	-0.06	-0.07	-0.08
RootFzb1 (kN)	332.67	-0.08	-0.11	-0.14	-0.15
RootMxb1 (kN.m)	6424.65	-0.01	-0.03	-0.06	-0.07
RootMyb1 (kN.m)	6675.36	-0.04	-0.07	-0.10	-0.12
RootMzb1 (kN.m)	127.52	0.42	0.19	0.00	0.04

Considering the tower first side-side modal damping, it provides higher amount of reductions in shear forces and bending moments in lateral directions, namely TwrBsFyt and TwrBsMxt, with 33.61% and 56.99%, as tabulated in Table 5.3. On the other hand, no significant load mitigation is achieved in other directions at the tower base or blade root. The high reductions in lateral loads are due to the fact that side-side vibrations on the tower are less aerodynamically damped due to low intensity of turbulence in the lateral direction.

Although first side-side tower modal damping provide significant amount of load

Table 5.3: Lifetime Damage Equivalent Loads for different tower first side-side modal damping ratios

Load / Improvement in Percentage	**Baseline Load**	**5%**	**10%**	**20%**	**30%**
TwrBsFxt (kN)	183.33	-0.04	-0.05	-0.06	-0.07
TwrBsFyt (kN)	74.77	-23.85	-29.20	-32.41	-33.61
TwrBsFzt (kN)	49.52	-0.06	-0.12	-0.26	-0.39
TwrBsMxt (kN.m)	5026.92	-37.89	-48.03	-54.52	-56.99
TwrBsMyt (kN.m)	12477.63	-0.06	-0.05	-0.07	-0.09
TwrBsMzt (kN.m)	2691.89	-0.01	-0.01	0.01	0.02
RootFxb1 (kN)	190.36	0.00	-0.01	-0.02	-0.03
RootFyb1 (kN)	304.82	-0.01	-0.01	-0.02	-0.02
RootFzb1 (kN)	332.67	0.01	0.01	0.02	0.02
RootMxb1 (kN.m)	6424.65	-0.01	-0.02	-0.04	-0.06
RootMyb1 (kN.m)	6675.36	-0.02	-0.04	-0.03	-0.05
RootMzb1 (kN.m)	127.52	0.24	0.12	0.27	0.46

mitigation in lateral direction, the second side-side mode is less effective in reducing loads according to Table 5.4. It provides 16.52% and 3.97% shear force and bending moment reductions with 30% structural damping ratio, respectively.

Considering the effect of all tower modes, it can be concluded that tower modes do not have significant load mitigation in blade root. While fore-aft modes provides fore-aft load mitigation at the tower base, which are TwrBsFxt and TwrBsMyt; side-side modes provide side-side load mitigation, namely TwrBsFyt and TwrBsMxt. None of the tower modes cause significant mitigation in axial shear force and torsion, namely TwrBsFzt and TwrBsMzt. Generally speaking, the first fore-aft and side-side modes provide more load mitigation compared to the second tower modes since the modal frequencies of the second modes are higher, making them difficult to be excited by ambient turbulence.

Considering the effect of blade modal damping to the fatigue loads, Table 5.5 shows the contribution of the first blade flapwise modal damping increase to the loads. It

Table 5.4: Lifetime Damage Equivalent Loads for different tower second side-side modal damping ratios

Load / Improvement in Percentage	**Baseline Load**	**5%**	**10%**	**20%**	**30%**
TwrBsFxt (kN)	183.33	0.04	0.09	0.07	0.00
TwrBsFyt (kN)	74.77	-10.49	-13.07	-15.20	-16.52
TwrBsFzt (kN)	49.52	-0.01	0.01	0.01	0.28
TwrBsMxt (kN.m)	5026.92	-2.40	-3.01	-3.50	-3.97
TwrBsMyt (kN.m)	12477.63	0.00	0.02	0.01	-0.08
TwrBsMzt (kN.m)	2691.89	0.01	-0.01	-0.02	0.10
RootFxb1 (kN)	190.36	0.00	-0.02	-0.02	-0.14
RootFyb1 (kN)	304.82	-0.02	-0.03	-0.04	-0.05
RootFzb1 (kN)	332.67	0.01	0.01	0.00	0.01
RootMxb1 (kN.m)	6424.65	-0.02	-0.03	-0.05	-0.06
RootMyb1 (kN.m)	6675.36	-0.01	-0.02	-0.01	-0.12
RootMzb1 (kN.m)	127.52	0.44	0.65	-0.20	-0.21

can be stated that lifetime DELs of blade flapwise shear force and flapwise bending moment are reduced by 3.81% and 4.29%, respectively with additional 30% modal damping for the first flapwise mode. In addition, it is interesting that blade flapwise modal damping have major effect on mitigating tower loads as representing in Table 5.5. Up to 9.88% tower shear force reductions are achievable in X direction. Moreover, it should be pointed out that the torsion at the tower base are reduced by 12.65% which is significantly high.

Considering Table 5.6, the increase in modal damping ratio of the second flapwise mode of the blade is also effective in reducing tower base lifetime DELs, yet it is less effective compared to the first flapwise mode. It is worth noting that the shear force mitigation at the tower base, which is TwrBsFxt, is higher with additional blade second flapwise modal damping ratio compared to the first flapwise modal damping ratio. The reason may be due to the coupling of tower vibrations and blade flapwise mode, the effect of which results in decrease in tower vibrations in X direction

Table 5.5: Lifetime Damage Equivalent Loads for different blade first flapwise modal damping ratios

Load Case / Improvement in Percentage	**Baseline Load**	**5%**	**10%**	**20%**	**30%**
TwrBsFxt (kN)	183.33	-2.73	-5.15	-8.16	-9.88
TwrBsFyt (kN)	74.77	-1.97	-3.61	-5.36	-5.91
TwrBsFzt (kN)	49.52	-2.22	-4.40	-7.18	-8.83
TwrBsMxt (kN.m)	5026.92	-0.41	-0.71	-1.08	-1.23
TwrBsMyt (kN.m)	12477.63	-1.13	-2.21	-3.86	-5.04
TwrBsMzt (kN.m)	2691.89	-3.22	-6.28	-10.31	-12.65
RootFxb1 (kN)	190.36	-0.76	-1.59	-2.82	-3.81
RootFyb1 (kN)	304.82	-0.14	-0.26	-0.42	-0.52
RootFzb1 (kN)	332.67	-0.05	-0.12	-0.21	-0.26
RootMxb1 (kN.m)	6424.65	-0.28	-0.53	-0.89	-1.10
RootMyb1 (kN.m)	6675.36	-0.97	-1.92	-3.36	-4.29
RootMzb1 (kN.m)	127.52	-0.26	-1.00	-1.83	-2.12

with additional blade flapwise modal damping. As in the case of blade first flapwise modal damping, the second flapwise mode also provides mitigation in tower torsion by 7.26%. On the other hand, both blade first and second flapwise modal damping do not mitigate blade DELs significantly since flapwise vibrations are heavily damped by aerodynamic force. Therefore, one can state that additional structural damping for the blade flapwise mode is unnecessary taking into account the trade-off between price and blade fatigue life improvement. However, it provides significant fatigue life improvements in the tower base, where the highest stresses are measured.

Considering the blade edgewise mode which is less likely damped by aerodynamic forces, the effect of edgewise modal damping to the lifetime DELs at the blade root is low as well, as tabulated in Table 5.7. The edgewise shear force and bending moment DELs are reduced by 0.82% and 2.25%, respectively with 30% modal structural damping ratio. The mitigation of flapwise loads are very low, lower than 0.5%.

In general, it can be concluded that the first fore-aft tower mode is highly effective in

Table 5.6: Lifetime Damage Equivalent Loads for different blade second flapwise modal damping ratios

Load Case / Improvement in Percentage	**Baseline Load**	**5%**	**10%**	**20%**	**30%**
TwrBsFxt (kN)	183.33	-4.87	-7.83	-10.34	-11.32
TwrBsFyt (kN)	74.77	-2.56	-4.22	-5.38	-5.37
TwrBsFzt (kN)	49.52	-0.80	-1.49	-2.48	-3.18
TwrBsMxt (kN.m)	5026.92	-0.57	-0.95	-1.23	-1.22
TwrBsMyt (kN.m)	12477.63	-1.08	-1.77	-2.37	-2.61
TwrBsMzt (kN.m)	2691.89	-2.70	-4.52	-6.38	-7.26
RootFxb1 (kN)	190.36	-0.87	-1.56	-2.33	-2.74
RootFyb1 (kN)	304.82	-0.05	-0.08	-0.13	-0.16
RootFzb1 (kN)	332.67	-0.05	-0.08	-0.12	-0.15
RootMxb1 (kN.m)	6424.65	-0.04	-0.09	-0.16	-0.23
RootMyb1 (kN.m)	6675.36	-0.54	-0.89	-1.24	-1.44
RootMzb1 (kN.m)	127.52	0.41	-0.09	-0.05	-0.29

reducing fore-aft loads, which create the highest stresses at the tower base. Therefore, a damping treatment to the first fore-aft tower mode could be profitable to increase fatigue life of the structure. The second fore-aft tower mode can also be damped for this purpose; however, its contribution to fatigue life would be lower compared to the first fore-aft mode. The first side-side tower modal damping increase provides the highest amount of load reduction in side-side direction since side-side vibrations are less damped by the aerodynamic forces. The second side-side tower modal damping increase also provides load reduction in side-side direction with a lower amount compared to the first side-side mode. Considering all the tower modes, the damping increase in any of the tower mode has negligible effect in the blade root loads. Considering the blade modes, it is worth pointing out that blade damping has incontrovertible effect in reducing tower base loads, rather than blade root loads. Howbeit, the first and second flapwise modes of the blade provide particular load reduction in flapwise direction. Besides, the first edgewise modal damping increase reduces edgewise loads. It could be a trade-off study between blade damping treatment cost and

fatigue life increase of the blade since the blade root load reductions are low. On the other hand, blade damping treatment could be profitable to increase tower fatigue life.

Table 5.7: Lifetime Damage Equivalent Loads for different blade first edgewise modal damping ratios

Load Case / Improvement in Percentage	**Baseline Load**	**5%**	**10%**	**20%**	**30%**
TwrBsFxt (kN)	183.33	-0.78	-1.50	-2.63	-3.45
TwrBsFyt (kN)	74.77	-8.53	-12.08	-14.36	-14.85
TwrBsFzt (kN)	49.52	-10.98	-13.34	-14.45	-14.50
TwrBsMxt (kN.m)	5026.92	-2.27	-3.50	-4.66	-5.26
TwrBsMyt (kN.m)	12477.63	-0.18	-0.34	-0.59	-0.76
TwrBsMzt (kN.m)	2691.89	-0.54	-0.82	-1.21	-1.55
RootFxb1 (kN)	190.36	-0.06	-0.09	-0.20	-0.32
RootFyb1 (kN)	304.82	-0.63	-0.76	-0.83	-0.82
RootFzb1 (kN)	332.67	-0.17	-0.21	-0.23	-0.24
RootMxb1 (kN.m)	6424.65	-1.76	-2.11	-2.27	-2.25
RootMyb1 (kN.m)	6675.36	-0.02	-0.06	-0.18	-0.28
RootMzb1 (kN.m)	127.52	-2.00	-1.92	-2.55	-2.46

5.6 Short-Term Damage Equivalent Loads for Offshore Wind Turbine

In this section, NREL 5 MW wind turbine model is established under the ocean by fixing the monopile to the ocean bottom in order to observe the system response and fatigue loads to the additional hydrodynamic load. The triggering reason for this analyses is that wind-wave misalignment induces fatigue damage for offshore wind turbines due to the fact that the misaligned waves causes large loads in side-side direction, which has very little damping compared to the fore-aft direction. In addition, metocean data reveals that wind and wave are often misaligned and thus misalignment should be taken into account during design procedure of offshore wind turbines.

For the analyses, the water depth is specified as 20 meters. The turbulence model is specified with 12 m/s mean speed. For the wave model, significant wave height H_s and peak spectral period T_p are given as 6 meters and 10 seconds, respectively. The direction of waves is iterated such that it is misaligned from the wind by 0, 30, 60, 90, 120, 150 and 180 degrees.

Figure 5.23 shows the effect of the wind/wave misalignment angle and structural damping ratio of the first tower fore-aft mode to the short-term DELs at the tower base. According to Figure 5.23a, around 20% load reductions are achievable with additional 30% structural damping ratio. However, the wind/wave misalignment does not have subtle effect on fore-aft tower loads. Considering Figure 5.23b, it is observed that the misalignment angle highly affects the lateral tower base shear loads, TwrBsFyt. It makes peak when the wind/wave misalignment angle becomes 90 degree; in other words, when wave hits the tower from lateral direction. In addition, the fore-aft modal damping does not have serious effect on reducing lateral damage equivalent shear load TwrBsFyt. For axial tower base force TwrBsFzt, the effect of wind/wave misalignment and structural damping ratio of the first fore-aft tower mode is negligible according to Figure 5.23c. As in the case of side-side shear force, the side-side bending moment is highly dependent on wind/wave misalignment angle and makes peak when wave is perpendicular to the wind, as illustrated in Figure 5.23d. When wind and wave is along X axis, in other words, wind/wave misalignment is 0 or 180 degrees, the side-side moments becomes minimum. In addition, the structural

damping ratio of the tower fore-aft mode does not have significant effect on side-side bending moment at the tower base, TwrBsMxt. For the fore-aft bending moment, additional fore-aft structural damping can provide considerable amount of load reduction for different wind/wave misalignment angles as illustrated in Figure 5.23e. Considering tower base torsion, according to Figure 5.23f, although additional structural damping reduce the loads, the reduction is negligible. In addition, the wind/wave misalignment angle does not alter torsion load remarkably, as expected.

The effect of wind/wave misalignment and structural damping ratio of the first tower side-side mode to the short-term DELs is illustrated in Figure 5.24 for the tower base. For the fore-aft shear loads and bending moments, no remarkable load reduction is achievable with additional side-side structural damping, according to Figure 5.24a and Figure 5.24e. Besides, tower base axial load and torsion are not effected significantly by wind/wave misalignment and structural damping, as illustrated in Figure 5.24c and 5.24f. On the other hand, predictably, there is huge amount of reduction in side-side shear forces and bending moments, as illustrated in Figure 5.24b and 5.24d, respectively. 70.6% shear force and 71.7% bending moment DEL reductions are provided with 30% side-side structural damping ratio. Reductions are very remarkable when considering the fact that lateral shear forces and bending moments may become critical and reach longitudinal shear forces and bending moments when the angle between main wind and wave approaches perpendicular, and the fact that lateral vibrations are less damped by aerodynamic forces, making lateral vibrations more serious. Therefore, it is recommended that a damping treatment to the first side-side mode of the tower would be helpful in increasing fatigue life of the offshore wind turbine system which encounters wind/wave misalignment during its lifetime.

Considering the effect of the wind/wave misalignment and structural damping ratio of the blade modes, it is observed that increase in any of the blade modal damping does not provide remarkable load reduction at the blade root, as represented in Figure 5.25 and 5.26. In addition, the wind/wave misalignment does not alter the blade loads significantly. Thus, a damping treatment for the blade modes would be unnecessary to increase the lifetime of the blades. However, additional blade damping may be helpful in reducing tower fatigue loads as in the case of onshore wind turbine system.

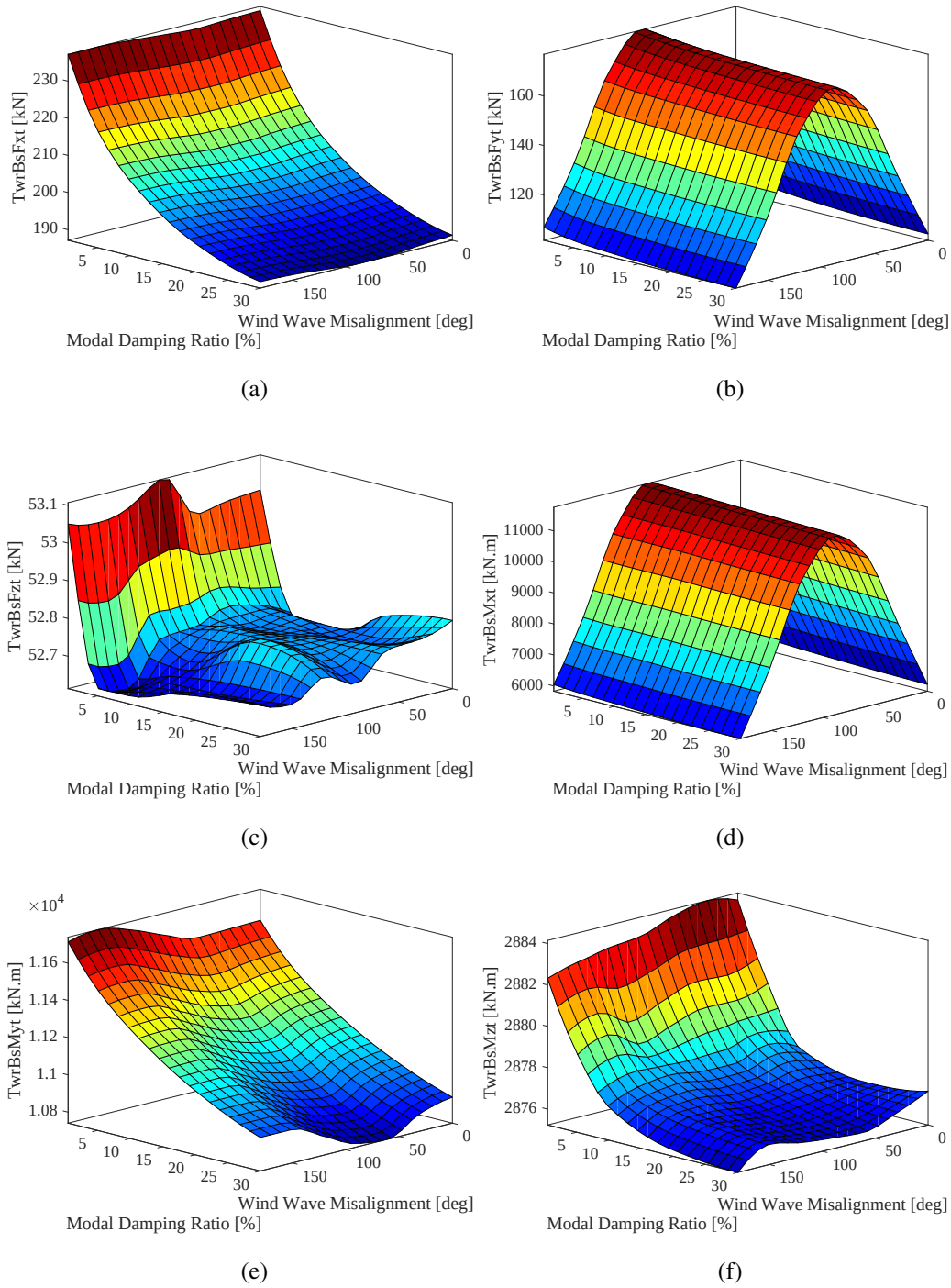

Figure 5.23: Damage Equivalent Loads for offshore wind turbine system with additional tower fore-aft modal damping

Generally speaking, for offshore wind turbines, damping increase for tower side-side modes provide high mitigation in side-side tower base loads. As wind/wave misalignment becomes 90 degree, the highest reduction is achieved. The second side-

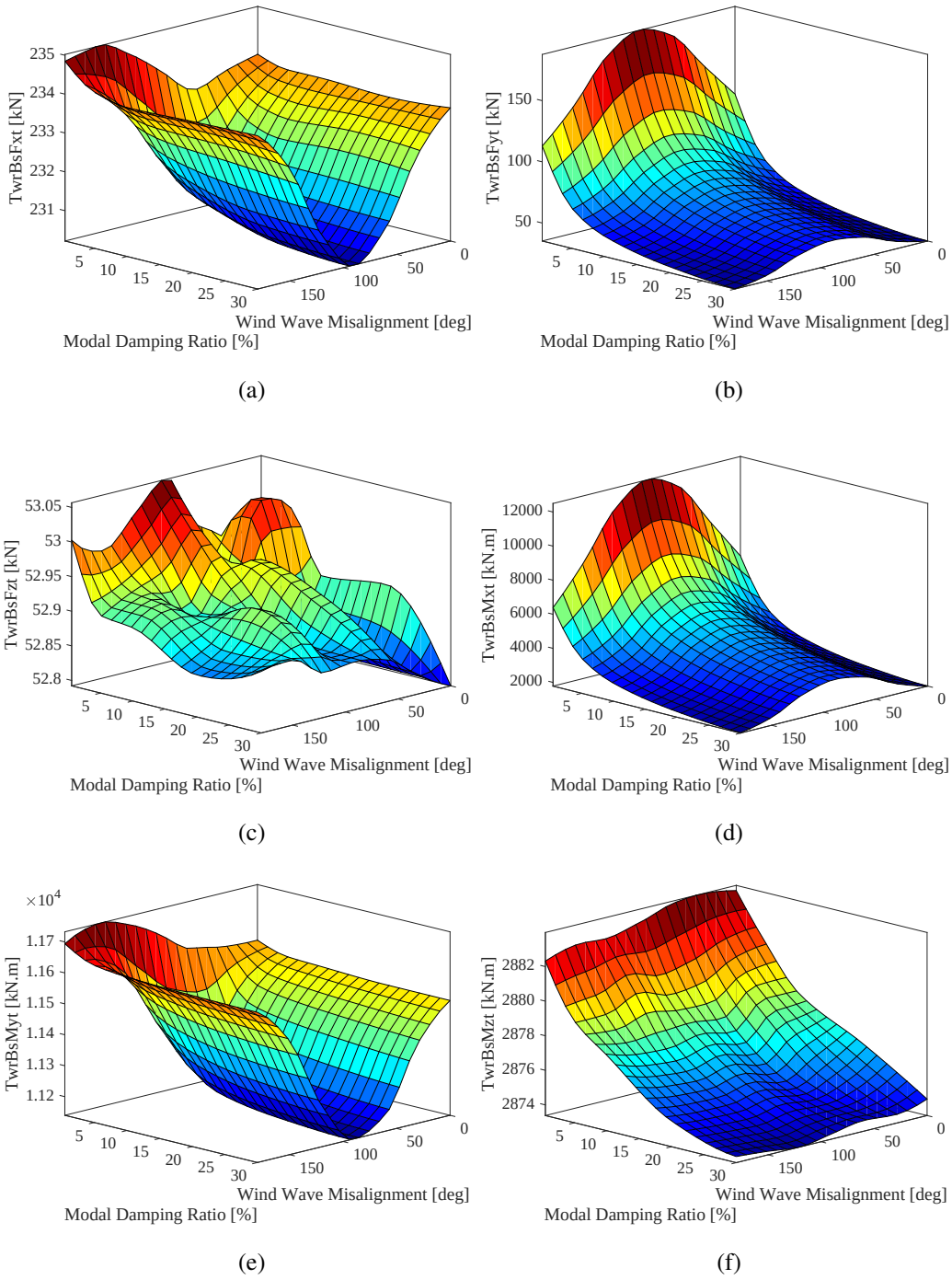

Figure 5.24: Damage Equivalent Loads for offshore wind turbine system with additional tower side-side modal damping

side tower mode also provides significant amount of reduction in side-side loads, yet with a lesser amount when compared to the first side-side tower mode. It is worth noting that wind/wave misalignment does not have significant effect on blade loads,

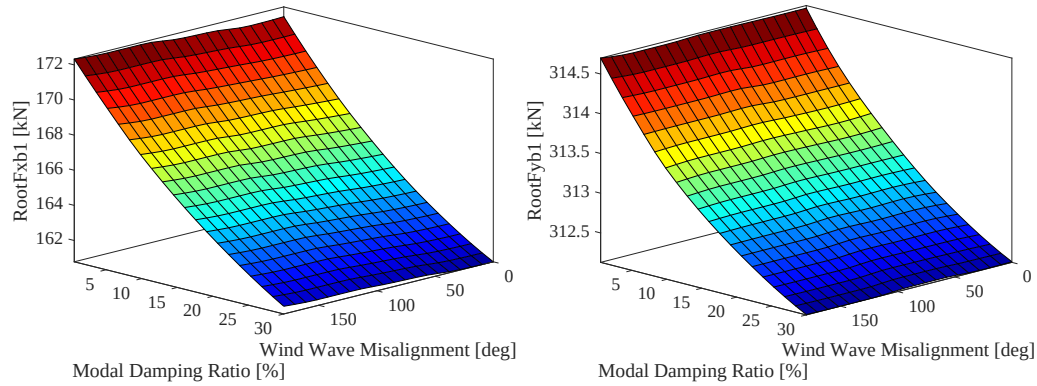

(a)

(b)

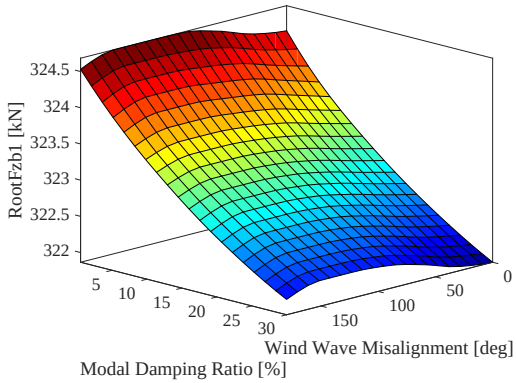

(c)

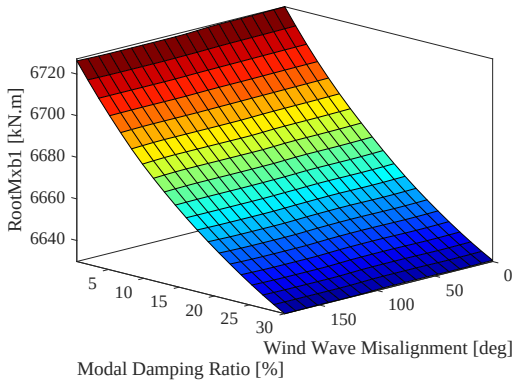

(d)

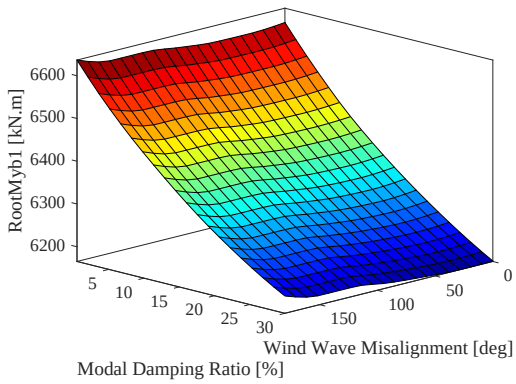

(e)

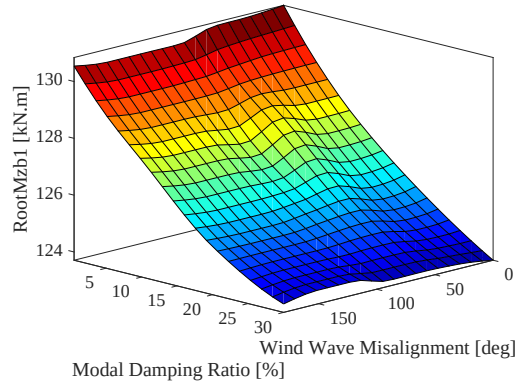

(f)

Figure 5.25: Damage Equivalent Loads for offshore wind turbine system with additional blade flapwise modal damping

as waves are applied to the tower base and thus vibrations are dampen out along the tower. However, blade damping provides mitigation in tower base loads as in the case of onshore wind turbine system. However, it requires a trade-off study between

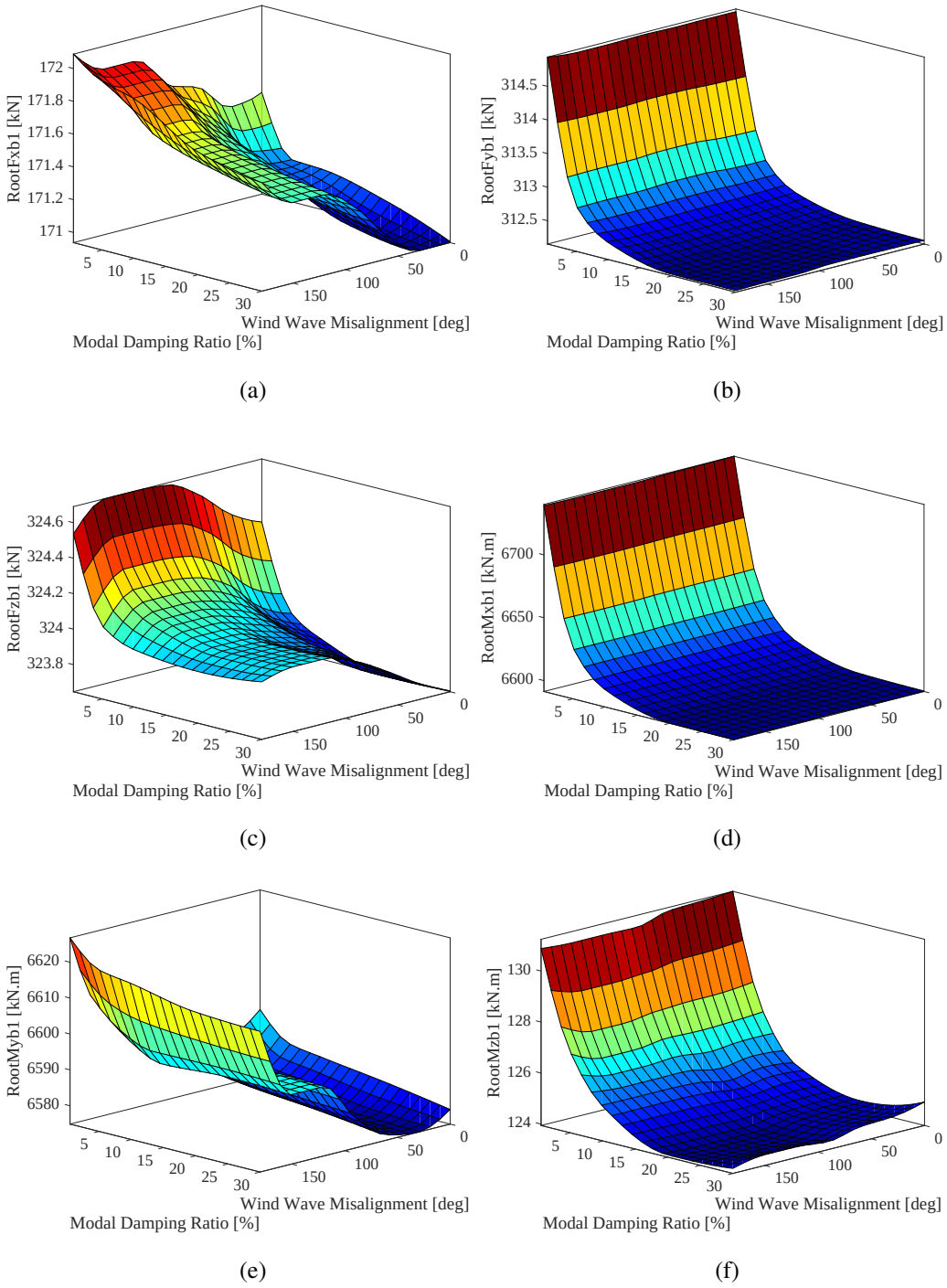

Figure 5.26: Damage Equivalent Loads for offshore wind turbine system with additional blade edgewise modal damping

damping treatment cost and tower fatigue life increase.

5.7 Gust Analysis

Gust is defined as a temporary change in the wind speed. According to IEC 61400-1, the wind turbine shall be designed to withstand the gusts. For a gust analysis, the ultimate loads are observed, rather than fatigue loads. In order to observe the characteristics of the wind turbine system to a gust and efect of structural damping for each tower and blade mode, a typical Design Load Case (DLC) of IEC 61400-1 is created by generating an Extreme Operating Gust (EOG) input at a 14 m/s steady wind speed, as represented in Figure 5.27. In this study, gust is applied only in X direction.

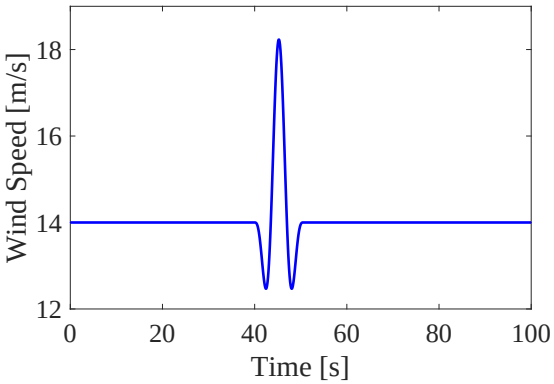

Figure 5.27: Extreme Coherent Gust input

Figure 5.28 and 5.29 shows the typical responses at the tower base and the blade root for no additional structural damping, respectively. According to the tower base responses, the fore-aft shear force and moment are highly affected by gust load and a sharp peak with following fluctuations are seen according to Figure 5.28a and 5.28e. They both make peak by increasing about 2.3 times the steady responses. Moreover, it is worth noting that when the gust passes, fore-aft responses become steady due to the fact that the cyclic load coming from the blade rotation is small compared to the load due to the steady wind input, thus buried under wind load. On the other hand, the side-side responses increase but does not show impulse response clearly, as illustrated in Figure 5.28b and 5.28d. In this case, the cyclic loads are dominant thus the impulse response behavior is not clearly seen. Considering axial force in 5.28c, it can be stated that although gust is discernible as an impulsive response, the change is negligible in percentage. On the other hand, the torsional moment increase is so

harsh that it increases to 800 kN.m and then returns to steady fluctuations between +300 kN.m and -200 kN.m.

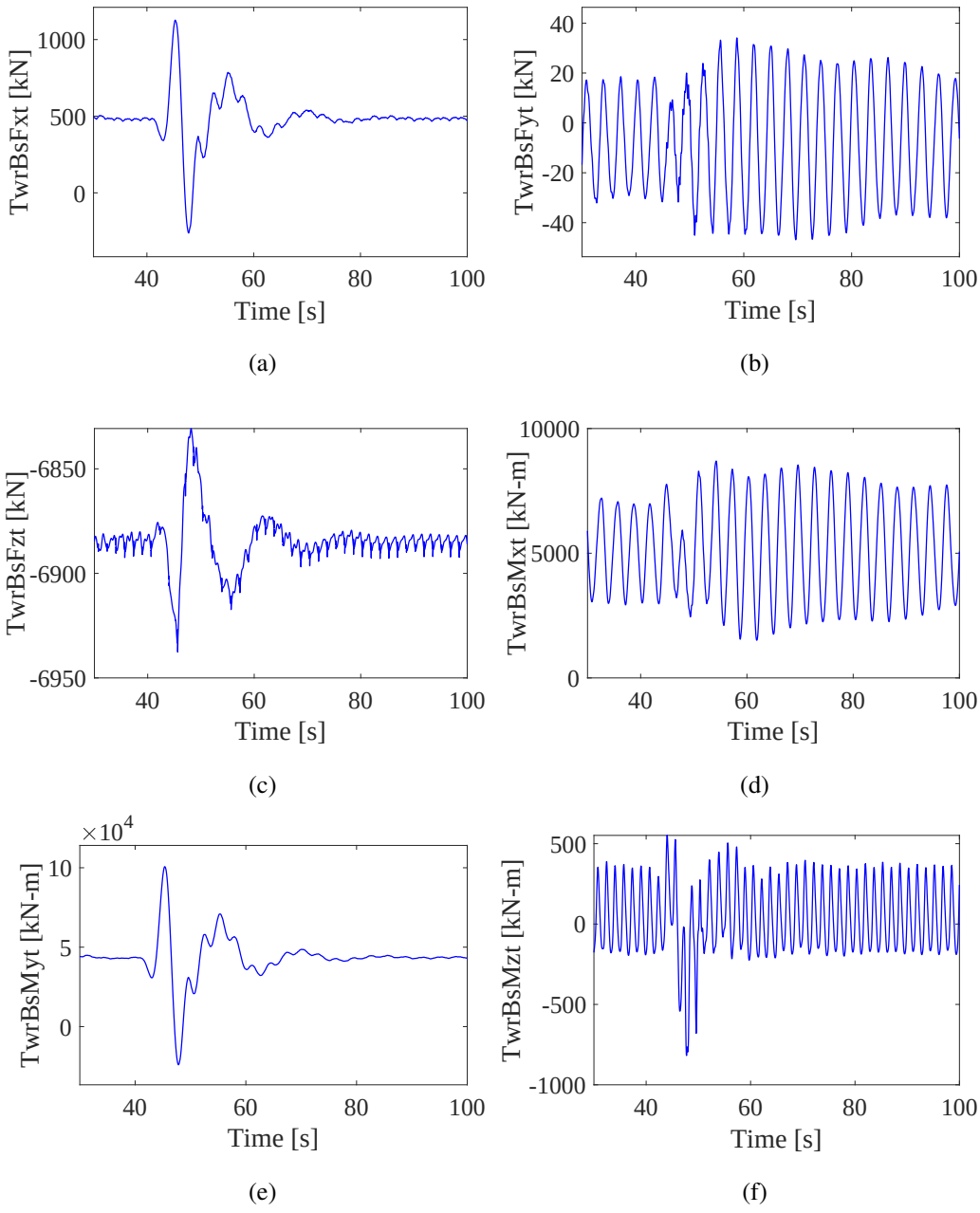

Figure 5.28: Tower base response to the Gust

Figure 5.29 reveals that the blade responses have cyclic fluctuations at 0.2 Hz corresponding to 12.1 rpm blade rotation in all directions. The flapwise shear force and moment responses show impulsive behaviour by increasing sharply to 378 kN and 12350 kN.m respectively as illustrated in Figure 5.29a and 5.29e. On the other hand,

the edgewise force and moment are not affected by gust considerably as shown in Figure 5.29b and 5.29d which is due to the fact that the gust is applied only in X direction and no coherent direction change exist. Considering axial force, it makes peak when gust hits due to the blade and tower interaction according to Figure 5.29c. The torsional moment makes dip in negative direction and it is not critical when considering the general trend of torsional moment, as plotted in Figure 5.29f.

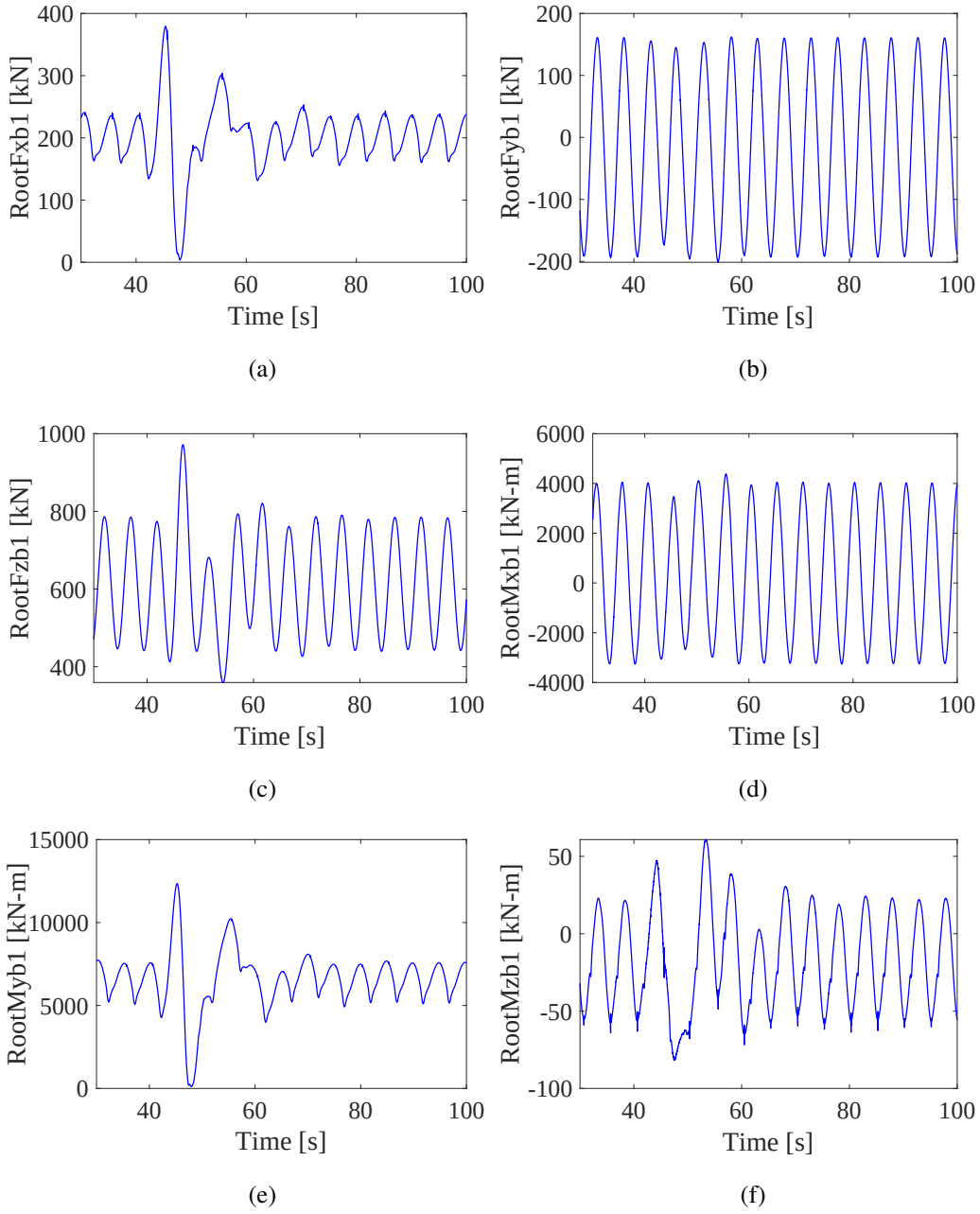

Figure 5.29: Blade root response to the Gust

CHAPTER 6

VISCOELASTIC LINK TREATMENT

6.1 Modeling Approach

6.1.1 Baseline Finite Element Model

In order to investigate the effectiveness of viscoelastic links on reducing vibrations, Finite Element Model (FEM) of the NREL 5 MW wind turbine is created in Nastran. In this model, the tower and blades are modeled by 2D quadrilateral and beam elements respectively with varying mass, inertia and stiffness properties to be compatible with FAST model. The nacelle and hub are modeled with lumped mass and rigidly connected to the blade roots and the tower top by using multi point constraint elements [80, 107]. The tower is rigidly connected to the ground from its base by neglecting the structural soil interaction. A schematic view of the wind turbine finite element model is illustrated in Figure 6.1.

In finite element model, the aerodynamic damping due to the incoming wind should be carefully modeled since it mainly drives the wind turbine responses especially in operating conditions. When the wind turbine is non-operating, which means the blades are stopped, it results insignificant aerodynamic damping. The aerodynamic damping is highly dependent on mean wind speed and varied between 4% and 9% for longitudinal modes in operating condition [108, 109]. For the lateral modes, the effect of aerodynamic damping to the structural response is much less effective and range from 0.08% to 1.43% [110]. In this study, the aerodynamic damping is modeled by creating a dashpot element at the top of the tower in the direction of wind which is fore-aft direction. With this element, 4.0% damping ratio is achieved for the first

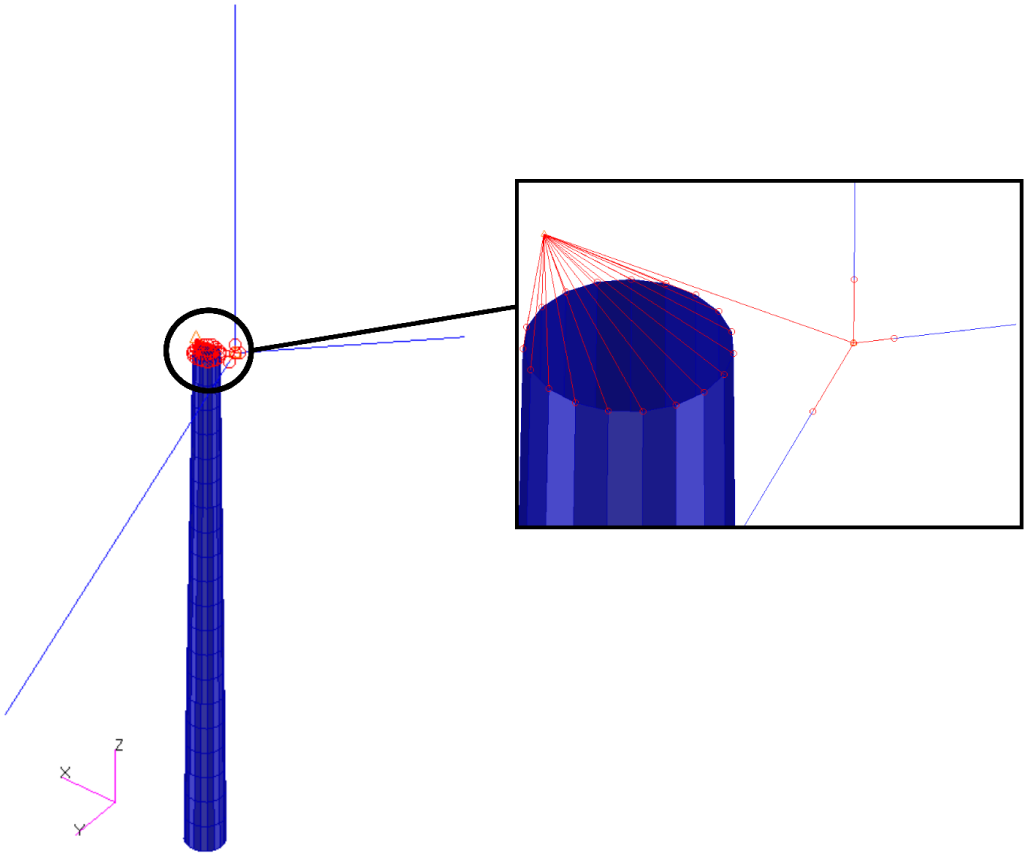

Figure 6.1: Finite Element Model of NREL 5 MW Wind Turbine

tower fore-aft mode for a main wind speed of 12.0 m/s.

As in aerodynamic damping, structural damping is also varied among the published studies and it is driven by the wind turbine size, connections and the material properties. According to IEC61400-1 [3], a structural damping ratio of 1.0% is recommended and it is applied for the finite element model for all the modes.

For above mentioned finite element model, in order to compare and corroborate the dynamic characteristics with FAST model, a modal analysis is made. Figure 6.2 shows the first five mode shapes of the finite element model. The first tower side-side and fore-aft tower modes have high contribution to the tower response and illustrated in Figure 6.2a and 6.2b, respectively. They are typical fundamental cantilever beam modes in which top displacement are observed at the tip. Figure 6.2c, 6.2d and 6.2e show the 1st blade asymmetric flapwise yaw, 1st blade asymmetric flapwise pitch and 1st blade collective flap modes, respectively. Although they are blade dominant

modes, there are slight amount of coupling with tower bending motion. In the studies related with blade vibrations, endeavors usually aim to reduce modal vibrations contributed by these blade modes.

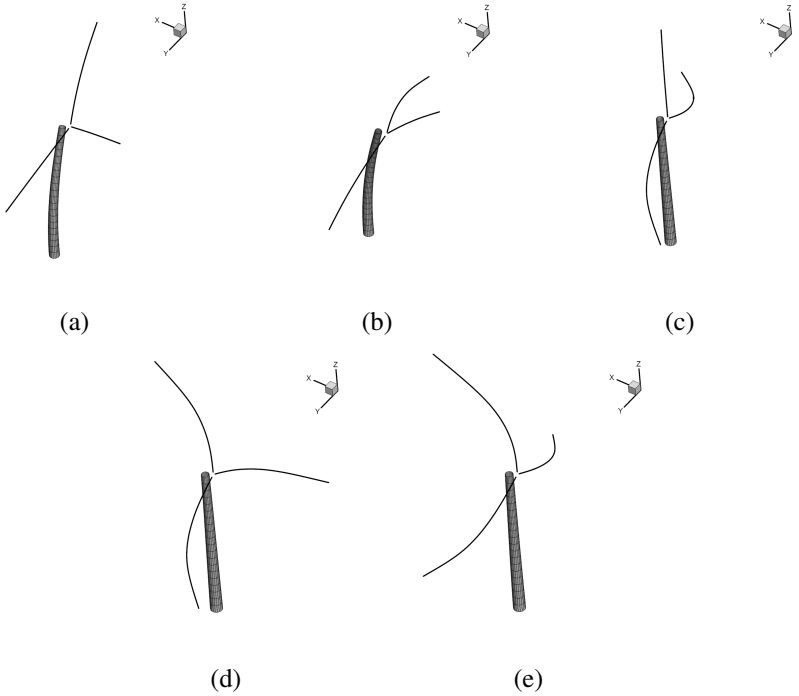

Figure 6.2: The first five mode shapes of the finite element model

The natural frequencies of FAST model and FEM are compared in Table 6.1. It is worth noting that above 3.0 Hz, FEM has buckling modes for the tower which are not observed in FAST model due to beam element formulation in FAST.

In order to investigate the effectiveness of viscoelastic link treatment in reducing vibrations, steady frequency response analysis is preferred since it allows to estimate modal damping ratios accurately. To determine the aerodynamic loads, steady CFD analysis is performed by using QBlade [111]. A steady wind speed with 12.0 m/s mean and 12.1 rpm blade rotation corresponding to the rated speed is simulated. An illustrative for QBlade analysis is shown in Figure 6.3.

Table 6.1: The natural frequencies of FAST model and FEM

Mode	**FAST [4]**	**FEM**
Tower 1st side-side	0.312	0.302
Tower 1st fore-aft	0.324	0.304
1st blade asymmetric flapwise yaw	0.666	0.624
1st blade asymmetric flapwise pitch	0.668	0.657
1st blade collective flap	0.699	0.686
1st blade asymmetric edgewise pitch	1.079	1.036
1st blade asymmetric edgewise yaw	1.090	1.053
2nd blade asymmetric flapwise yaw	1.934	1.848
2nd blade asymmetric flapwise pitch	1.922	1.704
2nd blade collective flap	2.021	1.952
2nd tower fore-aft	2.900	2.942
2nd tower side-side	2.936	2.797

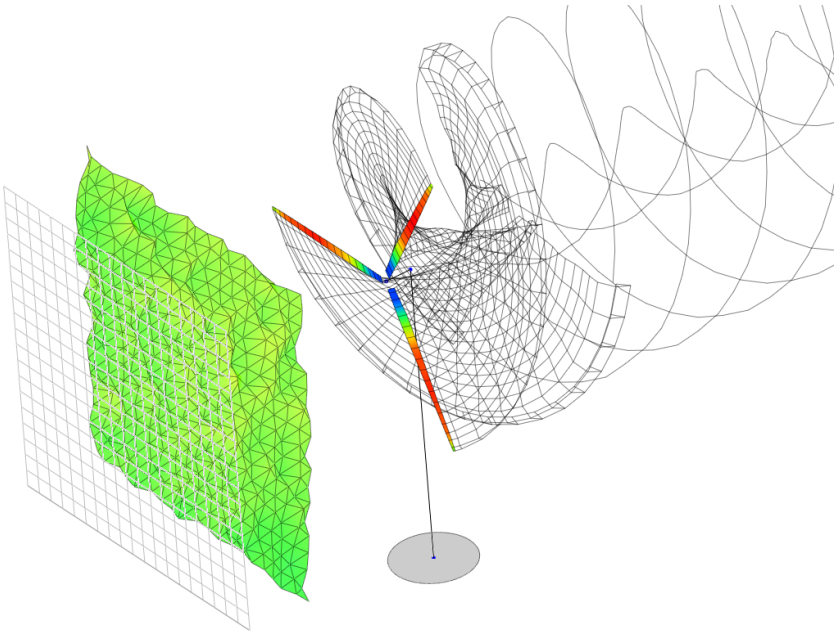

Figure 6.3: QBlade Analysis for 12 m/s wind speed

In Figure 6.4, the normal and tangential forces through the blade length are plotted.

For the tower loads, they are composed of drag and dependent on the mean velocity $V(z)$. To mathematically represent the wind velocity, a power law profile is used in

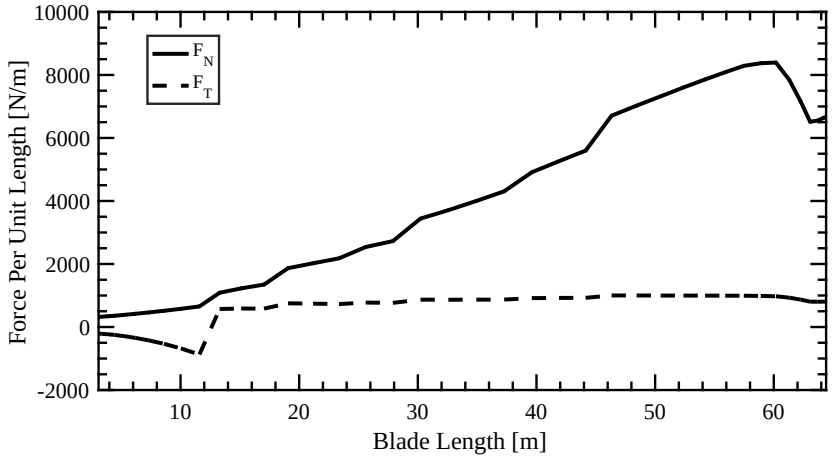

Figure 6.4: Normal and Tangential forces along the blade for 12.0 m/s wind speed

order to take into account the wind shear, defined by the following equation,

$$V(z) = V_r \left(\frac{z}{z_r} \right)^{\alpha} \tag{6.1}$$

Where V_r represents the reference wind speed measured at the nacelle altitude z_r, which is 87.6m in this study, and α is the roughness coefficient which can be taken as 0.14. The wind loads acting through the tower are then determined from,

$$F_{tower}(z) = \frac{1}{2} \rho_a C_{D,T} D\left(z\right) V_r^2\left(z\right) \tag{6.2}$$

Where $C_{D,T}$ is the drag coefficient of the tower, taken as 1.0 according to NREL database, $D(z)$ is the outer diameter of the tower at z, ρ_a is the air density.

The calculated blade and tower loads are mapped to the nodes of the FEM for frequency response analysis.

6.1.2 Viscoelastic Material Definition

Nastran has the capability of modeling viscoelastic materials with a complex frequency dependent material modulus as defined in Equation 2.9. Viscoelastic materials can be used in direct frequency analysis module of Nastran, called SOL 108.

Nastran requires the complex modulus in the form of $TR(f)$ and $TI(f)$ functions as defined in Equation 6.3 and 6.4, respectively. In these functions, g_{ref} is reference element damping, G_{REF} is reference modulus, g is overall structural damping, $G^{'}(f)$ is storage modulus and $G^{''}(f)$ is loss modulus. $TR(f)$ and $TI(f)$ are tabulated by using TABLED1 card. In Nastran, the complex material modulus is added to the global stiffness matrix in complex form rather than global damping matrix [112].

$$TR(f) = \frac{1}{g_{ref}} \left[\frac{G^{'}(f)}{G_{REF}} - 1 \right] \tag{6.3}$$

$$TI(f) = \frac{1}{g_{ref}} \left[\frac{G^{''}(f)}{G_{REF}} - g \right] \tag{6.4}$$

In this study, as the base viscoelastic material, LD-400 [86] is selected since it is effective and widely used. Various ambient temperatures, ranging from 0 to 20 degree Celcius are considered since the effectiveness of viscoelastic materials are highly dependent on the temperature. As an example, Figure 6.5 shows storage and loss modulus curves for 0 and 20 degree Celcius.

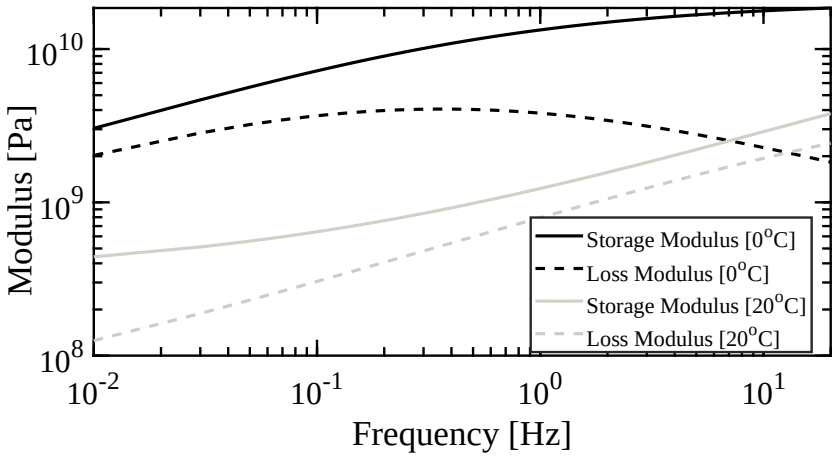

Figure 6.5: Material Modulus for LD-400

In viscoelastic materials, loss factor indicates the capability of dissipation. Figure 6.6 shows the loss factor for different temperatures between 0 and 20 degree Celcius. It can be stated that for the frequencies lower than 2.0 Hz and for 20 degree Celcius, LD-400 is more effective as it is in transition region. For 0 degree Celcius, LD-400

exhibits glassy behavior evinced by decrease in loss factor with frequency increase. For a typical wind turbine system, since the lower frequency modes are more critical for the tower, the dissipative characteristics of the selected viscoelastic materials should be higher for the lower frequencies. In addition, besides the loss factor, the storage modulus is also critical as it changes the stiffness of the structure thus the dynamic characteristics which may decrease the effectivity of the viscoelastic material.

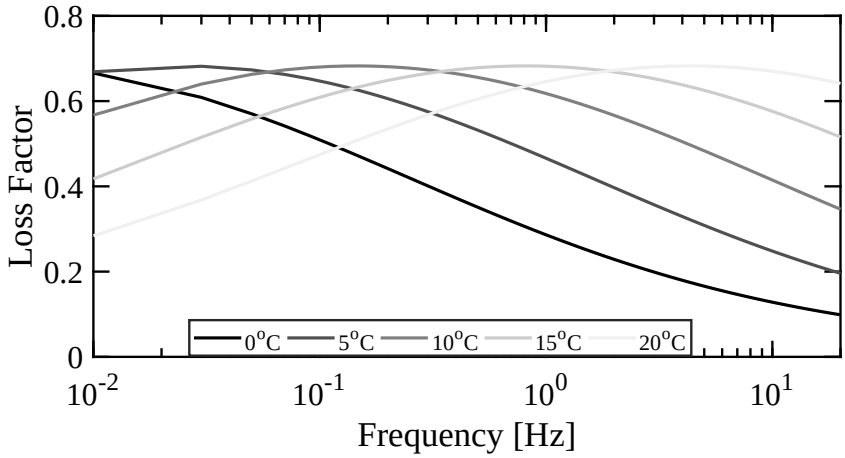

Figure 6.6: Loss factor for LD-400

6.1.3 Viscoelastic Link Modeling

As mentioned in Section 2.5.5, viscoelastic links, which link different locations of the tower are utilized to mitigate vibrations. They are implemented inside the wind turbine tower. As the tower is slender structure, the number of implemented viscoelastic links can be increased to increase dissipated mechanical energy. They can be implemented from the tower base to the tower top. In addition, they can be used at different locations inside the tower so as to alter the direction of strain developed in viscoelastic link to mitigate different modes.

Schematic representations of viscoelastic links inside a wind turbine tower are proposed in Figure 6.7.

As illustrated in Figure 6.7a, a viscoelastic link is rigidly connected to the inner wall

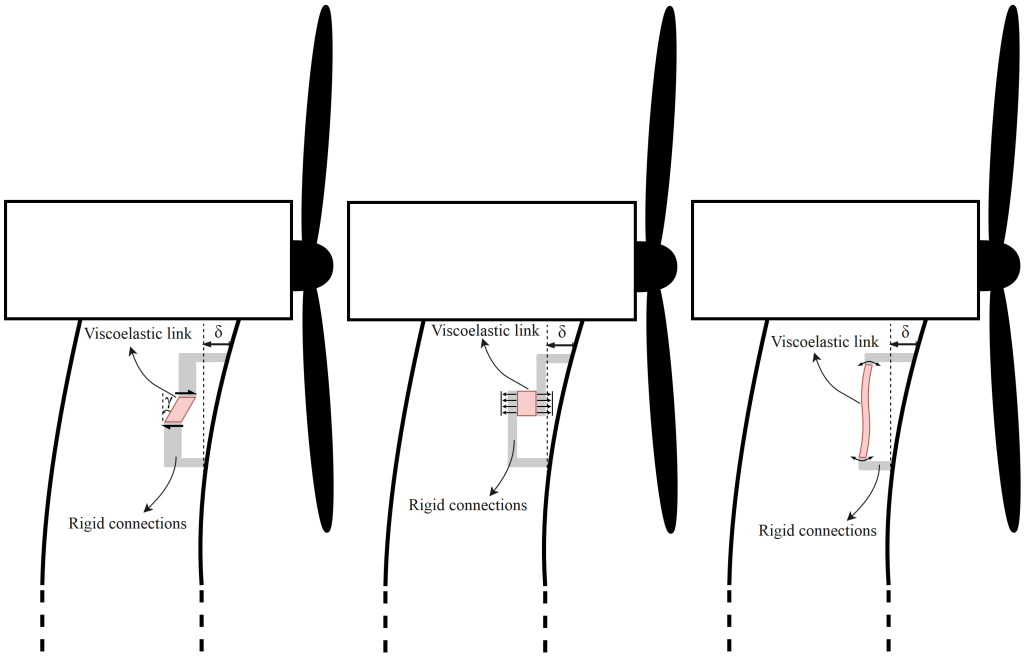

(a) Shear type (b) Tension-compression type (c) Bending type

Figure 6.7: Viscoelastic links

of the tower from upper and lower ends. As the tower bends, a relative motion will arise between upper and lower parts which causes shear strain in the viscoelastic link and consequently mechanical energy will be dissipated. With similar aspect, the tension-compression type viscoelastic link can be modeled by connecting it to the tower wall as illustrated in Figure 6.7b. With this type of link, mechanical energy is dissipated through normal strain. Besides, as viscoelastic link length increases with a length/thickness ratio greater than 10, it dissipates energy through bending as shown in 6.7c. Further dissipation mechanisms can be offered in this way provided that there is relative motion between connected locations. In addition, the number of viscoelastic links can be increased inside the tower in order to dissipate more mechanical energy.

The flexibility of the viscoelastic link design and implementation necessitates parametric approach to increase the effectiveness. Therefore, a Matlab code that works in collaboration with Nastran is created in which viscoelastic link thickness t, width w, height h, the offset distance between any two viscoelastic links x, the connection distance between upper and lower parts, l and the position of the center of viscoelastic

links, X_l, Y_l and Z_l are determined. The parameters are schematically shown in Figure 6.8 which is for a shear-type viscoelastic link layout. The type of the viscoelastic link can be changed by changing the connection nodes according to Figure 6.7.

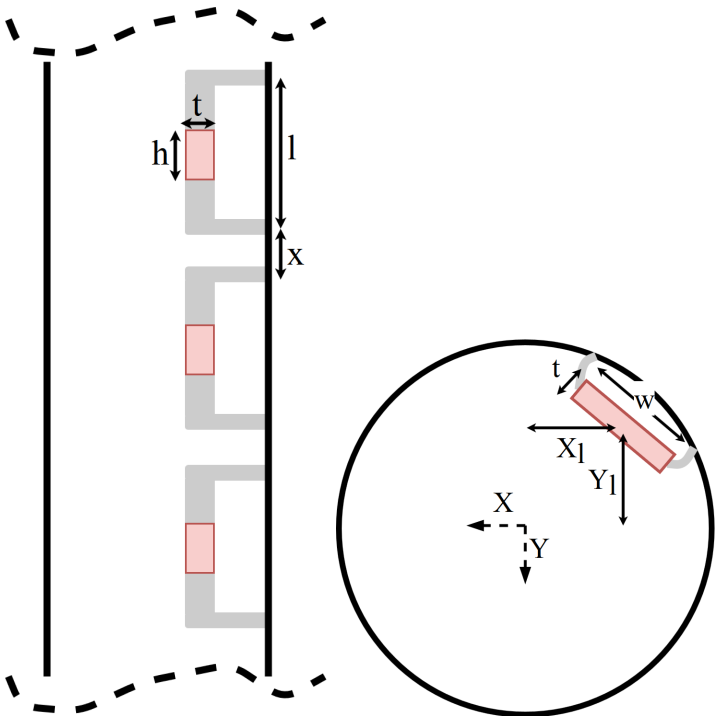

Figure 6.8: Viscoelastic link parameters

The Matlab code firstly creates the Bulk Data File (.bdf) including nodes and solid HEXA8 elements representing viscoelastic links in terms of the parameters given. Solid elements are automatically connected by a searching algorithm to the nearest tower nodes by RBAR elements representing rigid connection. It is worth pointing out that instead of the rigid connection elements, steel and aluminum beam elements are also investigated and observed that they behave rigid as well. Once the viscoelastic links are implemented between the tower top and base, Matlab code combines viscoelastic link input file with baseline FEM input file and performs a direct frequency response analysis for the given frequency interval. For the pre-determined critical nodes, the obtained frequency response functions are plotted graphically. Post-processing is performed on frequency response functions in order to obtain peak responses and modal damping ratios of the critical modes. The modal damping ratios are estimated by using peak-picking method. The process of creating viscoelastic link is shown in Figure 6.9.

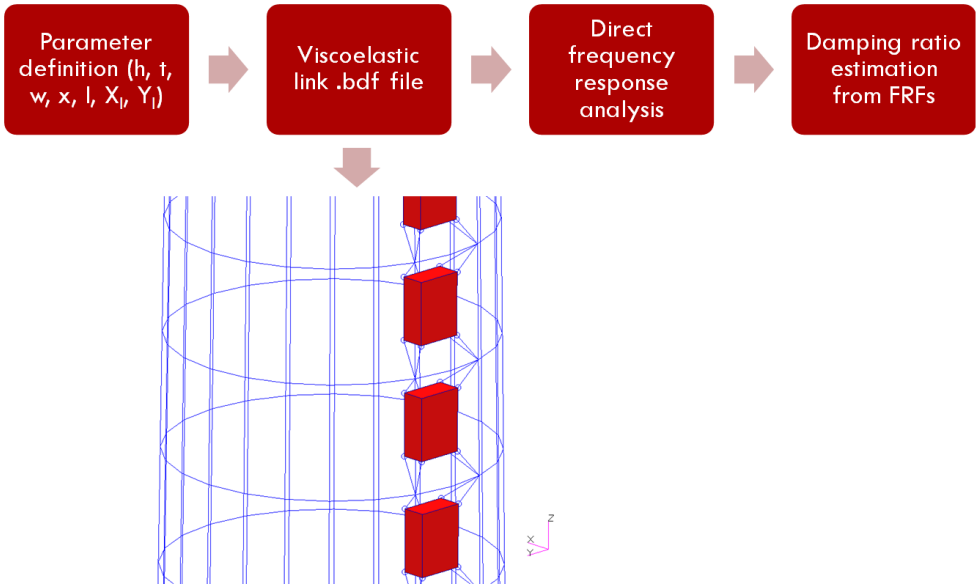

Figure 6.9: Process of analysis

6.2 Viscoelastic Link Simulations

6.2.1 Baseline FEM Simulation

Before estimating the effectiveness of viscoelastic links, the baseline finite element model without viscoelastic links is investigated in a direct frequency response analysis. The locations with the highest acceleration responses for the tower are determined between 0 and 5.0 Hz in Nastran. Figure 6.11 indicates the frequency response functions for the nodes selected as effectivity measurements along the tower. The modes which are critical and to be investigated in detail with the viscoelastic link treatment are numbered by their peaks. The selected critical modes and nodes are described in Table 6.2 and Table 6.3, respectively. The nodes are graphically shown in Figure 6.10.

In Figure 6.11, it is obvious that for X responses, the severest vibrations are exist at 0.68 Hz, corresponding to the 1st blade collective flap mode illustrated in Figure 6.2e. It is numbered as mode 2 in Table 6.2. Although there are additional blade dominant modes around 0.68 Hz, they are highly coupled with the tower, making fore-aft tower vibrations critical. Around 0.30 Hz, where the first tower fore-aft and side-side modes are exist, fore-aft tower vibrations represented by Node 572 and 432

Table 6.2: Description of the critical modes

Mode No.	**Description**
1	The first fore-aft tower mode
	The first side-side tower mode
2	The first blade collective flap mode
3	The second blade collective flap mode
4	The second side-side tower mode

Table 6.3: The critical nodes selected as effectivity measurements

Node ID	**Description**
Node 572	Tower top X acceleration response at z = 87.6 m
Node 568	Tower top Y acceleration response at z = 87.6 m
Node 432	Tower X acceleration response at z = 56.9 m
Node 428	Tower Y acceleration response at z = 56.9 m

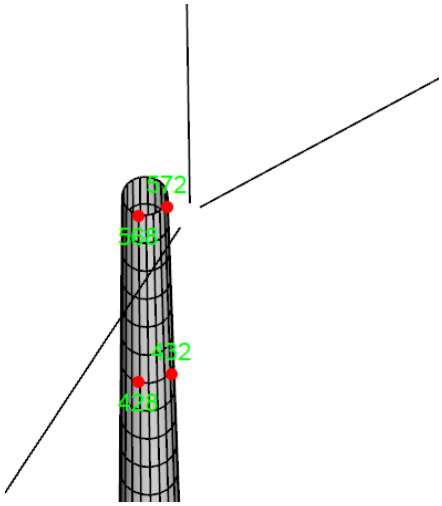

Figure 6.10: Critical node locations along the tower

are also critical but lower than those around 0.68 Hz. It may be due to the fact that the fore-aft aerodynamic damping provided by dashpot element is only applied at the tower top, resulting in higher damping in the tower compared to the blade modes. In addition, it is worth noting that around 1.95 Hz which corresponds to the 2nd blade collective flap mode, the fore-aft responses are high. 2nd tower fore-aft and side-side modes cause lower vibrations around 2.90 Hz compared to the first tower

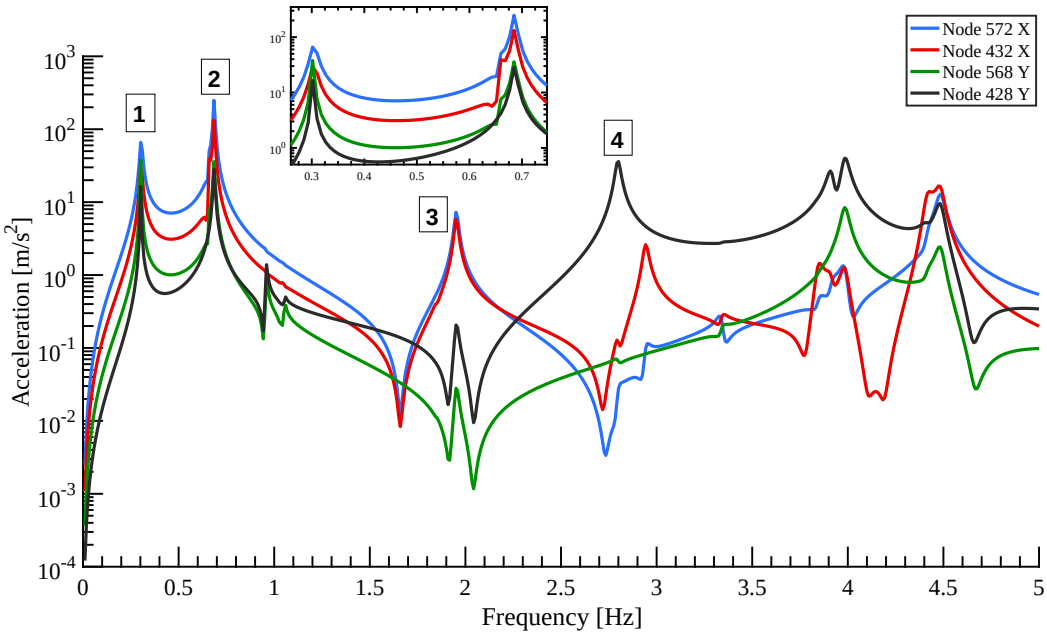

Figure 6.11: Frequency Response Functions for the nodes at the tower

bending modes. Considering the side-side responses indicated by Node 568 and 428, the first two spikes at 0.30 and 0.68 Hz are critical as well. At 2.80 Hz, the side-side acceleration response of Node 428 is also significant where tower second side-side mode couples with torsional movement of the body and the blade flapwise motion. It is worth pointing out that the first fore-aft and side-side tower modes are very close to each other around 0.30 Hz, making identification of each mode difficult. This is also valid for the first blade collective flap mode, where there are 3 blade modes between 0.66 and 0.69 Hz. Those closely spaced modes may complicate the identification of the modal damping ratios of each mode.

6.2.2 Parametric Viscoelastic Link Implementation

6.2.2.1 Influence of Viscoelastic Link Locations

Wind turbine monopile is large hollow cylinder in which there is enough space to implement viscoelastic links even though the ladder or lift used for maintenance purposes encloses significant space. The locations where viscoelastic links are connected determine the direction of the strain, hereby the direction of vibration dissipation. It

necessitates a parametric approach to investigate the effect of viscoelastic link position in mitigating vibrations.

In order to investigate the effect of viscoelastic link position inside the tower, a specific viscoelastic links are created with 0.5m width, w, 0.5m thickness, t and 4.38m height, h. By setting offset x to 0.05m, a viscoelastic link layout composed of 20 identical links is created between tower base to top. For different X_l and Y_l parameters shown in Figure 6.8, frequency responses analysis is made and the maximum acceleration responses at the critical nodes are investigated. Figure 6.12 illustrates the simulated viscoelastic link positions in the normalized coordinate system which is preferred to take into account the tapered cross section of the tower.

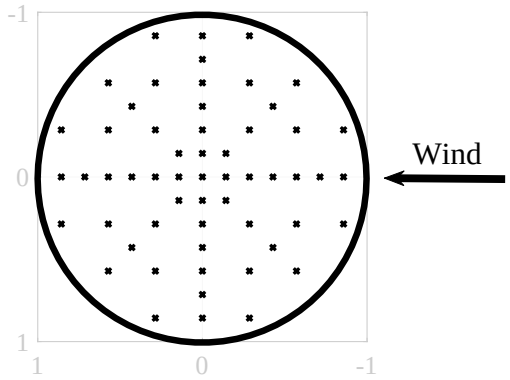

Figure 6.12: Investigated viscoelastic link positions

Figure 6.13 - 6.16 shows the contour plots indicating the maximum acceleration responses in X and Y directions for different viscoelastic link positions. While red regions indicate that the responses decrease when the viscoelastic links are implemented at that region, the blue regions indicate there is no change in acceleration responses. The investigated modes are numbered in Figure 6.11 with descriptions tabulated in Table 6.2. Figure 6.13 depicts the contour plot of maximum responses for the first mode that corresponds to the first tower bending mode for different nodes. It can be seen that Node 572 and Node 432 reflect the highest amount of decrease when viscoelastic links are placed to fore or aft wall of the tower as illustrated in Figure 6.13a and 6.13c. In addition, the amount of decrease is higher when viscoelastic links are implemented close to the wall. Settling the viscoelastic links in side-side walls is not effective in reducing fore-aft vibrations since side-side vibrations are lower

compared to fore-aft vibrations even though side-side aerodynamic damping is low. Considering the Y accelerations depicted in Figure 6.13b and 6.13d, the upper-right and lower-left settlement of viscoelastic links is highly effective in reducing Y responses, yet upper-left and lower-right positioning cause adverse affect. The reason can be stated by the fact that side-side responses are coupled with the fore-aft mode of the tower. Therefore, the position where the maximum reduction in Y direction is observed shifts from side-side wall to fore-aft wall slightly.

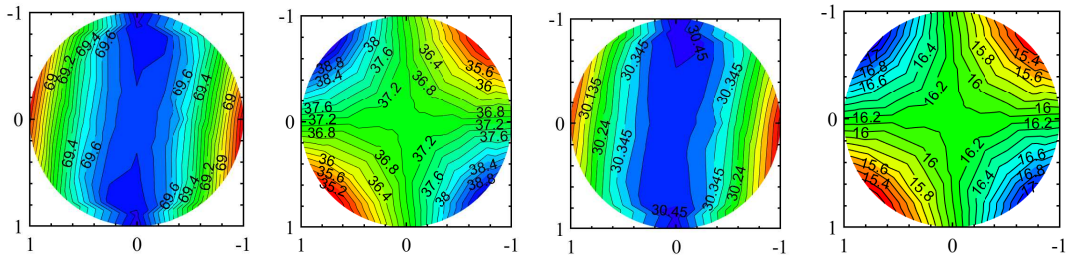

(a) Node 572 X (b) Node 568 Y (c) Node 432 X (d) Node 428 Y

Figure 6.13: Acceleration responses for Mode 1 for different viscoelastic link positions

Figure 6.14 shows the effectiveness of the position of viscoelastic links on mitigating the modal responses of the blade collective flap mode in which blade tip reaches to the highest deflection and blade motion is highly coupled with tower fore-aft bending. Considering the tower top accelerations illustrated in Figure 6.14a and 6.14b, fore and aft regions provide higher mitigation in fore-aft and side-side responses, yet side-side vibrations are not affected much with settlement of links to the side-side wall. For the responses of Node 432 and Node 428 in Figure 6.14c and 6.14d representing the tower 2nd bending mode, the relation between the viscoelastic link position and response is highly irrelevant. In addition, mitigations in Node 432 and Node 428 are low which reveal that the second tower bending modes do not contribute much to the total response.

Between 1.90 and 2.1 Hz, the second blade modes are dominant and cause remarkable vibration response for the tower top as depicted in Figure 6.11. In Figure 6.15a and 6.15b, although red and blue regions are extensively cleft for the tower top nodes, the mitigation levels are very low and can be neglected. Figure 6.15c and 6.15d also

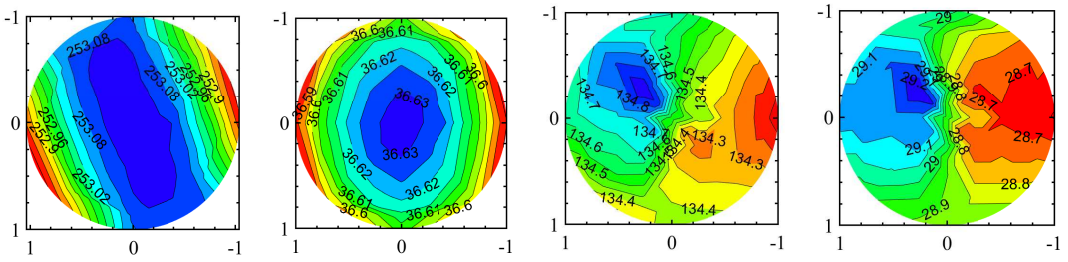

(a) Node 572 X (b) Node 568 Y (c) Node 432 X (d) Node 428 Y

Figure 6.14: Acceleration responses for Mode 2 for different viscoelastic link positions

indicate that the position of the viscoelastic link to the vibration mitigation is distinct and higher in fore of the tower wall, yet the amount of mitigation is lower. It can be stated that the effect of viscoelastic links to the tower vibrations around frequencies of the 2nd blade modes is negligible.

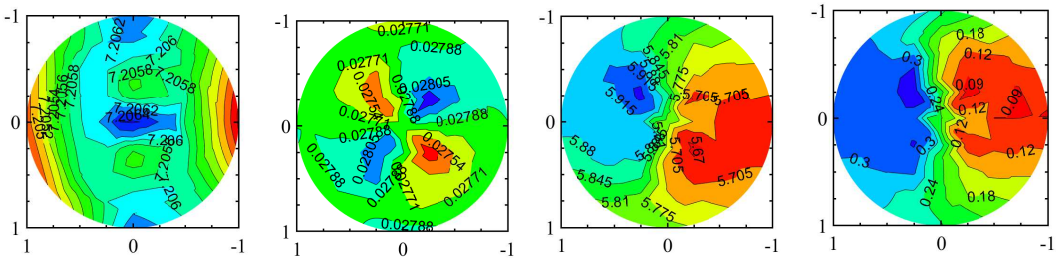

(a) Node 572 X (b) Node 568 Y (c) Node 432 X (d) Node 428 Y

Figure 6.15: Acceleration responses for Mode 3 for different viscoelastic link positions

The fourth critical mode corresponding to the fore-aft and side-side second tower bending modes are investigated in Figure 6.16. Although the vibrations in the tower top nodes are not effected with additional viscoelastic link treatment, nodes where the second mode of the tower cause the highest vibrations exhibit remarkable amount of vibration reduction especially for the red regions illustrated in Figure 6.16c and 6.16d. The fore-aft and side-side couplings are observable for the nodes where fore-aft responses are dominant as depicted in Figure 6.16a and 6.16c. For all 4 nodes, although distinct regions are exist for effective vibration mitigation, the levels are

very low except Node 428 in which by 12% of vibration can be mitigated when the links are settled to side-side wall as indicated with red region in Figure 6.16d.

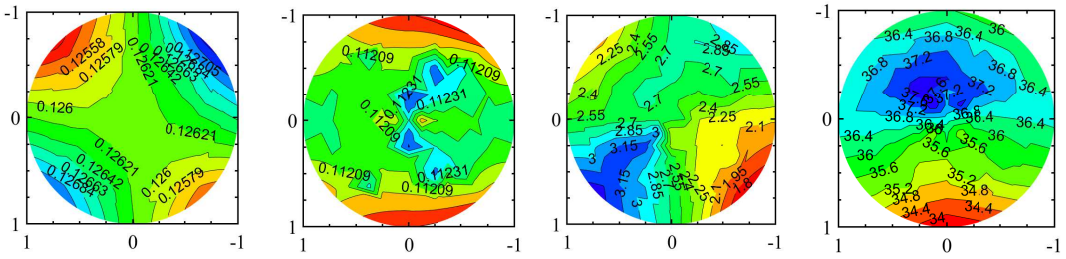

(a) Node 572 X (b) Node 568 Y (c) Node 432 X (d) Node 428 Y

Figure 6.16: Acceleration responses for Mode 4 for different viscoelastic link positions

In general, the viscoelastic links are more effective in reducing tower vibrations when they are installed closer to the tower wall especially for Mode 1 and Mode 2 which induce the highest responses in both fore-aft and side-side directions. For the fore-aft vibrations, placing the viscoelastic links in fore or aft directions is generally more suitable in reducing vibrations. On the other hand, for the first and the second tower side-side mode, side-side vibrations are slightly coupled with fore-aft vibrations, resulting that the optimum locations to mitigate side-side vibrations shift slightly to the fore or aft side of the inner tower wall.

In the following analyses, two viscoelastic link implementations are preferred as depicted in Figure 6.17 for fore-aft and side-side vibrations, respectively. While Case A is used to mitigate fore-aft vibrations, Case B is for side-side vibrations by taking into account the coupling between fore-aft and side-side vibrations. The distance between the origin of the tower and the viscoelastic link center is 1.70m at the tower top for both configurations. Considering the tapered cross section of the tower, it corresponds to 85% of the radius through the tower length.

6.2.2.2 Influence of Connection Distance, l

The effectiveness of viscoelastic link depends on the relative motion between upper and lower connection points. Therefore, the parameter l which is the connection

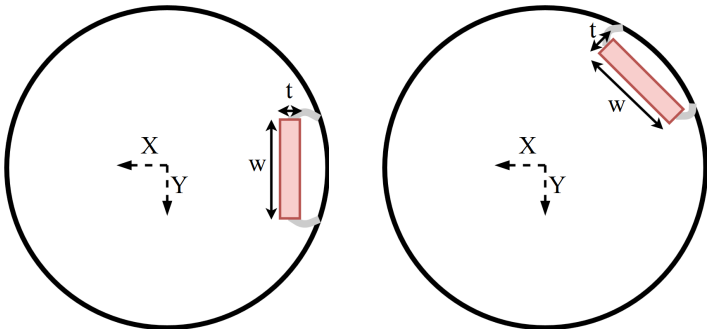

(a) Case A (b) Case B

Figure 6.17: Viscoelastic link implementations

distance between upper and lower parts of viscoelastic link is iterated by specifying h, t, w and x as 0.1m, 0.4m, 0.4m and 0.05m, respectively. The material is LD-400 and 20 degree Celcius ambient temperature is assumed. Figure 6.18 represents the modal damping ratios of the first fore-aft (F-A), side-side (S-S) tower bending and blade collective flap (BCF) bending modes for different l.

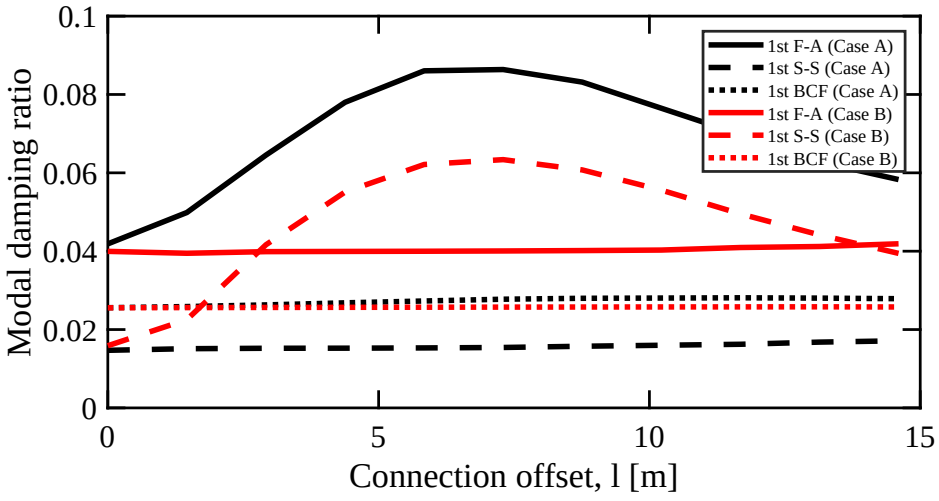

Figure 6.18: Modal damping ratios of the 1st tower fore-aft (F-A), side-side (S-S) and blade collective flap (BCF) modes with varying parameter l

The 1st fore-aft and side-side tower modal damping ratios increase when viscoelastic links are implemented as Case A and Case B, respectively. They both become maximum when l is around 5.5m and then decrease due to the abrupt change in modal frequencies of the tower first tower bending mode as l increases more. The modal

damping ratio of the 1st blade collective flap mode is not changed significantly for both Case A and Case B.

6.2.2.3 Influence of Geometric Parameters; t, h, w

In this section, the aspect of parametric design approach of viscoelastic links is enhanced with concern on the thickness, t, width, w, height, h and as schematically illustrated in Figure 6.8. For LD-400, the ambient temperature is assumed as 20 degree Celcius. Both Case A and Case B are considered for fore-aft and side-side tower modes as well as blade collective flap mode.

In order to determine the effectiveness of the viscoelastic links for different thickness in mitigating tower vibrations, a viscoelastic link scheme with varying thickness t is considered. l, w, h, x are specified as 5.0m, 0.4m, 0.1m and 0.05m, respectively. With these parameters, a total of 60 viscoelastic links are used from tower base to top. Figure 6.19 represents the modal damping ratios with varying t. The first fore-aft and side-side modal damping ratios increase up to a specific t value and then decreases slightly. The rest of the modes are not affected much with increase in viscoelastic link thickness.

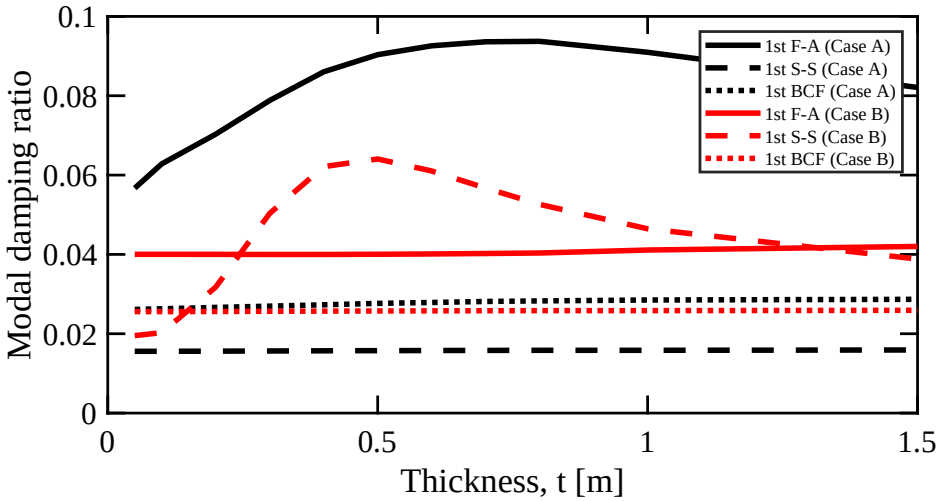

Figure 6.19: Modal damping ratios of the 1st tower fore-aft (F-A), side-side (S-S) and blade collective flap (BCF) with varying parameter t

Another parameter considered is h, which is the height of viscoelastic links. By

specifying width, w, t, x and l as 0.4m, 0.4m, 0.05m and 5.0m, h is iterated for Case A and Case B. Figure 6.20 shows the modal damping ratio of the three critical modes for varying height h. For lower h, viscoelastic links exhibit shear deformation rather than bending deformation. With shear deformation, since shear modulus is lower than the extensional modulus, they can more efficiently dissipate the vibrations and consequently modal damping ratios are higher. Expectedly, while Case A provides modal damping ratio increase for 1st F-A mode, Case B increases 1st S-S modal damping ratio.

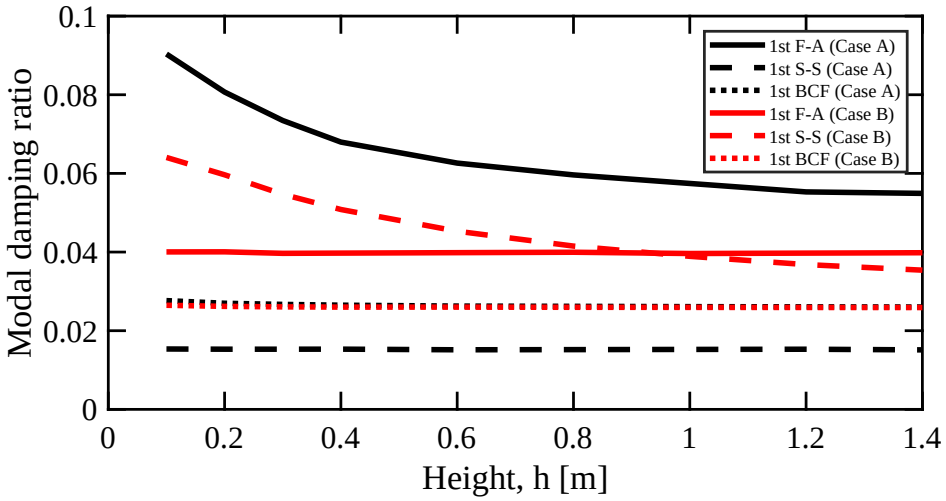

Figure 6.20: Modal damping ratios of the 1st tower fore-aft (F-A), side-side (S-S) and blade collective flap (BCF) modes with varying parameter h

Figure 6.21 illustrates the effect of width, w by specifying t, x, l and h as 0.4m, 0.05m, 5.0m and 0.1m, respectively. The first fore-aft and side-side modal damping ratios can increase up to 0.09 and 0.06, respectively. As width increases after a certain value, these modal damping ratios slightly decrease due to the change in the dynamic characteristics of the wind turbine tower causing fore-aft and side-side bending modes couple with the blade collective flap mode. It is worth noting that modal damping ratio of the blade collective flap mode increases slightly especially for Case A.

In general, by maintaining optimum parameters for viscoelastic link layout, the fore-aft and side-side modal damping ratios can be increased up to 0.09 and 0.06. For Case A and Case B, fore-aft and side-side tower vibrations are mitigated, respectively. However, the effect of viscoelastic links on blade collective flap mode is low and

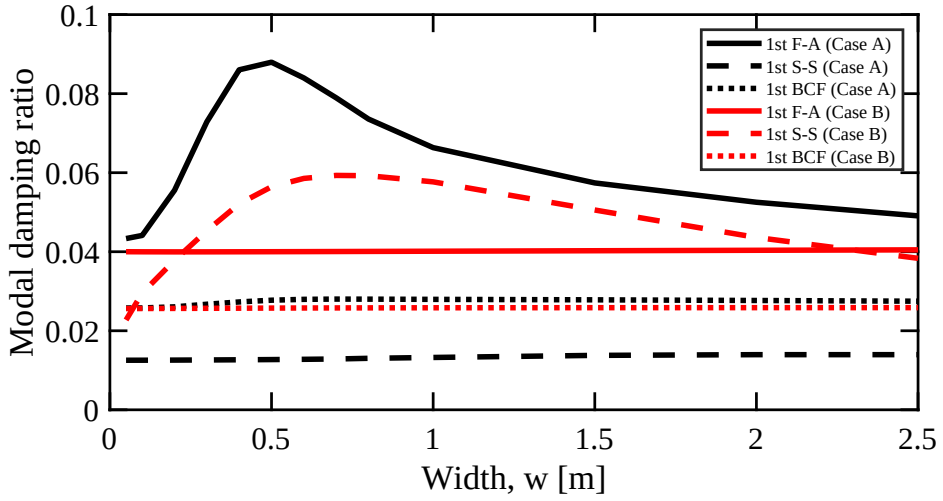

Figure 6.21: Modal damping ratios of the 1st tower fore-aft (F-A), side-side (S-S) and blade collective flap (BCF) modes with varying parameter w

negligible.

6.2.2.4 Effectiveness of Tension-Compression Type Link

In above mentioned analysis, the viscoelastic links are connected to exhibit shear deformation. With the same type of connection, when the parameter h increases, it starts to exhibit bending deformation. It can also be connected to the tower to make use of normal strain to dissipate vibrations as represented in Figure 6.7b.

In Figure 6.22, considering the material LD-400, the effectiveness of shear and tension-compression type viscoelastic links are compared for 0.4m w, 0.1m h, 5.84m l with varying thickness t. The tension-compression type links have worse effect compared to shear type links and the reason is they modify the modal characteristics of the structure as extensional modulus is higher than the shear modulus of LD-400. Therefore, it would be better to utilize shear modulus of LD-400 instead of extensional modulus.

To conclude, above results reveal that significant vibration reduction accompanied by structural damping ratio increase can be achieved with viscoelastic link treatment for the first tower fore-aft and side-side bending modes. In general, while implementing the viscoelastic links to the fore region of the tower wall provide structural damping

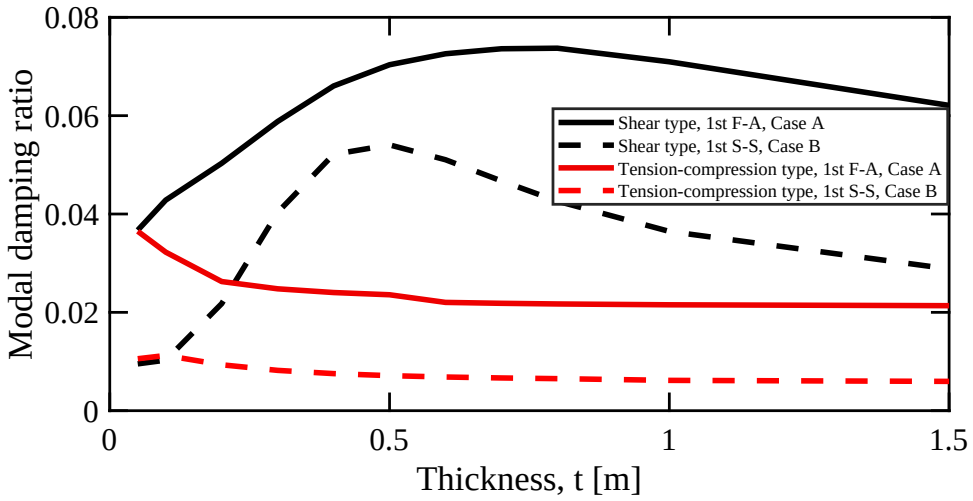

Figure 6.22: Modal damping ratios of the 1st tower fore-aft (F-A) and side-side (S-S) tower bending modes for shear and tension-compression type viscoelastic links

increase for fore-aft modes, implementing them between fore and side of the tower wall provide structural damping to side-side modes more effectively. It is worth noting that for the blade dominant modes such as blade flapwise and edgewise modes, viscoelastic link treatment does not provide significant reductions for tower vibrations contributed by these modes.

Considering the lifetime damage equivalent loads represented in Section 5.5, the increases in structural damping ratios for the first tower bending modes will come up with significant fatigue load reductions for the tower base, where maximum loads are observed. It can be also mentioned that the second tower side-side mode can be dampen out structurally with viscoelastic links and it results significant lifetime fatigue load reductions at the tower base. For the blade dominant modes, contribution of viscoelastic links is subtle yet better than nothing at all.

6.2.2.5 Influence of Ambient Temperature

As mentioned in the preceding sections, the dissipative and elastic characteristics of viscoelastic materials are highly dependent on the ambient temperature. As the average temperature of the wind turbine site may vary depending on the location and the season, the effectiveness of the viscoelastic links change. It may change from

day to night as well especially for the locations where high temperature deviations are observed between day and night. Generally speaking, a viscoelastic material performs the most efficient performance for the temperatures where it is in transition region. Therefore, it is a critical issue to select the optimum viscoelastic material for vibration dissipation.

Figure 6.23 illustrates the effect of different ambient temperatures for the four critical modes for Case A. According to Figure 6.23 (upper-left), as temperature increases, the effectiveness of the viscoelastic link increases significantly when t is above 0.5m. The reason may be due to frequency dependent characteristics of the viscoelastic links and the modal frequency change for the 1st fore-aft mode with thickness increase. Considering the 1st BCF, 2nd BCF and 2nd S-S modes, the effect of temperature differs. It can be stated that the elastic and dissipative characteristics of the LD-400 is highly sensitive to the temperature and frequency in investigated region.

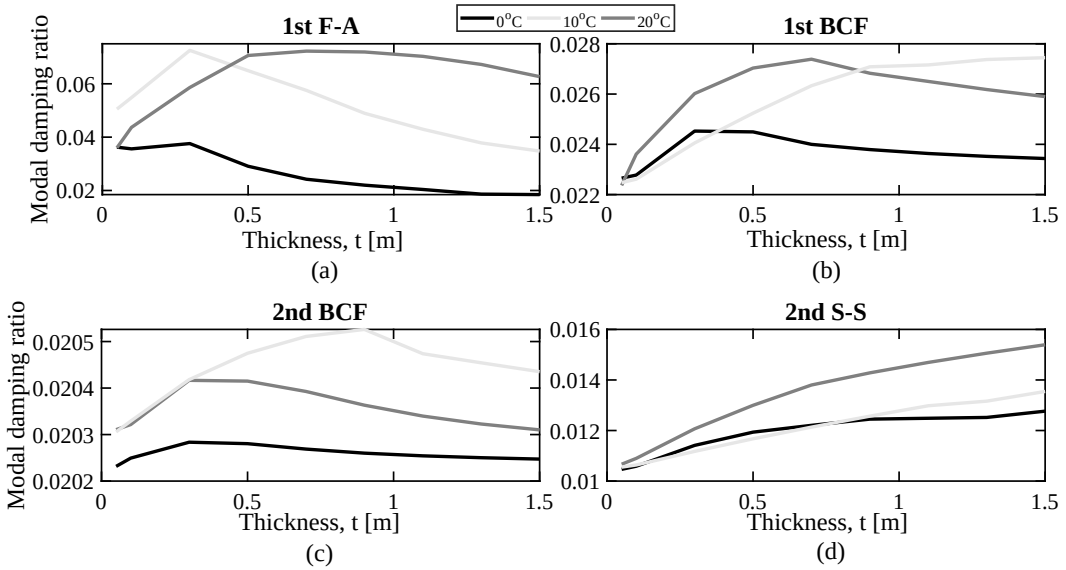

Figure 6.23: Modal damping ratios of the LD-400 for different temperatures and modes

CHAPTER 7

CONCLUSION

In this study, NREL 5 MW reference wind turbine is taken into account to investigate the effect of structural damping on fatigue loads and propose a vibration control approach by using viscoelastic links in order to increase fatigue life of the system. In this aspect, firstly aeroservoelastic model is developed in FAST. For the simulations, the environmental load conditions are defined according to the IEC 61400 standards. Firstly, a preliminary analyses are made in operating condition in order to estimate the modal characteristics of the wind turbine for different wind speeds and structural damping ratios. It is investigated that above 3 Hz, no significant excitations are observed since the turbulence is tended to excite lower frequencies better. The first tower fore-aft and side-side modes, as well as the first flapwise and edgewise blade modes are what contribute most to the total responses. In addition, the highest shear force and bending moments are measured at the tower base and blade root which make these locations critical in terms of fatigue damage. Therefore, the simulations mainly focus on the short-term and lifetime damage equivalent loads in these regions.

3 different wind turbine conditions are simulated which are pitch condition, parked condition and operating condition. In pitch condition, for different blade pitch angles, the effect of structural damping ratios of each modes are investigated for different wind speeds. It is observed that the blade pitch angle is dominant in determining both tower base and blade root loads. They generally decrease exponentially with increase in pitch angle. The structural damping increase in the side-side tower modes and blade edgewise modes have remarkable effect in the loads since they have low aerodynamic damping.

For parked condition in which the blades are feathered and the generator is stopped,

42% and 69% reductions can be provided around the rated wind speed in the fore-aft shear forces and bending moments with 30% structural damping for the first fore-aft tower mode. For 30% structural damping for the first side-side tower mode, the reductions are 40% and 42% for the side-side shear forces and bending moments, respectively. Considering the blade, the edgewise shear force and bending moment can be mitigated up to 28% and 42% with 30% structural damping for the first blade edgewise mode.

When the wind turbine system is operating, the aerodynamic damping increases and it results in decrease in the effectiveness of additional structural damping. Yet, up to 17% and 21% shear force and bending moment mitigation is provided in fore-aft direction at the tower base with the increase in fore-aft structural damping. For the side-side loads, by 31% and 54% reductions are achieved as they are less likely to be damped by the aerodynamic forces.

The short-term damage equivalent loads give information about the fatigue loads corresponding to the specific wind speed. In order to estimate the fatigue damage represented by the entire wind turbine system lifetime, the lifetime damage equivalent loads are calculated by extrapolating the short-term loads to the system lifetime using Weibull distribution. Up to 11.88% and 17.68% tower base shear force and bending moment mitigation in the fore-aft direction are provided with 30% tower fore-aft structural damping ratio. For the side-side tower loads, the reductions are 33.61% and 56.99% for the shear force and bending moment, respectively for 30% tower side-side structural damping ratio. It is worth pointing out that although increase in blade structural damping does not provide remarkable load mitigation for the blade root loads, it can help to reduce the tower base loads significantly.

In order to increase the structural damping ratios by using vibration control approaches, finite element model is created which exhibits approximately the same dynamic characteristics with FAST model. Viscoelastic links are implemented inside the tower wall. Parametric design approach is followed with the help of a tool created in Matlab which creates and implements the viscoelastic links inside the tower and makes frequency response analysis in Nastran. From the frequency response functions for the selected nodes, the modal damping ratios and maximum responses are obtained.

In the parametric approach, firstly optimum viscoelastic link positions are determined. It is observed that fore the tower fore-aft vibrations, implementing the viscoelastic links to the fore or aft of the tower wall provides higher vibration mitigation. On the other hand, for the side-side tower vibrations, as they are slightly coupled with fore-aft vibrations, the optimum viscoelastic link positions are somewhere between fore and side of the tower wall. In general, as viscoelastic links are closer to the tower wall, vibration mitigation becomes higher.

For the optimum viscoelastic link positions, thickness, width, height and offset parameters are iterated. For the first tower fore-aft bending mode, 0.094 structural damping ratio can be provided corresponding to 0.054 increase from the baseline model structural damping ratio. For the first side-side tower bending mode, structural damping ratio increases from 0.01 to 0.064 which is significantly high since the side-side modes are less damped by the aerodynamic load. It can be stated the optimum structural damping ratio increase can be obtained for w, 0.4m t, 0.4 x, 0.05m l, 5.0m and h, 0.1m. The blade related vibrations are not mitigated significantly as viscoelastic links are implemented inside the tower. In addition, the viscoelastic links exhibit more effective performance under shear deformation than tension-compression deformation. It is worth noting that the viscoelastic link height, which also determines the number of viscoelastic links along the tower wall, has significant effect on the vibration mitigation. In general, higher structural damping increase can be achieved with higher mass.

When the increase in damping ratios provided by viscoelastic links is compared with the reductions in damage equivalent loads in the equivalent FAST model for the same damping ratios, it is concluded viscoelastic links provide 6.2% and 9.5% reductions in the tower base fore-aft shear force and bending moments, respectively. Considering the tower base side-side loads, the reductions are 25.0% and 41.0% for shear force and bending moment.

The deficiency of using viscoelastic links in wind turbines arise from the temperature dependent characteristics of the viscoelastic materials. When the temperature changes in different seasons, the effectiveness of viscoelastic links may change. This deficiency can be handled by using different viscoelastic materials for different tem-

perature ranges. Heating can also be provided to optimize the temperature of viscoelastic materials. However, these remedies causes additional cost which should be investigated in the scope of another study.

As a future work, a comprehensive trade-off study can be made between the cost of added viscoelastic links and increase in fatigue life of the system. In addition, considering the effect of temperature, a more detailed optimization procedure can be performed in order to find optimum viscoelastic link parameters.

REFERENCES

[1] T. Corke and N. Robert, *Wind Energy Design*. CRC Press, 2018.

[2] GWEC, "Wind power capacity in the world," 2018. `http://gwec.net/global-figures/interactive-map/`, Accessed August 12, 2018.

[3] International Electrotechnical Commission, "IEC 61400-1 Ed.3: Wind turbines - Part 1: Design requirements," 2005.

[4] J. Jonkman, S. Butterfield, W. Musial, and G. Scott, "Definition of a 5-mw nrel reference wind turbine for offshore system development," Tech. Rep. NREL/TP-500-38060, National Renewable Energy Laboratory (NREL), 2009.

[5] J. F. Manwell, J. G. McGowan, and A. L. Rogers, *Wind Energy Explained: Theory, Design and Application*. John Wiley & Sonst, Ltd., 2010.

[6] GWEC, "Global Wind Energy Report: Annual Market Update 2017," p. 72, 2018.

[7] O. Edenhofer, R. Pichs-Madruga, and Y. Sokona, "Renewable energy sources and climate change mitigation," 2012.

[8] I. B. Løken and A. Kaynia, "Dynamic Response and Fatigue of Offshore Wind Turbines Effect of Foundation Type and Modelling Method Using Software FAST," no. June, 2017.

[9] N. C. Inc., "Offshore wind market and economic analysis, anual market assessment," February 22, 2013. `https://www1.eere.energy.gov/wind/pdfs/offshore_wind_market_and_economic_analysis.pdf`, Accessed August 12, 2018.

[10] W. Tong, *Wind Power Generation and Wind Turbine Design*. WIT Press, 2010.

[11] J. Van Der Tempel, *Design of Support Structures for Offshore Wind Turbines*. PhD thesis, 2006.

[12] J. G. Leishman, "Principles of helicopter aerodynamics," *Principles of Helicopter Aerodynamics*, 2000.

[13] M. Rahman, Z. C. Ong, W. T. Chong, S. Julai, and S. Y. Khoo, "Performance enhancement of wind turbine systems with vibration control: A review," *Renewable and Sustainable Energy Reviews*, vol. 51, pp. 43–54, 2015.

[14] B. Fitzgerald and B. Basu, "Cable connected active tuned mass dampers for control of in-plane vibrations of wind turbine blades," *Journal of Sound and Vibration*, 2014.

[15] R. Damiani, J. Jonkman, and G. Hayman, "SubDyn User's Guide and Theory Manual," no. March, 2015.

[16] J. M. Jonkman and J. Buhl, M. L., "FAST User' s Guide," 2005. NREL/EL-500-38230.

[17] B. J. Jonkman and J. M. Jonkman, "FAST v8.16.00a-bjj Change Log," 2016.

[18] C. Lalanne, *Mechanical Vibration and Shock Analysis: Third edition*. 2014.

[19] H. J. Sutherland, "On the Fatigue Analysis of Wind Turbines," 1999.

[20] Germanischer Lloyd, "Guideline for the certification of wind turbines," *Lloyd Rules and Guidelines, IV, Industrial Services*, 2010.

[21] M. Sathyajith and G. Philip, *Advances in Wind Energy Conversion*. Springer, 2011.

[22] US Department of Energy, "Increasing wind energy's contribution to U.S. electricity supply," July 2008. `https://www.nrel.gov/docs/fy08osti/41869.pdf`, Accessed August 12, 2018.

[23] P. C. Putnam, "Power from the wind," *Van Nostrand Reinhold, New York*, 1948.

[24] N. N, "Timeline: The history of wind power," *The Guardian*, October 2008.

[25] A. Schaffarczyk, *Understanding Wind Power Technology: Theory, Deployment and Optimization*. John Wiley & Sonst, Ltd., 2014.

[26] T. Kellner, "Making Waves: GE Unveils Plans To Build An Offshore Wind Turbine the Size Of A Skyscraper, the World's Most Powerful," 2018. https://www.ge.com/reports/making-waves-ge-unveils-plans-build-offshore-wind-turbine-size-skyscraper-worlds-powerful, Accessed December 16, 2018.

[27] M. Borg, A. Shires, and M. Collu, "Offshore floating vertical axis wind turbines, dynamics modelling state of the art. part i: Aerodynamics," *Renewable and Sustainable Energy Reviews*, vol. 39, pp. 1214 – 1225, 2014.

[28] S. Eriksson, H. Bernhoff, and M. Leijon, "Evaluation of different turbine concepts for wind power," *Renewable and Sustainable Energy Reviews*, vol. 12, no. 5, pp. 1419 – 1434, 2008.

[29] M. Islam, S. Mekhilef, and R. Saidur, "Progress and recent trends of wind energy technology," *Renewable and Sustainable Energy Reviews*, vol. 21, pp. 456 – 468, 2013.

[30] Det Norske Veritas, "DNV-OS-J101 Design of Offshore Wind Turbine Structures," *May*, 2014.

[31] T. von Kármán, "Progress in the Statistical Theory of Turbulence," *Proceedings of the National Academy of Sciences*, 1948.

[32] A. Davenport, "The dependence of wind loads on meteorological parameters," in *Proceedings International Research Seminar Wind effects on buildings and structures*, 1967.

[33] J. C. Kaimal, J. C. Wyngaard, Y. Izumi, and O. R. Coté, "Spectral characteristics of surface-layer turbulence," *Quarterly Journal of the Royal Meteorological Society*, 1972.

[34] J. R. Connell, "Turbulence spectrum observed by a fast-rotating wind turbine blade," *Report PNL-3426, Battelle Pacific Northwest Laboratory*, June 1, 1980.

[35] S. Beskhyroun, L. D. Wegner, and B. F. Sparling, "New methodology for the application of vibration-based damage detection techniques," *Structural Control and Health Monitoring*, vol. 19, no. 8, pp. 632–649.

[36] H. Zuo, K. Bi, and H. Hao, "Using multiple tuned mass dampers to control offshore wind turbine vibrations under multiple hazards," *Engineering Structures*, 2017.

[37] T. Burton, N. Jenkins, D. Sharpe, and E. Bossanyi, *Wind Energy Handbook, Second Edition*. 2011.

[38] J. G. Holierhoek, J. B. De Vaal, A. H. Van Zuijlen, and H. Bijl, "Comparing different dynamic stall models," *Wind Energy*, 2013.

[39] A. Choudhry, R. Leknys, M. Arjomandi, and R. Kelso, "An insight into the dynamic stall lift characteristics," *Experimental Thermal and Fluid Science*, 2014.

[40] L. Xiong, Z. Xianmin, L. Gangqiang, C. Yan, and Y. Zhiquan, "Dynamic Response Analysis of the Rotating Blade of Horizontal Axis Wind Turbine," *Wing Engineering*, 2010.

[41] P. J. Murtagh, B. Basu, and B. M. Broderick, "Mode acceleration approach for rotating wind turbine blades," *Proceedings of the Institution of Mechanical Engineers, Part K: Journal of Multi-body Dynamics*, vol. 218, no. 3, pp. 159–167, 2004.

[42] P. J. Murtagh, B. Basu, and B. M. Broderick, "Along-wind response of a wind turbine tower with blade coupling subjected to rotationally sampled wind loading," *Engineering Structures*, vol. 27, no. 8, pp. 1209–1219, 2005.

[43] P. J. Murtagh, A. Ghosh, B. Basu, and B. M. Broderick, "Passive control of wind turbine vibrations including blade/tower interaction and rotationally sampled turbulence," *Wind Energy*, vol. 11, no. 4, pp. 305–317, 2008.

[44] N. Caterino, "Semi-active control of a wind turbine via magnetorheological dampers," *Journal of Sound and Vibration*, vol. 345, pp. 1–17, 2015.

[45] K. Iijima, S. Srinivasamurthy, and M. Fujikubo, "Structural Modeling for Flexible Floating Offshore Wind Turbine," pp. 280–283, 2016.

[46] M. A. Lackner and M. A. , "Passive structural control of offshore wind turbines," *Wind Energy*, 2011.

[47] I. Prowell, A. Elgamal, and J. Jonkman, "FAST Simulation of Wind Turbine Seismic Response," *2010 European Wind Energy Conference (EWEC 2010)*, no. March, pp. 1–12, 2010.

[48] M. Hänler, U. Ritschel, and I. Warnke, "Systematic modelling of wind turbine dynamics and earthquake loads on wind turbines," *European Wind Energy Conference and Exhibition*, pp. 1–6, 2006.

[49] J. Li, Z. Zhang, and J. Chen, "Experimental Study on Vibration Control of Offshore Wind Turbines Using a Ball Vibration Absorber," *Energy and Power Engineering*, vol. 04, no. 03, pp. 153–157, 2012.

[50] X. Zhao and P. Maißer, "Seismic response analysis of wind turbine towers including soil-structure interaction," *Proceedings of the Institution of Mechanical Engineers, Part K: Journal of Multi-body Dynamics*, vol. 220, no. 1, pp. 53–61, 2006.

[51] Eurocode 8, "Design of structures for earthquake resistance," 2005.

[52] L. Moskowitz, "Estimates of the power spectrums for fully developed seas for wind speeds of 20 to 40 knots," *Journal of Geophysical Research*, 1964.

[53] K. Hasselmann, T. P. Barnett, E. Bouws, H. Carlson, D. E. Cartwright, K. Enke, J. A. Ewing, H. Gienapp, D. E. Hasselmann, P. Kruseman, A. Meerburg, P. Muller, D. J. Olbers, K. Richter, W. Sell, and H. Walden, "Measurements of Wind-Wave Growth and Swell Decay during the Joint North Sea Wave Project (JONSWAP)," *Ergnzungsheft zur Deutschen Hydrographischen Zeitschrift Reihe*, 1973.

[54] M. Damgaard, L. B. Ibsen, L. V. Andersen, and J. K. Andersen, "Cross-wind modal properties of offshore wind turbines identified by full scale testing," *Journal of Wind Engineering and Industrial Aerodynamics*, 2013.

[55] N. Tarp-Johansen, C. Mørch, L. Andersen, E. Christensen, and S. Frandsen, "Comparing sources of damping of cross-wind motion," in *European Offshore Wind 2009*, The European Wind Energy Association, 2009.

[56] G. M. Stewart and M. A. Lackner, "The impact of passive tuned mass dampers and wind-wave misalignment on offshore wind turbine loads," *Engineering Structures*, vol. 73, pp. 54–61, 2014.

[57] International Electrotechnical Commission, "Wind Turbines - Part 3: Design requirements for offshore wind turbines," tech. rep., 2009.

[58] S. Adhikari and S. Bhattacharya, "Dynamic analysis of wind turbine towers on flexible foundations," *Shock and Vibration*, vol. 19, no. 1, pp. 37–56, 2012.

[59] P. J. Murtagh, B. Basu, and B. M. Broderick, "Simple models for natural frequencies and mode shapes of towers supporting utilities," *Computers and Structures*, vol. 82, no. 20-21, pp. 1745–1750, 2004.

[60] S. Krenk, M. N. Svendsen, and J. Høgsberg, "Resonant Vibration Control of Three-Bladed Wind Turbine Rotors," *AIAA Journal*, vol. 50, no. 1, pp. 148–161, 2012.

[61] A. Staino and B. Basu, "Dynamics and control of vibrations in wind turbines with variable rotor speed," *Engineering Structures*, vol. 56, pp. 58–67, 2013.

[62] P. Martynowicz, "Vibration control of wind turbine tower-nacelle model with magnetorheological tuned vibration absorber," *JVC/Journal of Vibration and Control*, vol. 23, no. 20, pp. 3468–3489, 2017.

[63] I. Enevoldsen and K. J. Mørk, *Effects of a vibration mass damper in a wind turbine tower*, vol. 24. 1996.

[64] B. Fitzgerald and B. Basu, "Structural control of wind turbines with soil structure interaction included," *Engineering Structures*, vol. 111, pp. 131–151, 2016.

[65] L. Suja-Thauvin, J. R. Krokstad, and J. F. Frimann-Dahl, "Maximum Loads on a One Degree of Freedom Model-scale Offshore Wind Turbine," *Energy Procedia*, vol. 94, no. January, pp. 329–338, 2016.

[66] D. Matha, F. Lemmer, J. Galvan, H. Bredmose, and J. A. Norbeck, "Qualification of innovative floating substructures for 10MW wind turbines and water

depths greater than 50m Start date 2015-06-01 Deliverable D1 . 2 Wind turbine models for the design," pp. 1–29, 2015.

[67] S. Mazzoni, F. McKenna, M. H. Scott, and G. L. Fenves, "OpenSees command language manual," *Pacific Earthquake Engineering Research Center*, 2006.

[68] C. Roderick, "Vibration Reduction of Offshore Wind Turbines Using Tuned Liquid Column Dampers Vibration Reduction of Offshore Wind Turbines," no. September, 2012.

[69] M. Symans and M. Constantinou, "Semi active control systems for seismic protection of structures: a state-of-the-art review," *Eng Struct*, no. 21:469-87, 1999.

[70] G. Housner, L. Bergman, T. Caughey, A. Chassiakos, R. Claus, and S. Masri, "Structural control: past, present and future," *J Eng Mech*, no. 123:897971, 1997.

[71] J. P. D. Hartog, *Mechanical Vibrations*. McGraw-Hill, 1956.

[72] G. Stewart and M. Lackner, "Offshore wind turbine load reduction employing optimal passive tuned mass damping systems," *IEEE Transactions on Control Systems Technology*, vol. 21, no. 4, pp. 1090–1104, 2013.

[73] M. A. M. Shzu, M. Morais, Z. J. G. Del Prado, and S. Avila, "Finite element analysis of a wind turbine tower with a pendulum tuned mass damper," 02 2015.

[74] K. Bi and H. Hao, "Using pipe-in-pipe systems for subsea pipeline vibration control," *Engineering Structures*, 2016.

[75] J. Arrigan, V. Pakrashi, B. Basu, and S. Nagarajaiah, "Control of flapwise vibrations in wind turbine blades using semi-active tuned mass dampers," *Structural Control and Health Monitoring*, 2011.

[76] B. Fitzgerald, B. Basu, and S. R. K. Nielsen, "Active tuned mass dampers for control of in-plane vibrations of wind turbine blades," *Structural Control and Health Monitoring*, vol. 20, no. 12, pp. 1377–1396.

[77] Z. Zhang, A. Staino, B. Basu, and S. R. Nielsen, "Performance evaluation of full-scale tuned liquid dampers (TLDs) for vibration control of large wind turbines using real-time hybrid testing," *Engineering Structures*, vol. 126, pp. 417–431, 2016.

[78] S. Colwell and B. Basu, "Tuned liquid column dampers in offshore wind turbines for structural control," *Engineering Structures*, vol. 31, no. 2, pp. 358–368, 2009.

[79] Z. Zhang, J. Li, S. R. Nielsen, and B. Basu, "Mitigation of edgewise vibrations in wind turbine blades by means of roller dampers," *Journal of Sound and Vibration*, vol. 333, no. 21, pp. 5283–5298, 2014.

[80] T. Gentils, L. Wang, and A. Kolios, "Integrated structural optimisation of offshore wind turbine support structures based on finite element analysis and genetic algorithm," *Applied Energy*, vol. 199, pp. 187–204, 2017.

[81] C. L. Bottasso, A. Croce, F. Gualdoni, and P. Montinari, "Load mitigation for wind turbines by a passive aeroelastic device," *Journal of Wind Engineering and Industrial Aerodynamics*, vol. 148, pp. 57–69, 2016.

[82] J. C. Marín, A. Barroso, F. París, and J. Cañas, "Study of fatigue damage in wind turbine blades," *Engineering Failure Analysis*, vol. 16, no. 2, pp. 656–668, 2009.

[83] K. A. Matis, *Structural Optimization of a Horizontal Axis Wind Turbine Blade*. PhD thesis, 2016.

[84] G. Freebury and W. Musial, "Determining equivalent damage loading for full-scale wind turbine blade fatigue tests," in *2000 ASME Wind Energy Symposium*, 2000.

[85] G. Hayman, "MLife Theory Manual for Version 1.00," no. October, p. 12, 2012.

[86] A. Nashif, D. Jones, J. Henderson, and J. HENDERSON, *Vibration Damping*. Wiley-Interscience publication, Wiley, 1985.

[87] C. Sun and Y. Lu, *Vibration Damping of Structural Elements*. New Immigrants, Prentice Hall PTR, 1995.

[88] C. D. Johnson and D. A. Kienholzt, "Finite Element Prediction of Damping in Structures with Constrained Viscoelastic Layers," *AIAA Journal*, vol. 20, no. 9, pp. 1284–1290, 1982.

[89] G. Barone, M. Di Paola, F. Lo Iacono, and G. Navarra, "Viscoelastic bearings with fractional constitutive law for fractional tuned mass dampers," *Journal of Sound and Vibration*, 2015.

[90] D. Adams, "Efficient finite element modeling of thin-walled structures with constrained viscoelastic layer damping," 2009.

[91] A. Manjock, "Evaluation report: Design codes FAST and ADAMS for load calculations of onshore wind turbines. Report No. 72042," *Humburg Germany: Germanischer Lloyd WindEnergie GmbH*, May 26, 2005.

[92] G. S. Bir, "User's Guide to BModes (Software for Computing Rotating Beam Coupled Modes)," *National Renewable Energy Laboratory*, no. September, 2007.

[93] Z. Fu and J. He, *Modal Analysis*. Elsevier, 2001.

[94] T. R. Kane and D. A. Levinson, *Dynamics: Theory and Applications*. McGraw-Hill, 1985.

[95] B. J. Jonkman and J. Buhl, M. L., "TurbSim User's Guide," no. September, 2006.

[96] J. M. Jonkman, G. J. Hayman, B. J. Jonkman, and R. R. Damiani, "AeroDyn v15 User's Guide and Theory Manual," 2015.

[97] M. O. L. Hansen, *Aerodynamics of Wind Turbines*. 2011.

[98] J. M. Jonkman, A. N. Robertson, and G. J. Hayman, "HydroDyn User's Guide and Theory Manual," *National Renewable Energy Laboratory*, 2015.

[99] N. Troldborg and J. Sørensen, "Atmospheric stability-dependent infinite wind-farm models and the wake -decay coefficient," *Wind Energy*, vol. 17, no. April 2013, pp. 657–669, 2014.

[100] S. D. Downing and D. F. Socie, "Simple rainflow counting algorithms," *International Journal of Fatigue*, 1982.

[101] B. R. Resor, "Definition of a 5MW/61.5 m wind turbine blade reference model," *Albuquerque, New Mexico, USA, Sandia National Laboratories, SAND2013-2569 2013*, no. SAND2013-2569, p. 53, 2013.

[102] X. Chen, W. Zhao, X. L. Zhao, and J. Z. Xu, "Failure test and finite element simulation of a large wind turbine composite blade under static loading," *Energies*, vol. 7, no. 4, pp. 2274–2297, 2014.

[103] J. C. Berg and B. R. Resor, "Numerical Manufacturing and Design Tool (NuMADv2.0) for Wind Turbine Blades: User's Guide," 2012. SAND2012-7028.

[104] K. Thomsen, J. T. Petersen, E. Nim, S. Øye, and B. Petersen, "A Method for Determination of Damping for Edgewise Blade Vibrations," *Wind Energy*, 2000.

[105] Z. Zhang, B. Basu, and S. R. K. Nielsen, "Tuned liquid column dampers for mitigation of edgewise vibrations in rotating wind turbine blades," *Structural Control and Health Monitoring*, vol. 22, no. 3, pp. 500–517.

[106] D. Eggleston and F. Stoddard, *Wind turbine engineering design*. Van Nostrand Reinhold, 1987.

[107] J. L. Chen and C. T. , "Spherical tuned liquid damper for vibration control in wind turbines," *JVC/Journal of Vibration and Control*, vol. 21, no. 10, pp. 1875–1885, 2015.

[108] R. Rezaei, P. Fromme, and P. Duffour, "Fatigue life sensitivity of monopile-supported offshore wind turbines to damping," *Renewable Energy*, vol. 123, pp. 450–459, 2018.

[109] V. Valamanesh, S. M. Asce, A. T. Myers, and M. Asce, "Aerodynamic Damping and Seismic Response of Horizontal Axis Wind Turbine Towers," pp. 1–9, 2014.

[110] C. Chen and P. Duffour, "Modelling damping sources in monopile-supported offshore wind turbines," *Wind Energy*, 2018.

[111] D. Marten, J. Wendler, “QBlade Guidelines v0.6,” 2013.

[112] MSC Software, “MSC. Nastran Version 70, Advanced Dynamic Analysis User’s Guide,” 2004.

APPENDICES

A.1 The Main FAST Input File

```
----- FAST v8.16.* INPUT FILE -------------------------------
FAST Certification Test #26:  NREL 5.0 MW Baseline Wind Turbine (Onshore)
---------------- SIMULATION CONTROL ------------------------
False Echo - Echo input data to <RootName>.ech (flag)
"FATAL" AbortLevel - Error level when simulation should abort (string) "WARNING", "SEVERE", "FATAL"
600 TMax - Total run time (s)
0.005 DT - Recommended module time step (s)
2 InterpOrder - Interpolation order for input/output time history (-) 1=linear, 2=quadratic
0 NumCrctn - Number of correction iterations (-) 0=explicit calculation, i.e., no corrections
99999 DT_UJac - Time between calls to get Jacobians (s)
1E+06 UJacSclFact - Scaling factor used in Jacobians (-)
---------------- FEATURE SWITCHES AND FLAGS --------------------
1 CompElast - Compute structural dynamics (switch) 1=ElastoDyn; 2=ElastoDyn + BeamDyn for blades
1 CompInflow - Compute inflow wind velocities (switch) 0=still air; 1=InflowWind; 2=external from OpenFOAM
1 CompAero - Compute aerodynamic loads (switch) 0=None; 1=AeroDyn v14; 2=AeroDyn v15
1 CompServo - Compute control and electrical-drive dynamics (switch) 0=None; 1=ServoDyn
0 CompHydro - Compute hydrodynamic loads (switch) 0=None; 1=HydroDyn
0 CompSub - Compute sub-structural dynamics (switch) 0=None; 1=SubDyn
0 CompMooring - Compute mooring system (switch) 0=None; 1=MAP++; 2=FEAMooring; 3=MoorDyn; 4=OrcaFlex
0 CompIce - Compute ice loads (switch) 0=None; 1=IceFloe; 2=IceDyn
---------------- INPUT FILES -----------------------------
"5MW_Baseline/All_Cases/wb/NRELOffshrBsline5MW_Onshore_ElastoDyn_BDoutputs.dat" EDFile - Name of file containing ElastoDyn
input parameters (quoted string)
"5MW_Baseline/All_Cases/wb/NRELOffshrBsline5MW_BeamDyn.dat" BDBldFile(1) - Name of file containing BeamDyn input parameters
for blade 1 (quoted string)
"5MW_Baseline/All_Cases/wb/NRELOffshrBsline5MW_BeamDyn.dat" BDBldFile(2) - Name of file containing BeamDyn input parameters
for blade 2 (quoted string)
"5MW_Baseline/All_Cases/wb/NRELOffshrBsline5MW_BeamDyn.dat" BDBldFile(3) - Name of file containing BeamDyn input parameters
for blade 3 (quoted string)
"5MW_Baseline/All_Cases/wb/NRELOffshrBsline5MW_InflowWind_30mps.dat" InflowFile - Name of file containing inflow wind
input parameters (quoted string)
"5MW_Baseline/All_Cases/wb/NRELOffshrBsline5MW_Onshore_AeroDyn.dat" AeroFile - Name of file containing aerodynamic
input parameters (quoted string)
"5MW_Baseline/All_Cases/wb/NRELOffshrBsline5MW_Onshore_ServoDyn.dat" ServoFile - Name of file containing control and
electrical-drive input parameters (quoted string)
"unused" HydroFile - Name of file containing hydrodynamic input parameters (quoted string)
"unused" SubFile - Name of file containing sub-structural input parameters (quoted string)
"unused" MooringFile - Name of file containing mooring system input parameters (quoted string)
"unused" IceFile - Name of file containing ice input parameters (quoted string)
---------------- OUTPUT ----------------------------------
True SumPrint - Print summary data to "<RootName>.sum" (flag)
1 SttsTime - Amount of time between screen status messages (s)
99999 ChkptTime - Amount of time between creating checkpoint files for potential restart (s)
"default" DT_Out - Time step for tabular output (s) (or "default")
0 TStart - Time to begin tabular output (s)
3 OutFileFmt - Format for tabular (time-marching) output file (switch) 1:  text file [<RootName>.out], 2:  binary file
[<RootName>.outb], 3:  both
True TabDelim - Use tab delimiters in text tabular output file?  (flag) uses spaces if false
"ES10.3E2" OutFmt - Format used for text tabular output, excluding the time channel.  Resulting field should be 10
```

```
characters.  (quoted string)
---------- LINEARIZATION ----------------------------
False Linearize - Linearization analysis (flag)
2 NLinTimes - Number of times to linearize (-) [>=1] [unused if Linearize=False]
10, 15 LinTimes - List of times at which to linearize (s) [1 to NLinTimes] [unused if Linearize=False]
1 LinInputs - Inputs included in linearization (switch) 0=none; 1=standard; 2=all module inputs (debug) [unused if
Linearize=False]
1 LinOutputs - Outputs included in linearization (switch) 0=none; 1=from OutList(s); 2=all module outputs (debug) [unused
if Linearize=False]
False LinOutJac - Include full Jacobians in linearization output (for debug) (flag) [unused if Linearize=False; used
only if LinInputs=LinOutputs=2]
False LinOutMod - Write module-level linearization output files in addition to output for full system?  (flag) [unused
if Linearize=False]
---------- VISUALIZATION ----------------------------
0 WrVTK - VTK visualization data output:  (switch) 0=none; 1=initialization data only; 2=animation
1 VTK_type - Type of VTK visualization data:  (switch) 1=surfaces; 2=basic meshes (lines/points); 3=all meshes (debug)
[unused if WrVTK=0]
True VTK_fields - Write mesh fields to VTK data files?  (flag) true/false [unused if WrVTK=0]
1 VTK_fps - Frame rate for VTK output (frames per second)will use closest integer multiple of DT [used only if WrVTK=2]...
```

A.2 ElastoDyn Input File

```
----- ELASTODYN v1.03.* INPUT FILE ----------------------------
NREL 5.0 MW Baseline Wind Turbine for Use in Offshore Analysis.  Properties from Dutch Offshore Wind Energy
Converter (DOWEC) 6MW Pre-Design (10046_009.pdf) and REpower 5M 5MW (5m_uk.pdf)
--------------- SIMULATION CONTROL -------------------------
False Echo - Echo input data to "<RootName>.ech" (flag)
3 Method - Integration method:  1:  RK4, 2:  AB4, or 3:  ABM4 (-)
"DEFAULT" DT - Integration time step (s)
--------------- ENVIRONMENTAL CONDITION ---------------------
9.80665 Gravity - Gravitational acceleration (m/s^2)
--------------- DEGREES OF FREEDOM -------------------------
True FlapDOF1 - First flapwise blade mode DOF (flag)
True FlapDOF2 - Second flapwise blade mode DOF (flag)
True EdgeDOF - First edgewise blade mode DOF (flag)
False TeetDOF - Rotor-teeter DOF (flag) [unused for 3 blades]
True DrTrDOF - Drivetrain rotational-flexibility DOF (flag)
True GenDOF - Generator DOF (flag)
True YawDOF - Yaw DOF (flag)
True TwFADOF1 - First fore-aft tower bending-mode DOF (flag)
True TwFADOF2 - Second fore-aft tower bending-mode DOF (flag)
True TwSSDOF1 - First side-to-side tower bending-mode DOF (flag)
True TwSSDOF2 - Second side-to-side tower bending-mode DOF (flag)
False PtfmSgDOF - Platform horizontal surge translation DOF (flag)
False PtfmSwDOF - Platform horizontal sway translation DOF (flag)
False PtfmHvDOF - Platform vertical heave translation DOF (flag)
False PtfmRDOF - Platform roll tilt rotation DOF (flag)
False PtfmPDOF - Platform pitch tilt rotation DOF (flag)
False PtfmYDOF - Platform yaw rotation DOF (flag)
--------------- INITIAL CONDITIONS -------------------------
0 OoPDefl - Initial out-of-plane blade-tip displacement (meters)
0 IPDefl - Initial in-plane blade-tip deflection (meters)
0 BlPitch(1) - Blade 1 initial pitch (degrees)
0 BlPitch(2) - Blade 2 initial pitch (degrees)
0 BlPitch(3) - Blade 3 initial pitch (degrees) [unused for 2 blades]
0 TeetDefl - Initial or fixed teeter angle (degrees) [unused for 3 blades]
0 Azimuth - Initial azimuth angle for blade 1 (degrees)
12.1 RotSpeed - Initial or fixed rotor speed (rpm)
0 NacYaw - Initial or fixed nacelle-yaw angle (degrees)
0 TTDspFA - Initial fore-aft tower-top displacement (meters)
0 TTDspSS - Initial side-to-side tower-top displacement (meters)
0 PtfmSurge - Initial or fixed horizontal surge translational displacement of platform (meters)
0 PtfmSway - Initial or fixed horizontal sway translational displacement of platform (meters)
0 PtfmHeave - Initial or fixed vertical heave translational displacement of platform (meters)
0 PtfmRoll - Initial or fixed roll tilt rotational displacement of platform (degrees)
0 PtfmPitch - Initial or fixed pitch tilt rotational displacement of platform (degrees)
0 PtfmYaw - Initial or fixed yaw rotational displacement of platform (degrees)
--------------- TURBINE CONFIGURATION ------------------------
3 NumBl - Number of blades (-)
63 TipRad - The distance from the rotor apex to the blade tip (meters)
1.5 HubRad - The distance from the rotor apex to the blade root (meters)
-2.5 PreCone(1) - Blade 1 cone angle (degrees)
-2.5 PreCone(2) - Blade 2 cone angle (degrees)
-2.5 PreCone(3) - Blade 3 cone angle (degrees) [unused for 2 blades]
0 HubCM - Distance from rotor apex to hub mass [positive downwind] (meters)
0 UndSling - Undersling length [distance from teeter pin to the rotor apex] (meters) [unused for 3 blades]
0 Delta3 - Delta-3 angle for teetering rotors (degrees) [unused for 3 blades]
0 AzimB1Up - Azimuth value to use for I/O when blade 1 points up (degrees)
-5.0191 OverHang - Distance from yaw axis to rotor apex [3 blades] or teeter pin [2 blades] (meters)
1.912 ShftGagL - Distance from rotor apex [3 blades] or teeter pin [2 blades] to shaft strain gages (meters)
-5 ShftTilt - Rotor shaft tilt angle (degrees)
1.9 NacCMxn - Downwind distance from the tower-top to the nacelle CM (meters)
```

0 NacCMyn - Lateral distance from the tower-top to the nacelle CM (meters)
1.75 NacCMzn - Vertical distance from the tower-top to the nacelle CM (meters)
-3.09528 NcIMUxn - Downwind distance from the tower-top to the nacelle IMU (meters)
0 NcIMUyn - Lateral distance from the tower-top to the nacelle IMU (meters)
2.23336 NcIMUzn - Vertical distance from the tower-top to the nacelle IMU (meters)
1.96256 Twr2Shft - Vertical distance from the tower-top to the rotor shaft (meters)
87.7 TowerHt - Height of tower above ground level [onshore] or MSL [offshore] (meters)
0.1 TowerBsHt - Height of tower base above ground level [onshore] or MSL [offshore] (meters)
0 PtfmCMxt - Downwind distance from the ground level [onshore] or MSL [offshore] to the platform CM (meters)
0 PtfmCMyt - Lateral distance from the ground level [onshore] or MSL [offshore] to the platform CM (meters)
0 PtfmCMzt - Vertical distance from the ground level [onshore] or MSL [offshore] to the platform CM (meters)
0 PtfmRefzt - Vertical distance from the ground level [onshore] or MSL [offshore] to the platform reference point (meters)
---------- MASS AND INERTIA ----------
0 TipMass(1) - Tip-brake mass, blade 1 (kg)
0 TipMass(2) - Tip-brake mass, blade 2 (kg)
0 TipMass(3) - Tip-brake mass, blade 3 (kg) [unused for 2 blades]
56780 HubMass - Hub mass (kg)
115926 HubIner - Hub inertia about rotor axis [3 blades] or teeter axis [2 blades] (kg m^2
534.116 GenIner - Generator inertia about HSS (kg m^2)
240000 NacMass - Nacelle mass (kg)
2.60789E+06 NacYIner - Nacelle inertia about yaw axis (kg m^2)
0 YawBrMass - Yaw bearing mass (kg)
0 PtfmMass - Platform mass (kg)
0 PtfmRIner - Platform inertia for roll tilt rotation about the platform CM (kg m^2)
0 PtfmPIner - Platform inertia for pitch tilt rotation about the platform CM (kg m^2)
0 PtfmYIner - Platform inertia for yaw rotation about the platform CM (kg m^2)
---------- BLADE ----------
17 BldNodes - Number of blade nodes (per blade) used for analysis (-)
"NRELOffshrBsline5MW_Blade.dat" BldFile(1) - Name of file containing properties for blade 1 (quoted string)
"NRELOffshrBsline5MW_Blade.dat" BldFile(2) - Name of file containing properties for blade 2 (quoted string)
"NRELOffshrBsline5MW_Blade.dat" BldFile(3) - Name of file containing properties for blade 3 (quoted string) [unused
for 2 blades] ---------- ROTOR-TEETER ----------
0 TeetMod - Rotor-teeter spring/damper model 0: none, 1: standard, 2: user-defined from routine UserTeet (switch)
[unused for 3 blades]
0 TeetDmpP - Rotor-teeter damper position (degrees) [used only for 2 blades and when TeetMod=1]
0 TeetDmp - Rotor-teeter damping constant (N-m/(rad/s)) [used only for 2 blades and when TeetMod=1]
0 TeetCDmp - Rotor-teeter rate-independent Coulomb-damping moment (N-m) [used only for 2 blades and when TeetMod=1]
0 TeetSStP - Rotor-teeter soft-stop position (degrees) [used only for 2 blades and when TeetMod=1]
0 TeetHStP - Rotor-teeter hard-stop position (degrees) [used only for 2 blades and when TeetMod=1]
0 TeetSSSp - Rotor-teeter soft-stop linear-spring constant (N-m/rad) [used only for 2 blades and when TeetMod=1]
0 TeetHSSp - Rotor-teeter hard-stop linear-spring constant (N-m/rad) [used only for 2 blades and when TeetMod=1]
---------- DRIVETRAIN ----------
100 GBoxEff - Gearbox efficiency (%)
97 GBRatio - Gearbox ratio (-)
8.67637E+08 DTTorSpr - Drivetrain torsional spring (N-m/rad)
2.215E+06 DTTorDmp - Drivetrain torsional damper (N-m/(rad/s))
---------- FURLING ----------
False Furling - Read in additional model properties for furling turbine (flag) [must currently be FALSE)
"unused" FurlFile - Name of file containing furling properties (quoted string) [unused when Furling=False]
---------- TOWER ----------
20 TwrNodes - Number of tower nodes used for analysis (-)
"NRELOffshrBsline5MW_Onshore_ElastoDyn_Tower.dat" TwrFile - Name of file containing tower properties (quoted string)
---------- OUTPUT ----------
True SumPrint - Print summary data to "<RootName>.sum" (flag)
1 OutFile - Switch to determine where output will be placed: 1: in module output file only; 2: in glue code output
file only; 3: both (currently unused)
True TabDelim - Use tab delimiters in text tabular output file? (flag) (currently unused)
"ES10.3E2" OutFmt - Format used for text tabular output (except time). Resulting field should be 10 characters. (currently
unused)
0 TStart - Time to begin tabular output (s) (currently unused)
1 DecFact - Decimation factor for tabular output 1: output every time step (-) (currently unused)
0 NTwGages - Number of tower nodes that have strain gages for output [0 to 9] (-)
10, 19, 28 TwrGagNd - List of tower nodes that have strain gages [1 to TwrNodes] (-) [unused if NTwGages=0]

```
3 NBlGages - Number of blade nodes that have strain gages for output [0 to 9] (-)
3,4,5 BldGagNd - List of blade nodes that have strain gages [1 to BldNodes] (-) [unused if NBlGages=0]
OutList - The next line(s) contains a list of output parameters.  See OutListParameters.xlsx for a listing of available
output channels, (-)
"OoPDefl1" - Blade 1 out-of-plane and in-plane deflections and tip twist
"IPDefl1" - Blade 1 out-of-plane and in-plane deflections and tip twist
"TwstDefl1" - Blade 1 out-of-plane and in-plane deflections and tip twist
"BldPitch1" - Blade 1 pitch angle
"Azimuth" - Blade 1 azimuth angle
"RotSpeed" - Low-speed shaft and high-speed shaft speeds
"GenSpeed" - Low-speed shaft and high-speed shaft speeds
"TTDspFA" - Tower fore-aft and side-to-side displacements and top twist
"TTDspSS" - Tower fore-aft and side-to-side displacements and top twist
"TTDspTwst" - Tower fore-aft and side-to-side displacements and top twist
"Spn2MLxb1" - Blade 1 local edgewise and flapwise bending moments at span station 2 (approx.  50% span)
"Spn2MLyb1" - Blade 1 local edgewise and flapwise bending moments at span station 2 (approx.  50% span)
"RootFxb1" - Out-of-plane shear, in-plane shear, and axial forces at the root of blade 1
"RootFyb1" - Out-of-plane shear, in-plane shear, and axial forces at the root of blade 1
"RootFzb1" - Out-of-plane shear, in-plane shear, and axial forces at the root of blade 1
"RootMxb1" - In-plane bending, out-of-plane bending, and pitching moments at the root of blade 1
"RootMyb1" - In-plane bending, out-of-plane bending, and pitching moments at the root of blade 1
"RootMzb1" - In-plane bending, out-of-plane bending, and pitching moments at the root of blade 1
"RotTorq" - Rotor torque and low-speed shaft 0- and 90-bending moments at the main bearing
"LSSGagMya" - Rotor torque and low-speed shaft 0- and 90-bending moments at the main bearing
"LSSGagMza" - Rotor torque and low-speed shaft 0- and 90-bending moments at the main bearing
"TwrBsFxt" - Fore-aft shear, side-to-side shear, and vertical forces at the base of the tower (mudline)
"TwrBsFyt" - Fore-aft shear, side-to-side shear, and vertical forces at the base of the tower (mudline)
"TwrBsFzt" - Fore-aft shear, side-to-side shear, and vertical forces at the base of the tower (mudline)
"TwrBsMxt" - Side-to-side bending, fore-aft bending, and yaw moments at the base of the tower (mudline)
"TwrBsMyt" - Side-to-side bending, fore-aft bending, and yaw moments at the base of the tower (mudline)
"TwrBsMzt" - Side-to-side bending, fore-aft bending, and yaw moments at the base of the tower (mudline)
END of input file (the word "END" must appear in the first 3 columns of this last OutList line)
---------------------------------------------------------
```

A.3 InflowWind Input File

```
----- InflowWind v3.01.* INPUT FILE ------------------------------------------------
12 m/s turbulent winds on 31x31 FF grid and tower
---------------------------------------------------------------------------
False Echo - Echo input data to <RootName>.ech (flag)
3 WindType - switch for wind file type (1=steady; 2=uniform; 3=binary TurbSim FF; 4=binary Bladed-style FF; 5=HAWC
format; 6=User defined)
0 PropagationDir - Direction of wind propagation (meteoroligical rotation from aligned with X (positive rotates towards
-Y) - degrees)
1 NWindVel - Number of points to output the wind velocity (0 to 9)
0 WindVxiList - List of coordinates in the inertial X direction (m)
0 WindVyiList - List of coordinates in the inertial Y direction (m)
90 WindVziList - List of coordinates in the inertial Z direction (m)
================== Parameters for Steady Wind Conditions [used only for WindType = 1] =========================
0 HWindSpeed - Horizontal windspeed (m/s)
90 RefHt - Reference height for horizontal wind speed (m)
0.2 PLexp - Power law exponent (-)
================== Parameters for Uniform wind file [used only for WindType = 2] ============================
"Wind/nrel_5mw.bts" Filename - Filename of time series data for uniform wind field.  (-)
90 RefHt - Reference height for horizontal wind speed (m)
125.88 RefLength - Reference length for linear horizontal and vertical sheer (-)
================== Parameters for Binary TurbSim Full-Field files [used only for WindType = 3] ==============
"Wind/12ms.bts" Filename - Name of the Full field wind file to use (.bts)
================== Parameters for Binary Bladed-style Full-Field files [used only for WindType = 4] =========
"Wind/90m_12mps_twr" FilenameRoot - Rootname of the full-field wind file to use (.wnd, .sum)
False TowerFile - Have tower file (.twr) (flag)
================== Parameters for HAWC-format binary files [Only used with WindType = 5] =====================
"wasp\Output\basic_5u.bin" FileName_u - name of the file containing the u-component fluctuating wind (.bin)
"wasp\Output\basic_5v.bin" FileName_v - name of the file containing the v-component fluctuating wind (.bin)
"wasp\Output\basic_5w.bin" FileName_w - name of the file containing the w-component fluctuating wind (.bin)
64 nx - number of grids in the x direction (in the 3 files above) (-)
32 ny - number of grids in the y direction (in the 3 files above) (-)
32 nz - number of grids in the z direction (in the 3 files above) (-)
16 dx - distance (in meters) between points in the x direction (m)
3 dy - distance (in meters) between points in the y direction (m)
3 dz - distance (in meters) between points in the z direction (m)
90 RefHt - reference height; the height (in meters) of the vertical center of the grid (m)
--------- Scaling parameters for turbulence -------------------------------------
1 ScaleMethod - Turbulence scaling method [0 = none, 1 = direct scaling, 2 = calculate scaling factor based on a desired
standard deviation]
1 SFx - Turbulence scaling factor for the x direction (-) [ScaleMethod=1]
1 SFy - Turbulence scaling factor for the y direction (-) [ScaleMethod=1]
1 SFz - Turbulence scaling factor for the z direction (-) [ScaleMethod=1]
12 SigmaFx - Turbulence standard deviation to calculate scaling from in x direction (m/s) [ScaleMethod=2]
8 SigmaFy - Turbulence standard deviation to calculate scaling from in y direction (m/s) [ScaleMethod=2]
2 SigmaFz - Turbulence standard deviation to calculate scaling from in z direction (m/s) [ScaleMethod=2]
--------- Mean wind profile parameters (added to HAWC-format files) ----------------------
8 URef - Mean u-component wind speed at the reference height (m/s)
2 WindProfile - Wind profile type (0=constant;1=logarithmic,2=power law)
0.2 PLExp - Power law exponent (-) (used for PL wind profile type only)
0.03 Z0 - Surface roughness length (m) (used for LG wind profile type only)
====================== OUTPUT ==================================================
True SumPrint - Print summary data to <RootName>.IfW.sum (flag)
OutList - The next line(s) contains a list of output parameters.  See OutListParameters.xlsx for a listing of available
output channels, (-)
"Wind1VelX" X-direction wind velocity at point WindList(1)
"Wind1VelY" Y-direction wind velocity at point WindList(1)
"Wind1VelZ" Z-direction wind velocity at point WindList(1)
END of input file (the word "END" must appear in the first 3 columns of this last OutList line)
---------------------------------------------------------------
```

A.4 TurbSim Input File

```
TurbSim Input File.  Example file that can be used with simulations for the NREL 5MW Baseline Turbine
------Runtime Options-----------------------
13428 RandSeed1 - First random seed (-2147483648 to 2147483647)
RanLux RandSeed2 - Second random seed (-2147483648 to 2147483647) for intrinsic pRNG, or an alternative pRNG: "RanLux"
or "RNSNLW"
False WrBHHTP - Output hub-height turbulence parameters in binary form?  (Generates RootName.bin)
False WrFHHTP - Output hub-height turbulence parameters in formatted form?  (Generates RootName.dat)
False WrADHH - Output hub-height time-series data in AeroDyn form?  (Generates RootName.hh)
True WrADFF - Output full-field time-series data in TurbSim/AeroDyn form?  (Generates RootName.bts)
False WrBLFF - Output full-field time-series data in BLADED/AeroDyn form?  (Generates RootName.wnd)
True WrADTWR - Output tower time-series data?  (Generates RootName.twr)
False WrFMTFF - Output full-field time-series data in formatted (readable) form?  (Generates RootName.u, RootName.v,
RootName.w)
False WrACT - Output coherent turbulence time steps in AeroDyn form?  (Generates RootName.cts)
True Clockwise - Clockwise rotation looking downwind?  (used only for full-field binary files - not necessary for AeroDyn)
0 ScaleIEC - Scale IEC turbulence models to exact target standard deviation?  [0=no additional scaling; 1=use hub scale
uniformly; 2=use individual scales]
-----Turbine/Model Specifications---------------
31 NumGrid_Z - Vertical grid-point matrix dimension
31 NumGrid_Y - Horizontal grid-point matrix dimension
0.05 TimeStep - Time step [seconds]
630.0 AnalysisTime - Length of analysis time series [seconds]
630.0 UsableTime - Usable length of output time series [seconds] (program will add GridWidth/MeanHHWS seconds) [bjj:
was 630]
90.0 HubHt - Hub height [m] (should be > 0.5*GridHeight)
145.0 GridHeight - Grid height [m]
145.0 GridWidth - Grid width [m] (should be >= 2*(RotorRadius+ShaftLength))
0 VFlowAng - Vertical mean flow (uptilt) angle [degrees]
0 HFlowAng - Horizontal mean flow (skew) angle [degrees]
-----Meteorological Boundary Conditions-------------
IECKAI TurbModel - Turbulence model ("IECKAI"=Kaimal, "IECVKM"=von Karman, "GP_LLJ", "NWTCUP", "SMOOTH", "WF_UPW",
"WF_07D", "WF_14D", or "NONE")
"1-ed3" IECstandard - Number of IEC 61400-x standard (x=1,2, or 3 with optional 61400-1 edition number (i.e.  "1-Ed2")
)
"B" IECturbc - IEC turbulence characteristic ("A", "B", "C" or the turbulence intensity in percent) ("KHTEST" option
with NWTCUP, not used for other models)
NTM IEC_WindType - IEC turbulence type ("NTM"=normal, "xETM"=extreme turbulence, "xEWM1"=extreme 1-year wind, "xEWM50"=extreme
50-year wind, where x=wind turbine class 1, 2, or 3)
default ETMc - IEC Extreme turbulence model "c" parameter [m/s]
PL WindProfileType - Wind profile type ("JET"=Low-level jet,"LOG"=Logarithmic,"PL"=Power law, or "default", or "USR"=User-defined)
90.  RefHt - Height of the reference wind speed [m]
12.0 URef - Mean (total) wind speed at the reference height [m/s]
default ZJetMax - Jet height [m] (used only for JET wind profile, valid 70-490 m)
default PLExp - Power law exponent [-] (or "default")
default Z0 - Surface roughness length [m] (or "default")
-----Non-IEC Meteorological Boundary Conditions--------
default Latitude - Site latitude [degrees] (or "default")
0.05 RICH_NO - Gradient Richardson number
default UStar - Friction or shear velocity [m/s] (or "default")
default ZI - Mixing layer depth [m] (or "default")
default PC_UW - Hub mean u'w' Reynolds stress [(m/s)^2] (or "default")
default PC_UV - Hub mean u'v' Reynolds stress [(m/s)^2] (or "default")
default PC_VW - Hub mean v'w' Reynolds stress [(m/s)^2] (or "default")
default IncDec1 - u-component coherence parameters (e.g.  "10.0 0.3e-3" in quotes) (or "default")
default IncDec2 - v-component coherence parameters (e.g.  "10.0 0.3e-3" in quotes) (or "default")
default IncDec3 - w-component coherence parameters (e.g.  "10.0 0.3e-3" in quotes) (or "default")
default CohExp - Coherence exponent (or "default")
-----Coherent Turbulence Scaling Parameters-------------
"M:\coh_events\eventdata" CTEventPath - Name of the path where event data files are located
"Random" CTEventFile - Type of event files ("random", "les" or "dns")
```

```
true Randomize - Randomize disturbance scale and location?  (true/false)
1.0 DistScl - Disturbance scale (ratio of dataset height to rotor disk).
0.5 CTLy - Fractional location of tower centerline from right (looking downwind) to left side of the dataset.
0.5 CTLz - Fractional location of hub height from the bottom of the dataset.
10.0 CTStartTime - Minimum start time for coherent structures in RootName.cts [seconds]
================================================
```

A.5 AeroDyn Input File

```
----- AERODYN v15.03.* INPUT FILE ------------------------------
NREL 5.0 MW offshore baseline aerodynamic input properties.
====== General Options ============================================================================
False Echo - Echo the input to "<rootname>.AD.ech" (flag)
"default" DTAero - Time interval for aerodynamic calculations or "default" (s)
1 WakeMod - Type of wake/induction model (switch) 0=none, 1=BEMT
1 AFAeroMod - Type of blade airfoil aerodynamics model (switch) 1=steady model, 2=Beddoes-Leishman unsteady model
2 TwrPotent - Type tower influence on wind based on potential flow around the tower (switch) 0=none, 1=baseline potential
flow, 2=potential flow with Bak correction
False TwrShadow - Calculate tower influence on wind based on downstream tower shadow?  (flag)
False TwrAero - Calculate tower aerodynamic loads?  (flag)
False FrozenWake - Assume frozen wake during linearization?  (flag) [used only when WakeMod=1 and when linearizing]
====== Environmental Conditions ===================================================================
1.225 AirDens - Air density (kg/m^3)
1.464E-05 KinVisc - Kinematic air viscosity (m^2/s)
335 SpdSound - Speed of sound (m/s)
====== Blade-Element/Momentum Theory Options ========== [used only when
WakeMod=1]
2 SkewMod - Type of skewed-wake correction model (switch) 1=uncoupled, 2=Pitt/Peters, 3=coupled [used only when WakeMod=1]
True TipLoss - Use the Prandtl tip-loss model?  (flag) [used only when WakeMod=1]
True HubLoss - Use the Prandtl hub-loss model?  (flag) [used only when WakeMod=1]
true TanInd - Include tangential induction in BEMT calculations?  (flag) [used only when WakeMod=1]
False AIDrag - Include the drag term in the axial-induction calculation?  (flag) [used only when WakeMod=1]
False TIDrag - Include the drag term in the tangential-induction calculation?  (flag) [used only when WakeMod=1 and
TanInd=TRUE]
"Default" IndToler - Convergence tolerance for BEMT nonlinear solve residual equation or "default" (-) [used only when
WakeMod=1]
100 MaxIter - Maximum number of iteration steps (-) [used only when WakeMod=1]
====== Beddoes-Leishman Unsteady Airfoil Aerodynamics Options ========== [used only when
AFAeroMod=2]
3 UAMod - Unsteady Aero Model Switch (switch) 1=Baseline model (Original), 2=GonzalezŠs variant (changes in Cn,Cc,Cm),
3=Minemma/Pierce variant (changes in Cc and Cm) [used only when AFAeroMod=2]
True FLookup - Flag to indicate whether a lookup for f' will be calculated (TRUE) or whether best-fit exponential equations
will be used (FALSE); if FALSE S1-S4 must be provided in airfoil input files (flag) [used only when AFAeroMod=2]
====== Airfoil Information ========================================================================
1 InCol_Alfa - The column in the airfoil tables that contains the angle of attack (-)
2 InCol_Cl - The column in the airfoil tables that contains the lift coefficient (-)
3 InCol_Cd - The column in the airfoil tables that contains the drag coefficient (-)
4 InCol_Cm - The column in the airfoil tables that contains the pitching-moment coefficient; use zero if there is no
Cm column (-)
0 InCol_Cpmin - The column in the airfoil tables that contains the Cpmin coefficient; use zero if there is no Cpmin
column (-)
8 NumAFfiles - Number of airfoil files used (-)
"Airfoils/Cylinder1.dat" AFNames - Airfoil file names (NumAFfiles lines) (quoted strings)
"Airfoils/Cylinder2.dat"
"Airfoils/DU40_A17.dat"
"Airfoils/DU35_A17.dat"
"Airfoils/DU30_A17.dat"
"Airfoils/DU25_A17.dat"
"Airfoils/DU21_A17.dat"
"Airfoils/NACA64_A17.dat"
====== Rotor/Blade Properties =====================================================================
True UseBlCm - Include aerodynamic pitching moment in calculations?  (flag)
"NRELOffshrBsline5MW_AeroDyn_blade.dat" ADBlFile(1) - Name of file containing distributed aerodynamic properties for
Blade #1 (-)
"NRELOffshrBsline5MW_AeroDyn_blade.dat" ADBlFile(2) - Name of file containing distributed aerodynamic properties for
Blade #2 (-) [unused if NumBl < 2]
"NRELOffshrBsline5MW_AeroDyn_blade.dat" ADBlFile(3) - Name of file containing distributed aerodynamic properties for
Blade #3 (-) [unused if NumBl < 3]
====== Tower Influence and Aerodynamics ========================== used only when TwrPotent/=0, TwrShadow=True, or TwrAero=True]
```

```
12 NumTwrNds - Number of tower nodes used in the analysis (-) [used only when TwrPotent/=0, TwrShadow=True, or TwrAero=True]
TwrElev TwrDiam TwrCd
(m) (m) (-)
0.1000000E+00 6.0000000E+00 1.0000000E+00
8.5261000E+00 5.7870000E+00 1.0000000E+00
1.7053000E+01 5.5740000E+00 1.0000000E+00
2.5579000E+01 5.3610000E+00 1.0000000E+00
3.4105000E+01 5.1480000E+00 1.0000000E+00
4.2633000E+01 4.9350000E+00 1.0000000E+00
5.1158000E+01 4.7220000E+00 1.0000000E+00
5.9685000E+01 4.5090000E+00 1.0000000E+00
6.8211000E+01 4.2960000E+00 1.0000000E+00
7.6738000E+01 4.0830000E+00 1.0000000E+00
8.5268000E+01 3.8700000E+00 1.0000000E+00
8.7700000E+01 3.8700000E+00 1.0000000E+00
====== Outputs ==============================================================================
True SumPrint - Generate a summary file listing input options and interpolated properties to "<rootname>.AD.sum"?  (flag)
0 NBlOuts - Number of blade node outputs [0 - 9] (-)
1, 9, 19 BlOutNd - Blade nodes whose values will be output (-)
0 NTwOuts - Number of tower node outputs [0 - 9] (-)
1, 2, 6 TwOutNd - Tower nodes whose values will be output (-)
OutList - The next line(s) contains a list of output parameters.  See OutListParameters.xlsx for a listing of available
output channels, (-)
END of input file (the word "END" must appear in the first 3 columns of this last OutList line)
---------------------------------------------------------
```

A.6 ServoDyn Input File

```
 ----- SERVODYN v1.05.* INPUT FILE ------------------------------
NREL 5.0 MW Baseline Wind Turbine for Use in Offshore Analysis.  Properties from Dutch Offshore Wind Energy Converter
(DOWEC) 6MW Pre-Design (10046_009.pdf) and REpower 5M 5MW (5m_uk.pdf)
---------------- SIMULATION CONTROL --------------------------
False Echo - Echo input data to <RootName>.ech (flag)
"default" DT - Communication interval for controllers (s) (or "default")
---------------- PITCH CONTROL -------------------------------
5 PCMode - Pitch control mode 0:  none, 3:  user-defined from routine PitchCntrl, 4:  user-defined from Simulink/Labview,
5:  user-defined from Bladed-style DLL (switch)
0 TPCOn - Time to enable active pitch control (s) [unused when PCMode=0]
9999.9 TPitManS(1) - Time to start override pitch maneuver for blade 1 and end standard pitch control (s)
9999.9 TPitManS(2) - Time to start override pitch maneuver for blade 2 and end standard pitch control (s)
9999.9 TPitManS(3) - Time to start override pitch maneuver for blade 3 and end standard pitch control (s) [unused for
2 blades]
2 PitManRat(1) - Pitch rate at which override pitch maneuver heads toward final pitch angle for blade 1 (deg/s)
2 PitManRat(2) - Pitch rate at which override pitch maneuver heads toward final pitch angle for blade 2 (deg/s)
2 PitManRat(3) - Pitch rate at which override pitch maneuver heads toward final pitch angle for blade 3 (deg/s) [unused
for 2 blades]
0 BlPitchF(1) - Blade 1 final pitch for pitch maneuvers (degrees)
0 BlPitchF(2) - Blade 2 final pitch for pitch maneuvers (degrees)
0 BlPitchF(3) - Blade 3 final pitch for pitch maneuvers (degrees) [unused for 2 blades]
---------------- GENERATOR AND TORQUE CONTROL ---------------------
5 VSContrl - Variable-speed control mode 0:  none, 1:  simple VS, 3:  user-defined from routine UserVSCont, 4:  user-defined
from Simulink/Labview, 5:  user-defined from Bladed-style DLL (switch)
2 GenModel - Generator model 1:  simple, 2:  Thevenin, 3:  user-defined from routine UserGen (switch) [used only when
VSContrl=0]
94.4 GenEff - Generator efficiency [ignored by the Thevenin and user-defined generator models] (%)
True GenTiStr - Method to start the generator T: timed using TimGenOn, F: generator speed using SpdGenOn (flag)
True GenTiStp - Method to stop the generator T: timed using TimGenOf, F: when generator power = 0 (flag)
9999.9 SpdGenOn - Generator speed to turn on the generator for a startup (HSS speed) (rpm) [used only when GenTiStr=False]
0 TimGenOn - Time to turn on the generator for a startup (s) [used only when GenTiStr=True]
9999.9 TimGenOf - Time to turn off the generator (s) [used only when GenTiStp=True]
---------------- SIMPLE VARIABLE-SPEED TORQUE CONTROL -------------
9999.9 VS_RtGnSp - Rated generator speed for simple variable-speed generator control (HSS side) (rpm) [used only when
VSContrl=1]
9999.9 VS_RtTq - Rated generator torque/constant generator torque in Region 3 for simple variable-speed generator control
(HSS side) (N-m) [used only when VSContrl=1]
9999.9 VS_Rgn2K - Generator torque constant in Region 2 for simple variable-speed generator control (HSS side) (N-m/rpm^2)
[used only when VSContrl=1]
9999.9 VS_SlPc - Rated generator slip percentage in Region 2 1/2 for simple variable-speed generator control (%) [used
only when VSContrl=1]
---------------- SIMPLE INDUCTION GENERATOR ----------------------
9999.9 SIG_SlPc - Rated generator slip percentage (%) [used only when VSContrl=0 and GenModel=1]
9999.9 SIG_SySp - Synchronous (zero-torque) generator speed (rpm) [used only when VSContrl=0 and GenModel=1]
9999.9 SIG_RtTq - Rated torque (N-m) [used only when VSContrl=0 and GenModel=1]
9999.9 SIG_PORt - Pull-out ratio (Tpullout/Trated) (-) [used only when VSContrl=0 and GenModel=1]
---------------- THEVENIN-EQUIVALENT INDUCTION GENERATOR -----------
9999.9 TEC_Freq - Line frequency [50 or 60] (Hz) [used only when VSContrl=0 and GenModel=2]
9998 TEC_NPol - Number of poles [even integer > 0] (-) [used only when VSContrl=0 and GenModel=2]
9999.9 TEC_SRes - Stator resistance (ohms) [used only when VSContrl=0 and GenModel=2]
9999.9 TEC_RRes - Rotor resistance (ohms) [used only when VSContrl=0 and GenModel=2]
9999.9 TEC_VLL - Line-to-line RMS voltage (volts) [used only when VSContrl=0 and GenModel=2]
9999.9 TEC_SLR - Stator leakage reactance (ohms) [used only when VSContrl=0 and GenModel=2]
9999.9 TEC_RLR - Rotor leakage reactance (ohms) [used only when VSContrl=0 and GenModel=2]
9999.9 TEC_MR - Magnetizing reactance (ohms) [used only when VSContrl=0 and GenModel=2]
---------------- HIGH-SPEED SHAFT BRAKE ------------------------
0 HSSBrMode - HSS brake model 0:  none, 1:  simple, 3:  user-defined from routine UserHSSBr, 4:  user-defined from
Simulink/Labview, 5:  user-defined from Bladed-style DLL (switch)
9999.9 THSSBrDp - Time to initiate deployment of the HSS brake (s)
0.6 HSSBrDT - Time for HSS-brake to reach full deployment once initiated (sec) [used only when HSSBrMode=1]
```

28116.2 HSSBrTqF - Fully deployed HSS-brake torque (N-m)
--------------- NACELLE-YAW CONTROL -------------------------
0 YCMode - Yaw control mode 0: none, 3: user-defined from routine UserYawCont, 4: user-defined from Simulink/Labview, 5: user-defined from Bladed-style DLL (switch)
9999.9 TYCOn - Time to enable active yaw control (s) [unused when YCMode=0]
0 YawNeut - Neutral yaw position-yaw spring force is zero at this yaw (degrees)
9.02832E+09 YawSpr - Nacelle-yaw spring constant (N-m/rad)
1.916E+07 YawDamp - Nacelle-yaw damping constant (N-m/(rad/s))
9999.9 TYawManS - Time to start override yaw maneuver and end standard yaw control (s)
2 YawManRat - Yaw maneuver rate (in absolute value) (deg/s)
0 NacYawF - Final yaw angle for override yaw maneuvers (degrees)
--------------- TUNED MASS DAMPER -------------------------
False CompNTMD - Compute nacelle tuned mass damper true/false (flag)
"NRELOffshrBsline5MW_ServoDyn_TMD.dat" NTMDfile - Name of the file for nacelle tuned mass damper (quoted string) [unused when CompNTMD is false]
False CompTTMD - Compute tower tuned mass damper true/false (flag)
"NRELOffshrBsline5MW_ServoDyn_TMD.dat" TTMDfile - Name of the file for tower tuned mass damper (quoted string) [unused when CompTTMD is false]
--------------- BLADED INTERFACE ---------------------------- [used only with Bladed Interface]
"ServoData/DISCON_x64.dll" DLL_FileName - Name/location of the dynamic library .dll [Windows] or .so [Linux] in the Bladed-DLL format (-) [used only with Bladed Interface]
"DISCON.IN" DLL_InFile - Name of input file sent to the DLL (-) [used only with Bladed Interface]
"DISCON" DLL_ProcName - Name of procedure in DLL to be called (-) [case sensitive; used only with DLL Interface]
"default" DLL_DT - Communication interval for dynamic library (s) (or "default") [used only with Bladed Interface]
false DLL_Ramp - Whether a linear ramp should be used between DLL_DT time steps [introduces time shift when true] (flag) [used only with Bladed Interface]
9999.9 BPCutoff - Cuttoff frequency for low-pass filter on blade pitch from DLL (Hz) [used only with Bladed Interface]
0 NacYaw_North - Reference yaw angle of the nacelle when the upwind end points due North (deg) [used only with Bladed Interface]
0 Ptch_Cntrl - Record 28: Use individual pitch control 0: collective pitch; 1: individual pitch control (switch) [used only with Bladed Interface]
0 Ptch_SetPnt - Record 5: Below-rated pitch angle set-point (deg) [used only with Bladed Interface]
0 Ptch_Min - Record 6: Minimum pitch angle (deg) [used only with Bladed Interface]
0 Ptch_Max - Record 7: Maximum pitch angle (deg) [used only with Bladed Interface]
0 PtchRate_Min - Record 8: Minimum pitch rate (most negative value allowed) (deg/s) [used only with Bladed Interface]
0 PtchRate_Max - Record 9: Maximum pitch rate (deg/s) [used only with Bladed Interface]
0 Gain_OM - Record 16: Optimal mode gain (Nm/(rad/s)^2) [used only with Bladed Interface]
0 GenSpd_MinOM - Record 17: Minimum generator speed (rpm) [used only with Bladed Interface]
0 GenSpd_MaxOM - Record 18: Optimal mode maximum speed (rpm) [used only with Bladed Interface]
0 GenSpd_Dem - Record 19: Demanded generator speed above rated (rpm) [used only with Bladed Interface]
0 GenTrq_Dem - Record 22: Demanded generator torque above rated (Nm) [used only with Bladed Interface]
0 GenPwr_Dem - Record 13: Demanded power (W) [used only with Bladed Interface]
--------------- BLADED INTERFACE TORQUE-SPEED LOOK-UP TABLE ---------
0 DLL_NumTrq - Record 26: No. of points in torque-speed look-up table 0 = none and use the optimal mode parameters; nonzero = ignore the optimal mode PARAMETERs by setting Record 16 to 0.0 (-) [used only with Bladed Interface] GenSpd_TLU GenTrq_TLU
(rpm) (Nm)
--------------- OUTPUT ----------------------------------
True SumPrint - Print summary data to <RootName>.sum (flag) (currently unused)
1 OutFile - Switch to determine where output will be placed: 1: in module output file only; 2: in glue code output file only; 3: both (currently unused)
True TabDelim - Use tab delimiters in text tabular output file? (flag) (currently unused)
"ES10.3E2" OutFmt - Format used for text tabular output (except time). Resulting field should be 10 characters. (quoted string) (currently unused)
0 TStart - Time to begin tabular output (s) (currently unused)
OutList - The next line(s) contains a list of output parameters. See OutListParameters.xlsx for a listing of available output channels, (-)
"GenPwr" - Electrical generator power and torque
"GenTq" - Electrical generator power and torque
END of input file (the word "END" must appear in the first 3 columns of this last OutList line)

A.7 HydroDyn Input File

```
 ----- HydroDyn v2.03.* Input File ------------------------------
NREL 5.0 MW offshore baseline floating platform input properties for the OC3 Monopile.
False Echo - Echo the input file data (flag)
---------------- ENVIRONMENTAL CONDITIONS ---------------------
1027 WtrDens - Water density (kg/m^3)
20 WtrDpth - Water depth (meters)
0 MSL2SWL - Offset between still-water level and mean sea level (meters) ---------------- WAVES ---------------------------------
2 WaveMod - Incident wave kinematics model 0:  none=still water, 1:  regular (periodic), 1P#:  regular with user-specified
phase, 2:  JONSWAP/Pierson-Moskowitz spectrum (irregular), 3:  White noise spectrum (irregular), 4:  user-defined spectrum
from routine UserWaveSpctrm (irregular), 5:  Externally generated wave-elevation time series, 6:  Externally generated
full wave-kinematics time series [option 6 is invalid for PotMod/=0] (switch)
0 WaveStMod - Model for stretching incident wave kinematics to instantaneous free surface 0:  none=no stretching, 1:
vertical stretching, 2:  extrapolation stretching, 3:  Wheeler stretching (switch) [unused when WaveMod=0 or when PotMod/=0]
3630 WaveTMax - Analysis time for incident wave calculations (sec) [unused when WaveMod=0; determines WaveDOmega=2Pi/WaveTMax
in the IFFT]
0.25 WaveDT - Time step for incident wave calculations (sec) [unused when WaveMod=0; 0.1<=WaveDT<=1.0 recommended;
determines WaveOmegaMax=Pi/WaveDT in the IFFT]
6 WaveHs - Significant wave height of incident waves (meters) [used only when WaveMod=1, 2, or 3]
10 WaveTp - Peak-spectral period of incident waves (sec) [used only when WaveMod=1 or 2]
"DEFAULT" WavePkShp - Peak-shape parameter of incident wave spectrum (-) or DEFAULT (string) [used only when WaveMod=2;
use 1.0 for Pierson-Moskowitz]
0.15708 WvLowCOff - Low cut-off frequency or lower frequency limit of the wave spectrum beyond which the wave spectrum
is zeroed (rad/s) [unused when WaveMod=0, 1, or 6]
3.2 WvHiCOff - High cut-off frequency or upper frequency limit of the wave spectrum beyond which the wave spectrum
is zeroed (rad/s) [unused when WaveMod=0, 1, or 6]
0 WaveDir - Incident wave propagation heading direction (degrees) [unused when WaveMod=0 or 6]
0 WaveDirMod - Directional spreading function 0:  none, 1:  COS2S (-) [only used when WaveMod=2,3, or 4]
1 WaveDirSpread - Wave direction spreading coefficient ( > 0 ) (-) [only used when WaveMod=2,3, or 4 and WaveDirMod=1]
1 WaveNDir - Number of wave directions (-) [only used when WaveMod=2,3, or 4 and WaveDirMod=1; odd number only]
90 WaveDirRange - Range of wave directions (full range:  WaveDir +/- 1/2*WaveDirRange) (degrees) [only used when WaveMod=2,3,or
4 and WaveDirMod=1]
123456789 WaveSeed(1) - First random seed of incident waves [-2147483648 to 2147483647] (-) [unused when WaveMod=0,
5, or 6]
1011121314 WaveSeed(2) - Second random seed of incident waves [-2147483648 to 2147483647] (-) [unused when WaveMod=0,
5, or 6]
TRUE WaveNDAmp - Flag for normally distributed amplitudes (flag) [only used when WaveMod=2, 3, or 4]
"" WvKinFile - Root name of externally generated wave data file(s) (quoted string) [used only when WaveMod=5 or 6]
1 NWaveElev - Number of points where the incident wave elevations can be computed (-)
0 WaveElevxi - List of xi-coordinates for points where the incident wave elevations can be output (meters)
0 WaveElevyi - List of yi-coordinates for points where the incident wave elevations can be output (meters)
---------------- 2ND-ORDER WAVES ---------------------------- [unused with WaveMod=0 or 6]
True WvDiffQTF - Full difference-frequency 2nd-order wave kinematics (flag)
True WvSumQTF - Full summation-frequency 2nd-order wave kinematics (flag)
0 WvLowCOffD - Low frequency cutoff used in the difference-frequencies (rad/s) [Only used with a difference-frequency
method]
3.04292 WvHiCOffD - High frequency cutoff used in the difference-frequencies (rad/s) [Only used with a difference-frequency
method]
0.314159 WvLowCOffS - Low frequency cutoff used in the summation-frequencies (rad/s) [Only used with a summation-frequency
method]
3.2 WvHiCOffS - High frequency cutoff used in the summation-frequencies (rad/s) [Only used with a summation-frequency
method]
---------------- CURRENT ---------------------------------- [unused with WaveMod=6]
0 CurrMod - Current profile model 0:  none=no current, 1:  standard, 2:  user-defined from routine UserCurrent (switch)
0 CurrSSV0 - Sub-surface current velocity at still water level (m/s) [used only when CurrMod=1]
"DEFAULT" CurrSSDir - Sub-surface current heading direction (degrees) or DEFAULT (string) [used only when CurrMod=1]
20 CurrNSRef - Near-surface current reference depth (meters) [used only when CurrMod=1]
0 CurrNSV0 - Near-surface current velocity at still water level (m/s) [used only when CurrMod=1]
0 CurrNSDir - Near-surface current heading direction (degrees) [used only when CurrMod=1]
0 CurrDIV - Depth-independent current velocity (m/s) [used only when CurrMod=1]
0 CurrDIDir - Depth-independent current heading direction (degrees) [used only when CurrMod=1]
```

---------- FLOATING PLATFORM ---------- [unused with WaveMod=6]
0 PotMod - Potential-flow model 0: none=no potential flow, 1: frequency-to-time-domain transforms based on WAMIT output, 2: fluid-impulse theory (FIT) (switch)
"unused" PotFile - Root name of potential-flow model data; WAMIT output files containing the linear, nondimensionalized, hydrostatic restoring matrix (.hst), frequency-dependent hydrodynamic added mass matrix and damping matrix (.1), and frequency- and direction-dependent wave excitation force vector per unit wave amplitude (.3) (quoted string) [MAKE SURE THE FREQUENCIES INHERENT IN THESE WAMIT FILES SPAN THE PHYSICALLY-SIGNIFICANT RANGE OF FREQUENCIES FOR THE GIVEN PLATFORM; THEY MUST CONTAIN THE ZERO- AND INFINITE-FREQUENCY LIMITS!]
1 WAMITULEN - Characteristic body length scale used to redimensionalize WAMIT output (meters) [only used when PotMod=1]
0 PtfmVol0 - Displaced volume of water when the platform is in its undisplaced position (m^3) [only used when PotMod=1; USE THE SAME VALUE COMPUTED BY WAMIT AS OUTPUT IN THE .OUT FILE!]
0 PtfmCOBxt - The xt offset of the center of buoyancy (COB) from the platform reference point (meters) [only used when PotMod=1]
0 PtfmCOByt - The yt offset of the center of buoyancy (COB) from the platform reference point (meters) [only used when PotMod=1]
1 RdtnMod - Radiation memory-effect model 0: no memory-effect calculation, 1: convolution, 2: state-space (switch) [only used when PotMod=1; STATE-SPACE REQUIRES *.ss INPUT FILE]
60 RdtnTMax - Analysis time for wave radiation kernel calculations (sec) [only used when PotMod=1; determines RdtnDOmega=Pi/RdtnTMax in the cosine transform; MAKE SURE THIS IS LONG ENOUGH FOR THE RADIATION IMPULSE RESPONSE FUNCTIONS TO DECAY TO NEAR-ZERO FOR THE GIVEN PLATFORM!]
0.005 RdtnDT - Time step for wave radiation kernel calculations (sec) [only used when PotMod=1; DT<=RdtnDT<=0.1 recommended; determines RdtnOmegaMax=Pi/RdtnDT in the cosine transform]
---------- 2ND-ORDER FLOATING PLATFORM FORCES ---------- [unused with WaveMod=0 or 6, or PotMod=0 or 2]
0 MnDrift - Mean-drift 2nd-order forces computed 0: None; [7, 8, 9, 10, 11, or 12]: WAMIT file to use [Only one of MnDrift, NewmanApp, or DiffQTF can be non-zero]
0 NewmanApp - Mean- and slow-drift 2nd-order forces computed with Newman's approximation 0: None; [7, 8, 9, 10, 11, or 12]: WAMIT file to use [Only one of MnDrift, NewmanApp, or DiffQTF can be non-zero. Used only when WaveDirMod=0]
0 DiffQTF - Full difference-frequency 2nd-order forces computed with full QTF 0: None; [10, 11, or 12]: WAMIT file to use [Only one of MnDrift, NewmanApp, or DiffQTF can be non-zero]
0 SumQTF - Full summation -frequency 2nd-order forces computed with full QTF 0: None; [10, 11, or 12]: WAMIT file to use
---------- FLOATING PLATFORM FORCE FLAGS ---------- [unused with WaveMod=6]
TRUE PtfmSgF - Platform horizontal surge translation force (flag) or DEFAULT
TRUE PtfmSwF - Platform horizontal sway translation force (flag) or DEFAULT
TRUE PtfmHvF - Platform vertical heave translation force (flag) or DEFAULT
TRUE PtfmRF - Platform roll tilt rotation force (flag) or DEFAULT
TRUE PtfmPF - Platform pitch tilt rotation force (flag) or DEFAULT
TRUE PtfmYF - Platform yaw rotation force (flag) or DEFAULT
---------- PLATFORM ADDITIONAL STIFFNESS AND DAMPING ---------
0 0 0 0 0 0 AddF0 - Additional preload (N, N-m)
0 0 0 0 0 0 AddCLin - Additional linear stiffness (N/m, N/rad, N-m/m, N-m/rad)
0 0 0 0 0 0
0 0 0 0 0 0
0 0 0 0 0 0
0 0 0 0 0 0
0 0 0 0 0 0
0 0 0 0 0 0 AddBLin - Additional linear damping(N/(m/s), N/(rad/s), N-m/(m/s), N-m/(rad/s))
0 0 0 0 0 0
0 0 1462500 0 0 0
0 0 0 0 0 0
0 0 0 0 0 0
0 0 0 0 0 0
0 0 0 0 0 0 AddBQuad - Additional quadratic drag($N/(m/s)^2$, $N/(rad/s)^2$, $N-m(m/s)^2$, $N-m/(rad/s)^2$)
0 0 0 0 0 0
0 0 0 0 0 0
0 0 0 0 0 0
0 0 0 0 0 0
0 0 0 0 0 0
---------- AXIAL COEFFICIENTS ----------
1 NAxCoef - Number of axial coefficients (-)
AxCoefID AxCd AxCa AxCp
(-) (-) (-) (-)
1 0.00 0.00 1.00

---------- MEMBER JOINTS ----------
2 NJoints - Number of joints (-) [must be exactly 0 or at least 2]
JointID Jointxi Jointyi Jointzi JointAxID JointOvrlp [JointOvrlp= 0: do nothing at joint, 1: eliminate overlaps by calculating super member]
(-) (m) (m) (m) (-) (switch)
1 0.00000 0.00000 -20.00010 1 0
2 0.00000 0.00000 10.00000 1 0
---------- MEMBER CROSS-SECTION PROPERTIES ----------
1 NPropSets - Number of member property sets (-)
PropSetID PropD PropThck
(-) (m) (m)
1 6.00000 0.06000
---------- SIMPLE HYDRODYNAMIC COEFFICIENTS (model 1) ---------
SimplCd SimplCdMG SimplCa SimplCaMG SimplCp SimplCpMG SimplAxCa SimplAxCaMG SimplAxCp SimplAxCpMG
(-) (-) (-) (-) (-) (-) (-) (-) (-) (-)
1.00 1.00 1.00 1.00 1.00 1.00 1.00 1.00 1.00 1.00
---------- DEPTH-BASED HYDRODYNAMIC COEFFICIENTS (model 2) ------
0 NCoefDpth - Number of depth-dependent coefficients (-)
Dpth DpthCd DpthCdMG DpthCa DpthCaMG DpthCp DpthCpMG DpthAxCa DpthAxCaMG DpthAxCp DpthAxCpMG
(m) (-) (-) (-) (-) (-) (-) (-) (-) (-) (-)
---------- MEMBER-BASED HYDRODYNAMIC COEFFICIENTS (model 3) -----
0 NCoefMembers - Number of member-based coefficients (-)
MemberID MemberCd1 MemberCd2 MemberCdMG1 MemberCdMG2 MemberCa1 MemberCa2 MemberCaMG1 MemberCaMG2 MemberCp1 MemberCp2 MemberCpMG1 MemberCpMG2 MemberAxCa1 MemberAxCa2 MemberAxCaMG1 MemberAxCaMG2 MemberAxCp1 MemberAxCp2 MemberAxCpMG1 MemberAxCpMG2
(-) (-)
---------- MEMBERS ----------
1 NMembers - Number of members (-)
MemberID MJointID1 MJointID2 MPropSetID1 MPropSetID2 MDivSize MCoefMod PropPot [MCoefMod=1: use simple coeff table, 2: use depth-based coeff table, 3: use member-based coeff table] [PropPot/=0 if member is modeled with potential-flow theory]
(-) (-) (-) (-) (-) (m) (switch) (flag)
1 1 2 1 1 0.5000 1 FALSE
---------- FILLED MEMBERS ----------
0 NFillGroups - Number of filled member groups (-) [If FillDens = DEFAULT, then FillDens = WtrDens; FillFSLoc is related to MSL2SWL]
FillNumM FillMList FillFSLoc FillDens
(-) (-) (m) (kg/m^3)
---------- MARINE GROWTH ----------
0 NMGDepths - Number of marine-growth depths specified (-)
MGDpth MGThck MGDens
(m) (m) (kg/m^3)
---------- MEMBER OUTPUT LIST ----------
0 NMOutputs - Number of member outputs (-) [must be < 10]
MemberID NOutLoc NodeLocs [NOutLoc < 10; node locations are normalized distance from the start of the member, and must be >=0 and <= 1] [unused if NMOutputs=0]
(-) (-) (-)
---------- JOINT OUTPUT LIST ----------
0 NJOutputs - Number of joint outputs [Must be < 10]
0 JOutLst - List of JointIDs which are to be output (-)[unused if NJOutputs=0]
---------- OUTPUT ----------
True HDSum - Output a summary file [flag]
False OutAll - Output all user-specified member and joint loads (only at each member end, not interior locations) [flag]
2 OutSwtch - Output requested channels to: [1=Hydrodyn.out, 2=GlueCode.out, 3=both files]
"ES11.4e2" OutFmt - Output format for numerical results (quoted string) [not checked for validity!]
"A11" OutSFmt - Output format for header strings (quoted string) [not checked for validity!]
---------- OUTPUT CHANNELS ----------
"Wave1Elev" - Wave elevation at the WAMIT reference point (0,0)
END of output channels and end of file.

A.8 MLife Input File

```
--- MLife version 1.0 Input File ---------------
Test#25
--- Job Options --------------------------
false EchoInp Echo input to <rootname>.echo as this file is being read.
true StrNames Use channel names following a "$" instead of numbers when specifying channels in this input file.
false OutData Output modified data array after scaling and calculated channels.  (currently unavailable)
"%6.2e" RealFmt Format for outputting floating-point values.
"Test26" RootName Root name for aggregate output files.
--- Input-Data Layout ----------------------------------
5 TitleLine The row with the file title on it (zero if no title is available).
7 NamesLine The row with the channel names on it (zero if no names are available or are specified below).
8 UnitsLine The row with the channel units on it (zero if no units are available or are specified below).
9 FirstDataLine The first row of data.
39 NumChans:  The number of channels in each input file.
ChanTitle ChanUnits Scale Offset PSFtype NumCols rows of data follow.
"Time" "(sec)" 1.0 0.0
"WindVxi" "(m/sec)" 1.0 0.0
"WindVyi" "(m/sec)" 1.0 0.0
"WindVzi" "(m/sec)" 1.0 0.0
"GenPwr" "(kW)" 1.0 0.0
"GenTq" "(kN.m)" 1.0 0.0
"HSSBrTq" "(kN.m)" 1.0 0.0 0
"Azimuth" "(deg)" 1.0 0.0
"GenSpeed" "(rpm)" 1.0 0.0
"NacYaw" "(deg)" 1.0 0.0
"NacYawErr" "(deg)" 1.0 0.0
"OoPDefl1" "(m)" 1.0 0.0 0
"IPDefl1" "(m)" 1.0 0.0 0
"TTDspFA" "(m)" 1.0 0.0 0
"TTDspSS" "(m)" 1.0 0.0 0
"PtfmTAxt" "(m/sec^2)" 1.0 0.0 0
"PtfmTAyt" "(m/sec^2)" 1.0 0.0 0
"PtfmTAzt" "(m/sec^2)" 1.0 0.0 0
"RootFxc1" "(kN)" 1.0 0.0 3
"RootFyc1" "(kN)" 1.0 0.0 3
"RootFzc1" "(kN)" 1.0 0.0 3
"RootMxc1" "(kN.m)" 1.0 0.0 3
"RootMyc1" "(kN.m)" 1.0 0.0 3
"RootMzc1" "(kN.m)" 1.0 0.0 3
"Spn1MLxb1" "(kN.m)" 1.0 0.0 3
"Spn1MLyb1" "(kN.m)" 1.0 0.0 3
"Spn1MLzb1" "(kN.m)" 1.0 0.0 3
"RotThrust" "(kN)" 1.0 0.0 3
"LSSGagFya" "(kN)" 1.0 0.0 3
"LSSGagFza" "(kN)" 1.0 0.0 3
"RotTorq" "(kN.m)" 1.0 0.0 3
"LSSGagMya" "(kN.m)" 1.0 0.0 3
"LSSGagMza" "(kN.m)" 1.0 0.0 3
"TwrBsFxt" "(kN)" 1.0 0.0 3
"TwrBsFyt" "(kN)" 1.0 0.0 3
"TwrBsFzt" "(kN)" 1.0 0.0 3
"TwrBsMxt" "(kN.m)" 1.0 0.0 3
"TwrBsMyt" "(kN.m)" 1.0 0.0 3
"TwrBsMzt" "(kN.m)" 1.0 0.0 3
--- Calculated Channels ------------------------------------
10 NumCChan The number calculated channels to generate.
1234567890 Seed The integer seed for the random number generator (-2,147,483,648 to 2,147,483,647)
Col_Title Units Equation Put each field in quotes.  Titles and units are limited to 10 characters.  "RootFMxy1" "(kN)"
"sqrt( timeSeriesData(:,50)^2 + timeSeriesData(:,51)^2 )"
"RootMMxy1" "(kN.m)" "sqrt( timeSeriesData(:,53)^2 + timeSeriesData(:,54)^2 )"
```

"RootFMxy2" "(kN)" "sqrt(timeSeriesData(:,56)^2 + timeSeriesData(:,57)^2)"
"RootMMxy2" "(kN.m)" "sqrt(timeSeriesData(:,59)^2 + timeSeriesData(:,60)^2)"
"RootFMxy3" "(kN)" "sqrt(timeSeriesData(:,62)^2 + timeSeriesData(:,63)^2)"
"RootMMxy3" "(kN.m)" "sqrt(timeSeriesData(:,65)^2 + timeSeriesData(:,66)^2)"
"LSSGagFMyz" "(kN)" "sqrt(timeSeriesData(:,78)^2 + timeSeriesData(:,79)^2)"
"LSSGagMMyz" "(kN.m)" "sqrt(timeSeriesData(:,81)^2 + timeSeriesData(:,82)^2)"
"TwrBsFMxy" "(kN)" "sqrt(timeSeriesData(:,89)^2 + timeSeriesData(:,90)^2)"
"TwrBsMMxy" "(kN.m)" "sqrt(timeSeriesData(:,92)^2 + timeSeriesData(:,93)^2)"
--- Load Roses --
2 NumRoses The number of load roses to generate.
Rose Name Units Channel1 Channel2 nSectors
"RootFxyc1" "(kN)" $RootFxc1$ $RootFyc1$ 12
"TwHt1MLxyt" "(kN.m)" $TwHt1MLxt$ $TwHt1MLyt$ 6
--- Time and Wind Speed -----------------------------------
$Time$ TimeChan The channel containing time.
$WindVxi$ WSChan The primary wind-speed channel (used for mean wind speed and turbulence intensity, 0 for none)
--- Statistics and Extreme Events ---------------------------
true DoStats Generate statistics of all the channels.
true WrStatsTxt Write the stats to a text file?
false WrStatsXLS Write the stats to an Excel file?
4 NumSFChans Number of channels that will have summary statistics generated for them.
$RootFxyc1_3$ $RootFxyc1_7$ $TwHt1MLxyt_2$ $TwHt1MLxyt_4$ SFChans List of channels that will have summary statistics generated for them.
--- Distributions --------------------------------------
false UserDistrib true = load user-specified distribution, false = only use Weibull wind distribution
2.4 WeibullShape Weibull shape factor. If WeibullShape=2, enter the mean wind speed for WeibullScale.
3 WeibullScale Weibull scale factor. If WeibullShape<>2. Otherwise, enter the mean wind speed.
3 WSin Cut-in wind speed for the turbine.
21 WSout Cut-out wind speed for the turbine.
44 WSmax Maximum wind speed value for the wind-speed bins.
1 WSMaxBinSize Maximum width of a wind-speed bin.
0 nDistribVars Number of independent variables in the user-specified distribution, ignored if UserDistrib = false
"" DistribName Filename of the user-supplied distribution table, ignored if UserDistrib = false
--- Fatigue ---
9 nFatigueChannels The number of fatigue channels. Next six lines ignored if zero.
0.0 FiltRatio The fraction of the maximum range of each channel used as a cutoff range for the racetrack filter. Use zero for no filter.
630720000 DesignLife Number of seconds in the design lifetime (20 years = 630720000 seconds).
1 Availability Fraction of the design life the turbine is operating when winds are between Vin and Vout
false BinCycles Bin the rainflow cycles?
0.5 UCMult Multiplier for binning unclosed cycles. (0 discards, 1 counts as a full cycle)
true DoShortTerm Compute simple (unweighted) damage-equivalent loads and damage rates.
true DoLife Do lifetime-related calculations?
true DoAggregate Compute a DELs and a damage result based on an aggregate of all the input files
true WrShortTermTxt Write short-term results to plain-text files?
false WrShortTermXLS Write short-term resultsto an Excel workbook?
true WrLifeTxt Write lifetime results to plain-text files?
false WrLifeXLS Write lifetime results to an Excel workbook?
1 EquivalentFrequency The frequency of the damage equivalent load (Hz)
false DEL_AsRange true = report DELs as a range value, false = report as a one-sided amplitude
2 DEL_Type 1 = fixed mean, 2 = zero mean, 3 = both
0 GoodmanFlag 0 = no Goodman correction, 1 = use Goodman correction, 2 = compute results for both
Channel# NSlopes SNslopeLst BinFlag BinWidth/Number TypeLMF LUlt BinWidth not used when BinCycles is false. nFatigueChannels rows of data follow. LUlt » LMF
$OoPDefl1$ 1 10 BN 30 AM 25e6
$IPDefl1$ 1 10 BN 30 AM 25e6
$TwstDefl1$ 1 10 BN 30 AM 25e6
$OoPDefl2$ 1 10 BN 30 AM 25e6
$IPDefl2$ 1 10 BN 30 AM 25e6
$TwstDefl2$ 1 10 BN 30 AM 25e6
$OoPDefl3$ 1 10 BN 30 AM 25e6
$IPDefl3$ 1 10 BN 30 AM 25e6
$TwstDefl3$ 1 10 BN 30 AM 25e6

```
1 NumDELGroups
Name NChannels ChannelList
"Blade Deflections" 9 1 3 4 5 6 7 8 2 9
--- Input Files ----------------------------------------
2 FileFormat Flag determining input file format.  1 = ascii, 2 = binary
3 1.1 1.3 1.1 1.7 (Weibull-Weighted Normal Operation:  NumNormFiles, PSF1, PSF2, PSF3, PSF4)
"Test1.outb"
"Test2.outb"
"Test3.outb"
0 1.1 1.3 1.5 1.7 (Weibull-Weighted Idling:  NumIdleFiles, PSF1, PSF2, PSF3, PSF4)
0 1.2 1.3 1.4 1.6 (Discrete Events:  NumDiscFiles, PSF1, PSF2, PSF3, PSF4)9 NumFiles The number of input files to read.

==EOF== DO NOT REMOVE OR CHANGE. MUST COME JUST AFTER LAST LINE OF VALID INPUT.
```